Chem Soc Rev

REVIEW ARTICLE

View Article Online
View Journal | View Issue

Cite this: *Chem. Soc. Rev.*, 2024, **53**, 11519

Molecular recognition of peptides and proteins by cucurbit[*n*]urils: systems and applications

Lilyanna Armstrong,[a] Sarah L. Chang,[a] Nia Clements,[a] Zoheb Hirani,[a] Lauren B. Kimberly,[a] Keturah Odoi-Adams,[b] Paolo Suating,[a] Hailey F. Taylor,[a] Sara A. Trauth[a] and Adam R. Urbach*[a]

Received 7th June 2024

DOI: 10.1039/d4cs00569d

rsc.li/chem-soc-rev

The development of methodology for attaching ligand binding sites to proteins of interest has accelerated biomedical science. Such protein tags have widespread applications as well as properties that significantly limit their utility. This review describes the mechanisms and applications of supramolecular systems comprising the synthetic receptors cucurbit[7]uril (Q7) or cucurbit[8]uril (Q8) and their polypeptide ligands. Molecular recognition of peptides and proteins occurs at sites of 1–3 amino acids with high selectivity and affinity *via* several distinct mechanisms, which are supported by extensive thermodynamic and structural studies in aqueous media. The commercial availability, low cost, high stability, and biocompatibility of these synthetic receptors has led to the development of myriad applications. This comprehensive review compiles the molecular recognition studies and the resulting applications with the goals of providing a valuable resource to the community and inspiring the next generation of innovation.

1. Introduction

Protein affinity tags are an essential tool of modern chemical biology with many established uses, including the detection of proteins and their isolation from complex mixtures, the addition of new functionality, and both the enhancement of solubility and the promotion of crystallization.[1–4] Affinity tags can be added to proteins *via* several different approaches, most commonly with genetic engineering but also *via* posttranslational and chemical modification. Compared to the size of the target protein, a tag may be relatively small (*e.g.*, peptide epitopes His_6, FLAG, or Myc) or large (*e.g.*, glutathione-*S*-transferase or maltose-binding protein) and often alters the

[a] *Department of Chemistry, Trinity University, San Antonio, TX, 78212, USA. E-mail: aurbach@trinity.edu*
[b] *Department of Chemistry and Physics, Southwestern Oklahoma State University, Weatherford, OK, 73096, USA*

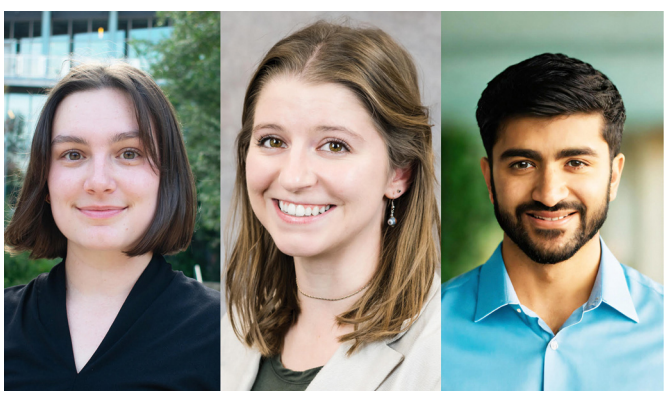

From left to right: Lilyanna Armstrong, Nia Clements and Zoheb Hirani

Lilyanna Armstrong, Nia Clements, and Zoheb Hirani did undergraduate research with Prof. Adam R. Urbach at Trinity University. Lilyanna is an undergraduate student at Trinity University studying biochemistry/molecular biology and Spanish. Upon graduation in 2025, she plans to study public and global health throughout the US and Latin America before pursuing an MD. Nia Clements completed a BS in biochemistry and molecular biology at Trinity University, followed by a Master of Public Health degree in infectious disease epidemiology at Cornell and is currently a PhD student in epidemiology at the University of Michigan at Ann Arbor. Her research interests include measuring health disparities related to climate and environmental justice issues caused by chemical exposures. Zoheb completed a BS in chemistry at Trinity University and recently finished his PhD in chemistry at Northwestern University with Prof. William R. Dichtel. His research interests are related to the synthesis and applications of porous, covalent organic frameworks.

structure and/or function of the protein in undesirable ways, necessitating removal of the tag.[4–7] The binding partners for an affinity tag (*e.g.*, monoclonal antibodies) can be costly to obtain or develop. His tags are an important exception to these general limitations because they are small and can be bound with commercially available and chemically modifiable metal complexes. Some major disadvantages of His tags are the need for low pH or high concentrations of imidazole to dissociate the complex, the limited binding affinity, and the incompatibility with reducing conditions, EDTA, and certain detergents.[6–8] The proven utility, future potential, and general limitations of affinity tags justify their further development. This review focuses on protein tags composed of 1–3 amino acid residues, *i.e.*, "minimal" protein tags, which are bound tightly and selectively by small, stable, inexpensive, and biocompatible synthetic receptors (Fig. 1). A 1–3 residue site cannot form a predictably folded structure, and when installed at the terminus of a protein, the site is even more likely to be structurally disordered and fully solvent-exposed, thus facilitating encapsulation by a synthetic receptor.

The complex between an affinity tag and its binding partner requires a substantial interfacial surface area.[9] In contrast to a folded protein, which can create a large binding interface by including a small molecule ligand within a well-defined binding cavity (Fig. 2a), the solvent-accessible surface of a minimal affinity tag is convex in shape and requires its binding partner to have a cavity (Fig. 2b). Natural protein/peptide receptors and enzymes, such as antibodies, N-recognins, proteases, and kinases have defined target binding sites within cavities.[10]

Small peptides are conformationally disordered and highly solvent-accessible. Therefore, they are good models for intrinsically disordered regions (IDRs) of proteins, while being less expensive to make and modify and easier to characterize by chemical methods. We hypothesize that receptors for small peptides should, in general, translate to intrinsically disordered regions of proteins such as termini and disordered loops.[13]

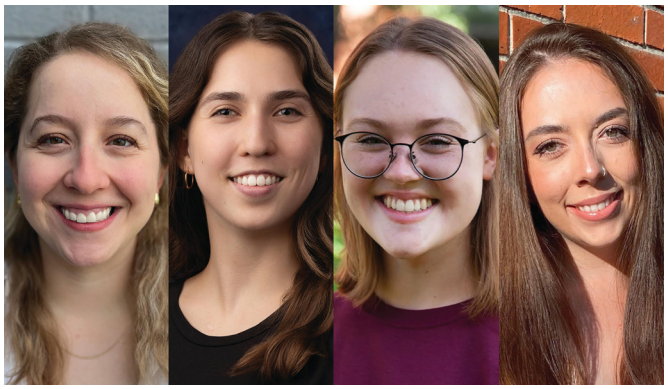

From left to right: Hailey Taylor, Sarah Chang, Lauren Kimberly, and Sara Trauth

Hailey Taylor, Sarah Chang, Lauren Kimberly, and Sara Trauth received bachelor degrees from Trinity University and did research in biomolecular recognition with Prof. Adam R. Urbach. Hailey earned her MS in chemistry from University of North Carolina at Chapel Hill and is currently a research associate at EpiCypher Inc. Her current research interests lie in developing novel assays to further epigenetic research. Sarah is currently pursuing an MD at the Joe R. and Teresa Lozano Long School of Medicine at the University of Texas Health San Antonio. Lauren is currently pursuing a PhD at the University of Texas at Austin with Prof. Emily Que. Her current research is focused on developing tools for cellular metal sensing. Sara Trauth was a Cottrell Postbaccalaureate Scholar with Prof. Adam R. Urbach for one year, and she is currently a PhD student in pharmacology and molecular sciences at The Johns Hopkins School of Medicine.

Keturah Adams

Keturah Adams earned her BS in chemistry from Southwestern Oklahoma State University (SWOSU) and her MS and PhD degrees in chemistry at Texas A&M University. She was a postdoctoral fellow at Trinity University with Prof. Adam R. Urbach before starting as an Assistant Professor of Chemistry (tenure-track) in the Department of Chemistry and Physics at SWOSU. Her research focuses on the functional characterization of the ELOVL4 protein, linked to macular dystrophy and neurodegenerative disorders. She is actively involved in programs supporting STEM education for high school students, rural teachers, and non-traditional students.

Paolo Suating

Paolo Suating received his PhD under the supervision of Prof. Bruce Gibb at Tulane University, where he studied the solvation properties of functionalized deep-cavity cavitands. He is currently a postdoctoral fellow with Prof. Adam R. Urbach at Trinity University studying sequence-selective peptide recognition by cucurbit[n]urils. His research interests include the syntheses of novel water-soluble macrocycles, ion–solute and solute–solute interactions in water, and long-range chirality transfer and induction.

Extensive work on developing synthetic receptors for peptides in aqueous solution was pioneered by Breslow, Hamilton, Kelly, Nowick, Schneider, Schmuck, Still, and others and has led to various strategies for targeting the ionic, polar, aromatic, and aliphatic functional groups of peptides.[14,15] Having a target site limited to 1–3 amino acid residues dictates that binding must be highly efficient on a per-residue basis. Although binding affinity and selectivity in the early systems was modest when compared with what is possible in biology, the highest affinity noncovalent complexes between synthetic receptors and peptides in aqueous solution have involved the inclusion of aromatic residues,[16–19] which are extraordinarily efficient on a per-residue basis, as discussed further below.

Targeting small sites, however, has the inherent problem of selectivity in a proteomic context. As an illustration of this problem, the crystal structure of cytochrome *c* bound to *p*-sulfonatocalix[4]calixarene shows multiple receptors bound to the surface of this relatively small protein (Fig. 1b).[12] In this review, we describe in detail how the properties of the cucurbit[*n*]uril (Q*n*) family of synthetic receptors have allowed them to target peptides and proteins in aqueous solution with sequence-selectively and with high affinity, and how these applications have enabled the development of myriad applications as affinity tags for peptides and proteins.

Cucurbit[*n*]urils (Q*n*'s) are a family of synthetic macrocyclic receptors composed of bis(methylene)-linked glycoluril units (Fig. 3).[20–22] The cavities of Q*n*'s are hydrophobic, which drives the inclusion of nonpolar groups *via* the exothermic release of water molecules upon guest binding.[23] The two identical and constricted entrances to a Q*n* cavity are lined with C═O groups that bind cations such as organic ammonium groups and metal cations.[24] The smaller cavity of cucurbit[6]uril (Q6) can accommodate alkyl groups, whereas the larger cavity of Q7 can accommodate larger guests, with optimal size complementarity for adamantane and ferrocene.[25,26] The cavity of Q8 can accommodate even larger guests and, importantly, two guests simultaneously.[27,28] Q*n*'s bind to a wide range of guests in aqueous solution with equilibrium association constant (K_a) values up to 10^{18} M^{-1},[29] which has led to applications in sensing, separations, remediation, catalysis, drug delivery, polymerization, and gelation, among many others.[22] Here, we focus on the basic science and applications of the molecular recognition of peptides and proteins by Q*n* receptors.

The vast majority of the work on peptide recognition by Q*n* receptors has involved Q7 and Q8, which have an inner cavity volume sufficient to accommodate the side chain(s) of one or two amino acid residue(s). Our first studies in this area followed the pioneering work of Kimoon Kim and coworkers, who reported the formation of ternary complexes in which Q8 binds either two of the same guest (*i.e.*, homoternary)[27] or two different guests (*i.e.*, heteroternary).[28] They showed that Q8 binds methyl viologen (MV) but not 2,6-dihydroxynaphthalene (HN), and that the Q8·MV complex binds HN as a second guest to form the heteroternary Q8·MV·HN complex (Fig. 4). A crystal structure shows HN and a viologen stacking face-to-face in the cavity of Q8 in the solid state, and NMR data show that both MV and HN are included simultaneously within the Q8 cavity in the solution state. The binding of HN to Q8·MV results in the growth and red-shifting of a visible charge-transfer absorbance and a quenching of naphthalene fluorescence, which corroborates the simultaneous inclusion of both aromatic guests in the Q8 cavity.[28]

In parallel with their report on hetero-guest pairs, Kim and coworkers filed a patent claiming that Q8·MV can also bind to aromatic second guests including tryptophan, tyrosine, and dopamine.[31] This finding inspired us to further explore the binding of amino acids by Q8·MV.[30] We measured the solubility of Q8 in our standard buffer, 10 mM sodium phosphate, pH 7.0 (100 μM), and the K_a value (8.5×10^5 M^{-1}) for the formation of the Q8·MV complex. Isothermal titration calorimetry (ITC) experiments showed that the Q8·MV complex binds to tryptophan with a K_a value of 4.3×10^4 M^{-1} and with 8-fold selectivity over phenylalanine and 20-fold selectivity over tyrosine.[30] No binding was observed for the other 17 amino acids by ITC or by NMR spectroscopy.[30,32] Based on the driving forces for cucurbituril binding, we would expect hydrophobic and basic (*i.e.*, cationic) amino acids to be preferred, but only tryptophan, phenylalanine, and tyrosine bind measurably. A comparative analysis of the side chains of the 20 genetically encoded amino acids, in terms of their solvent-exposed surface areas and their transfer energies from water to cyclohexane solution (Fig. 5),[33–35] is consistent with a combination of size and hydrophobicity driving the binding of tryptophan, phenylalanine, and tyrosine. Leucine and isoleucine are more hydrophobic but smaller than tryptophan and thus would not displace as many water molecules upon binding. Arginine and lysine are large but too hydrophilic to bind stably within the Q8 cavity.

Synthetic receptors need efficient ligands, and aromatic residues are particularly efficient. Aromatic residues are especially versatile for intermolecular interactions, with binding driven significantly by electrostatic, van der Waals, and

Adam R. Urbach

Adam R. Urbach earned a BS in chemistry from UT Austin, doing undergraduate research with Profs Jonathan L. Sessler and Thomas J. Kodadek. Following a PhD in organic chemistry at Caltech with Prof. Peter B. Dervan and a postdoc at Harvard with Prof. George M. Whitesides, he moved to Trinity University, where he is Professor of Chemistry. His research has primarily involved studies of biomolecular recognition, with his independent work focused on the sequence-selective molecular recognition of peptides and proteins by cucurbit[n]uril synthetic receptors. Prof. Urbach is a Fellow of the American Association for the Advancement of Science.

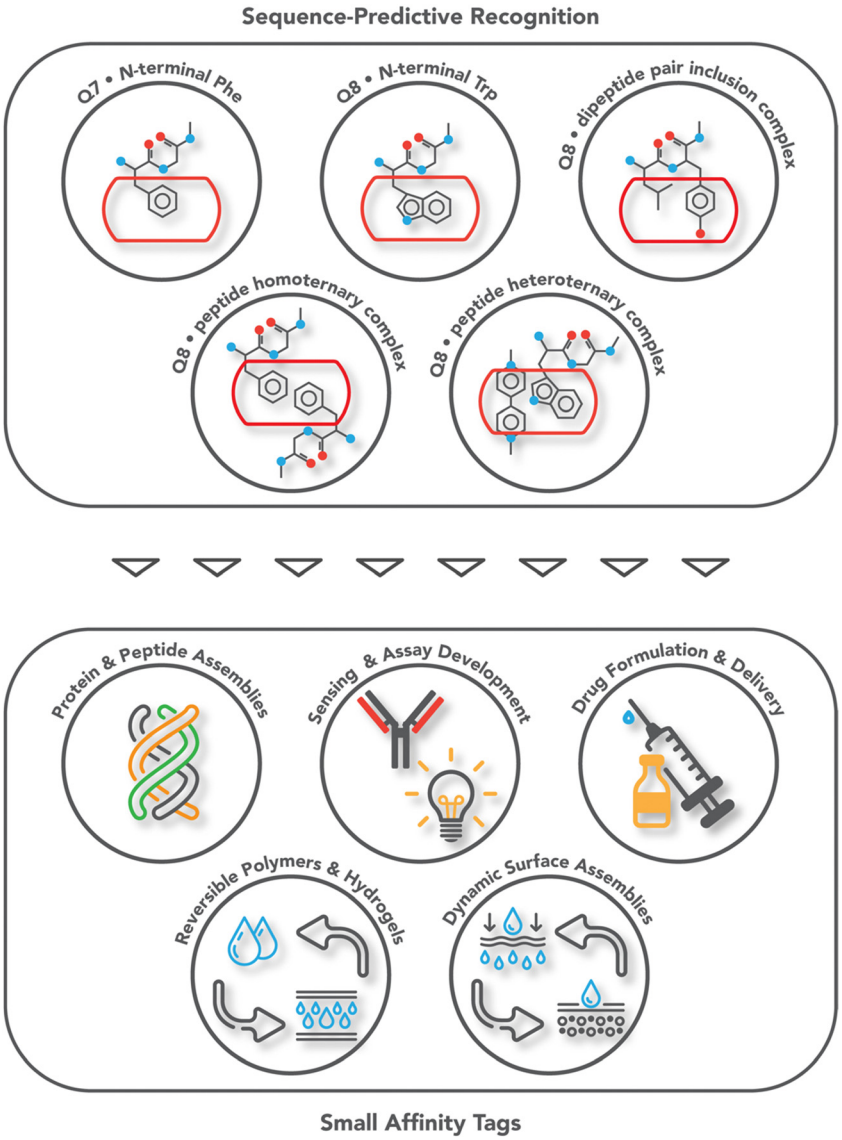

Fig. 1 Overview of the systems of sequence-predictive molecular recognition by cucurbit[*n*]urils and the applications they have enabled.

hydrophobic interactions.[36] Aromatic groups bind electrostatically to cations, hydrogen bond donors, and other aromatic groups *via* their quadrupole moments. The large, nonpolar surface areas of aromatic groups allow extensive van der Waals interactions and the release of many water molecules upon binding. The high structural rigidity minimizes the loss of conformational entropy upon binding. The aromatic residues tryptophan (Trp), phenylalanine (Phe), and tyrosine (Tyr) have a unique combination of characteristics, being the largest and most hydrophobic residues. Mutational studies of protein–protein interactions have found that on a per-residue basis, aromatic residues contribute significantly more than non-aromatic residues to the stability of protein–protein interactions.[37–39] It is perhaps not surprising, therefore, that aromatic residues can be bound with high affinity by synthetic receptors.

2. Mechanisms of peptide and protein recognition by cucurbit[*n*]urils

2.1. Discovery of sequence-selective peptide recognition by cucurbit[8]uril

In the Q8·MV·Trp aqueous complex at pH 7.0,[30] there is unusually high electrostatic charge density, including the dicationic MV, the zwitterionic tryptophan, and the concentrated negative electrostatic potential of the C═O groups of Q8. To probe the influence of charge on binding, we studied the binding of Q8·MV with a series of tryptophan derivatives that vary in the type, number, and location of charge (Fig. 6). Compared to tryptophan, tryptamine (TrpA) and tryptophan methyl ester (Trp-OMe) lack a negative charge, and indole propionic acid (IPA) and *N*-acetyl tryptophan (*N*-AcTrp) lack a positive charge. ITC studies showed that Q8·MV binds TrpA,

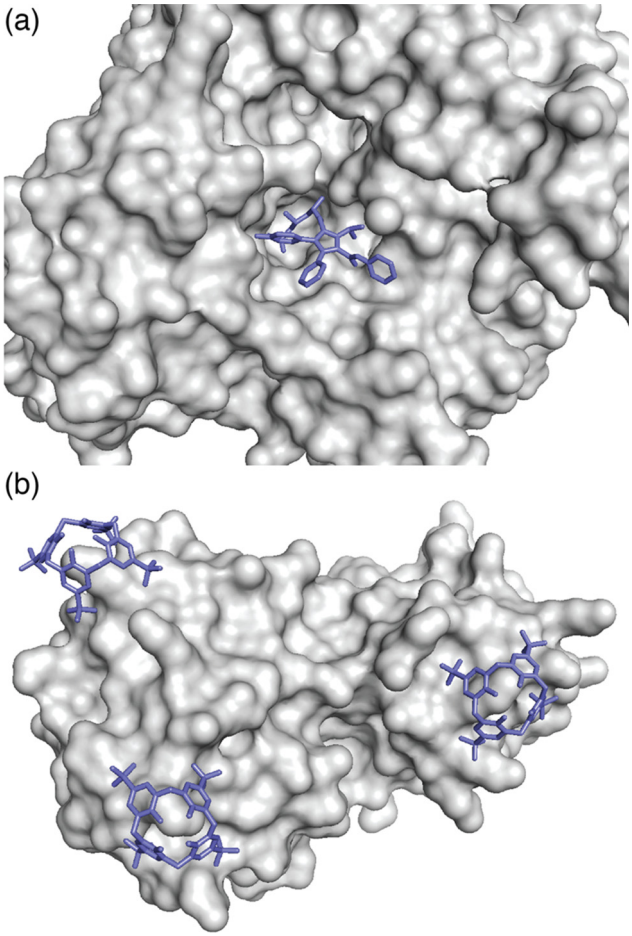

Fig. 2 (a) Binding of a ligand within a protein cavity. Crystal structure of atorvastatin (blue sticks) bound within the active site cavity of HMG CoA reductase, shown as a grey solvent-accessible surface (PDB ID: 1 HWK).[11] (b) Binding of a synthetic receptor on the surface of a protein. Crystal structure of three sulfonatocalix[4]arene hosts (blue sticks) bound to lysine residues on the surface of cytochrome *c*, shown as a grey solvent-accessible surface (PDB ID: 3TYI).[12] Reproduced from ref. 10 with permission from the Royal Society of Chemistry.

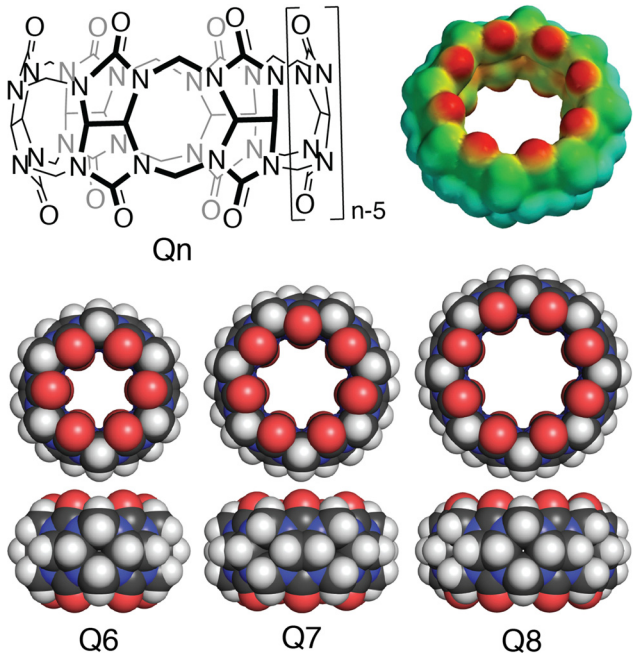

Fig. 3 (top left) Structural formula of cucurbit[*n*]uril; (top right) Electrostatic potential mapped onto the solvent accessible surface of cucurbit[8]uril; (bottom) Space-filling models of cucurbit[*n*]urils showing the variation in size based on the number of glycoluril units.

Trp-OMe, and tryptophan with similar affinity and with approximately 20-fold selectivity over IPA and *N*-AcTrp. It was particularly interesting to learn that the binding affinity of tryptophan correlates more with the cationic derivatives than with the anionic derivatives. These results suggested that binding selectivity is driven by electrostatic stabilization of the cationic ammonium group, most likely *via* its interaction with the C=O groups on Q8.

We reasoned that the singly charged tryptophan derivatives, especially *N*-AcTrp and Trp-OMe, are structurally analogous to a Trp residue positioned at the N- or C-terminal position of a peptide chain (Fig. 6).[30] *N*-AcTrp retains its carboxylate group, akin to a C-terminal Trp, and Trp-OMe retains its ammonium group, akin to an N-terminal Trp. Therefore, we hypothesized that Q8·MV should bind selectively to an N-terminal Trp residue *versus* a C-terminal Trp residue due to stabilization by the proximal ammonium group. ITC studies showed that Q8·MV binds to the peptide H-Trp-Gly-Gly-OH (Gly = glycine; H- indicates unprotected N-terminal amine; –OH indicates unprotected C-terminal carboxylic acid), which contains an N-terminal Trp residue, with a K_a value of 1.3×10^5 M^{-1} and with 6-fold selectivity over H-Gly-Trp-Gly-OH and 40-fold selectivity over H-Gly-Gly-Trp-OH (Table 1).[30] Both peptides containing a non-terminal Trp residue, H-Gly-Trp-Gly-OH and H-Gly-Gly-Trp-Gly-Gly-OH, bound Q8·MV with similar affinities. NMR data showed that in each complex, both the indole side chain and the viologen group are bound simultaneously within the Q8 cavity, as revealed by upfield chemical shift perturbation of the aromatic signals of both compounds in the presence of Q8. These results demonstrated that Q8·MV can recognize N-terminal Trp in a sequence-selective manner, and that the N-terminal residue, comprising the indole sidechain and the N-terminal ammonium group, comprises a unique epitope for site-selective binding.

Methyl viologen has intrinsic optical and electronic properties that have enabled several applications in the sensing of peptides and proteins, as discussed in detail in Section 3.1. The binding of Trp-containing peptides to Q8·MV induces the growth of a charge-transfer absorbance and the quenching of indole fluorescence.[30] Both of these effects are likely due to electron-transfer from indole to viologen in the excited electronic state and do not contribute significantly to the stability of the complexes in the ground state.[46] The viologen therefore provides the means for a convenient, built-in optical sensor for peptide binding *via* absorbance and fluorescence spectroscopy.

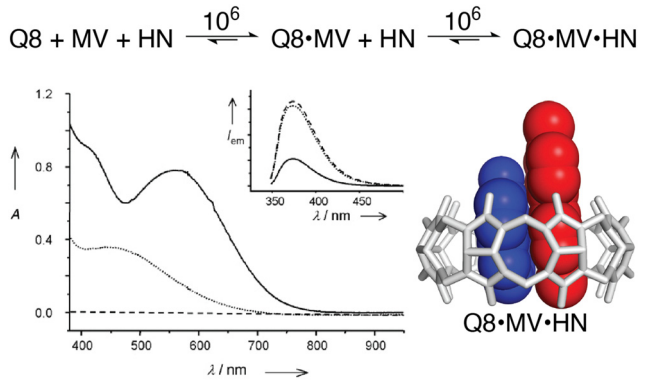

Fig. 4 (top) Two-step formation of the heteroternary Q8·MV·HN complex with equilibrium association constant (K_a) values (M^{-1}) shown over the arrows (10 mM sodium phosphate, pH 7.0, 300 K).[30] (bottom left) UV-visible absorption and emission (inset) spectra of HN (dashed line), a 1 : 1 mixture of HN and MV (dotted line), and a 1 : 1 : 1 mixture of Q8, HN, and MV (solid line). (bottom right) Structure of the Q8·MV·HN complex modeled from the crystal structure of an analogue. CCDC ID 154114.[28] Adapted with permission from ref. 28. © 2001 Wiley-VCH Verlag GmbH, Weinheim, Fed. Rep. of Germany.

With the indole side chain of the Trp residue bound within the Q8 cavity, the neighboring residue would be forced into proximity to Q8·MV. For example, a basic residue could possibly bind to the Q8 portal or be repelled by MV. Therefore, we hypothesized that the identity of the second residue could influence binding. We synthesized a library comprising 104 peptides, each containing a Trp binding site positioned either at the N-terminus of a tripeptide (H-Trp-X-Ala-NH_2 and H-Trp-Ala-X-NH_2) or at the center of a pentapeptide (H-X-Ala-Trp-Ala-Ala-NH_2, H-Ala-X-Trp-Ala-Ala-NH_2, H-Ala-Ala-Trp-X-Ala-NH_2, and H-Ala-Ala-Trp-Ala-X-NH_2), with a single variable position (X varied to all 20 amino acids except Trp and Cys) and with Ala residues at the other positions.[40] We used the sensing properties of Trp binding to Q8·MV to facilitate the parallel screening of peptide binding by measuring the relative quenching of Trp fluorescence as a surrogate for relative binding affinity. There were insignificant differences observed among the peptides in each of the two series, with the exception of H-Lys-Ala-Trp-Ala-Ala-NH_2 *versus* H-Ala-Lys-Trp-Ala-Ala-NH_2. These two peptides were tested by ITC (Table 1) and shown to have only 2-fold difference in affinity. Therefore, the screening assay was sensitive to changes in binding affinity, but in this particular motif (*i.e.*, Q8·MV binding to a peptide with a Trp residue), the sequence context of the target Trp residue does not significantly influence the binding affinity.

2.2. Multivalent peptide binding by self-assembled receptors

In an effort to expand the peptide binding properties of this system, we considered linking Q8 molecules to form multivalent receptors. Although the MV and Q8 work together as co-hosts, the viologen is more synthetically modifiable than the macrocycle. Therefore, we linked viologens together and recruited Q8 molecules to each viologen site to form multivalent receptors (Fig. 7).[47] One, two, and three viologen groups were conjugated to flexible, peptide-based scaffolds and used to recruit the same numbers of Q8 groups to form self-assembled monovalent, divalent, and trivalent receptors, which bound to peptides containing the same numbers of Trp residues in monovalent, divalent, and trivalent fashion. The extent of valency in each complex was quantified directly *via* the additive charge-transfer absorptivities of the Q8·viologen·Trp complexes (Fig. 7). Isothermal titration calorimetry studies showed that

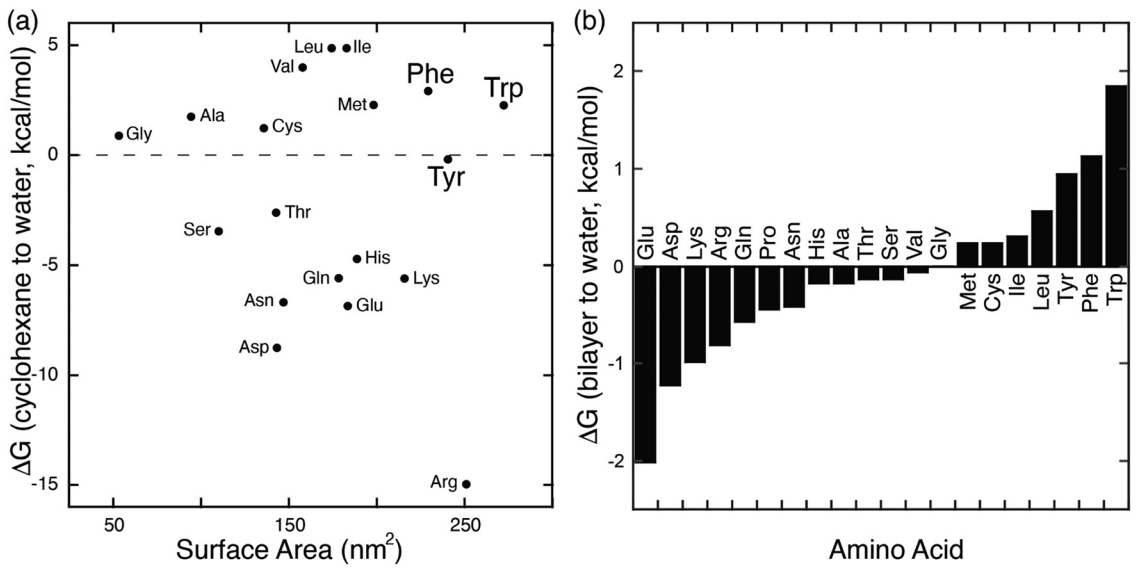

Fig. 5 (a) Plot of the transfer energy from cyclohexane solution to neutral aqueous solution *versus* the solvent-exposed surface area of side chain analogues of the 20 amino acids (*i.e.*, methane for alanine; 3-methylindole for tryptophan). The transfer energies were reported by Radzicka and Wolfenden.[34] The surface areas were calculated for tripeptides Gly-X-Gly by Chothia.[33] (b) Calculated hydrophobicity at pH 8 for all residues except Arg and Lys, which were calculated at pH 2.[35] Extremes on this plot are defined by charged residues at the negative end and aromatic residues at the positive end. Reproduced from ref. 10 with permission from the Royal Society of Chemistry.

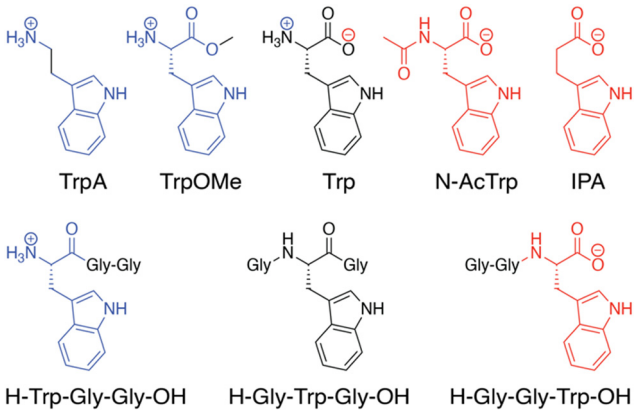

Fig. 6 Chemical formulas of tryptophan derivatives and their structurally analogous Trp-containing peptides.[30] Reproduced from ref. 10 with permission from the Royal Society of Chemistry.

the enthalpy of binding was additive with the extent of valency (average ΔH monovalent = −10.9 kcal mol^{-1}, divalent = −24.2 kcal mol^{-1}, trivalent −39.4 kcal mol^{-1}, Table 2), which corroborated the simultaneous formation of all Q8·viologen·indole complexes. The free energies of peptide binding, however, were not additive (average ΔG monovalent = −6.0 kcal mol^{-1}, divalent = −7.8 kcal mol^{-1}, trivalent −9.2 kcal mol^{-1}), which is in contrast to what would be expected for optimal multivalent binding.[48] The deviation from optimal binding was due to an entropic penalty for binding that was more than additive with the extent of valency (average $-T\Delta S$ monovalent = 4.9 kcal mol^{-1}, divalent = 16.4 kcal mol^{-1}, trivalent 30.2 kcal mol^{-1}).[47] This resulted in only a modest increase in peptide binding affinity of 30-fold for divalent *versus* monovalent and 300-fold for trivalent *vs.* monovalent (Table 2). For the set of four divalent complexes, the length of the oligo(Gly) linker between the two binding sites was varied between four or six Gly units. It

Table 1 Thermodynamic data for Q8 heteroternary complexes

Host	Peptide or protein	K_a (M^{-1})	ΔH (kcal mol^{-1})	$-T\Delta S$ (kcal mol^{-1})
Q8·MV[a]	H-**Trp**-Gly-Gly-OH	1.3×10^5	−14.8	7.8
Q8·MV[a]	H-Gly-**Trp**-Gly-OH	2.1×10^4	−11.4	5.5
Q8·MV[a]	H-Gly-Gly-**Trp**-OH	3.1×10^3	−8.8	4.0
Q8·MV[a]	H-Gly-Gly-**Trp**-Gly-Gly-OH	2.5×10^4	−12.1	6.1
Q8·MV[b]	H-Lys-Ala-**Trp**-Ala-Ala-NH_2	6.2×10^3	nr[j]	nr
Q8·MV[b]	H-Ala-Lys-**Trp**-Ala-Ala-NH_2	1.7×10^4	nr	nr
Q8·MV[c]	H-**Trp**-Gly-Gly-OH	3.0×10^5	−12.6	5.1
Q8·MV[c]	H-Met-Gly-Gly-OH	nd[i]	nr	nr
Q8·MV[c]	YFP-**Trp**-Gly-Gly	2.3×10^5	−7.2	−0.3
Q8·MV[c]	YFP-**Met**-Gly-Gly	1.2×10^5	−4.3	−2.7
Q8·MV[d]	H-Ala-Cys-Asn-Thr-Gly-Ser-Pro-**Tyr**-Glu-Cys-NH_2	4.3×10^4	−1.3	−5.0
Q8·MV[d]	H-Ala-Cys-Gln-Asn-Pro-Asn-Gln-Lys-**Phe**-Cys-NH_2	2.2×10^5	−11.0	3.9
Q8·MV[d]	H-Ala-Cys-Leu-Lys-Leu-Gly-Glu-Lys-**Trp**-Cys-NH_2	4.4×10^4	−12.0	5.5
Q8·MV[e]	H-Ala-Cys*-Asn-Thr-Gly-Ser-Pro-**Tyr**-Glu-Cys*-NH_2	nd	nr	nr
Q8·MV[e]	H-Ala-Cys*-Gln-Asn-Pro-Asn-Gln-Lys-**Phe**-Cys*-NH_2	5.9×10^4	−11.0	4.6
Q8·MV[e]	H-Ala-Cys*-Leu-Lys-Leu-Gly-Glu-Lys-**Trp**-Cys*-NH_2	nd	nr	nr
Q8·MV[d]	Tn3 (Gln-Lys-**Phe** in BC loop)	6.1×10^5	−11.0	2.8
Q8·MV[d]	Tn3 (Gln-Lys-**Phe** in DE loop)	8.9×10^4	−2.1	−4.7
Q8·MV[d]	Tn3 (Gln-Lys-**Phe** in FG loop)	6.4×10^4	−1.4	−5.2
Q8·MBBI[f]	H-**Trp**-Gly-Gly-OH	1.2×10^5	−15.6	8.6
Q8·MBBI[f]	H-Gly-**Trp**-Gly-OH	1.7×10^4	−16.5	10.7
Q8·MBBI[f]	H-Gly-Gly-**Trp**-OH	4.1×10^3	−13.0	8.0
Q8·MDAP[g]	H-Arg_7-OH	nd	nr	nr
Q8·MDAP[g]	H-Leu-Arg-Arg-**Trp**-Ser-Leu-Gly-OH	nd	nr	nr
Q8·MDAP[g]	H-Leu-Arg-Arg-**Trp**-pSer-Leu-Gly-OH	nd	nr	nr
Q8·MDAP[g]	H-**Trp**-Lys-Arg-Thr-Leu-Arg-Arg-Leu-OH	4.3×10^5	nr	nr
Q8·MDAP[g]	H-**Trp**-Lys-Arg-pThr-Leu-Arg-Arg-Leu-OH	4.1×10^5	nr	nr
Q8·MDAP[g]	H-**Phe**-Arg_7-OH	2.0×10^6	nr	nr
Q8·F′GG[h]	H-**Trp**-Gly-Gly-OH	4.6×10^5	−13.3	5.6
Q8·F′GG[h]	H-Gly-**Trp**-Gly-OH	1.0×10^5	−11.9	5.0
Q8·F′GG[h]	H-Gly-Gly-**Trp**-OH	9.0×10^4	−14.5	7.8
Q8·F′GG[h]	H-**Phe**-Gly-Gly-OH	3.6×10^5	−14.4	6.8
Q8·F′GG[h]	H-Gly-**Phe**-Gly-OH	5.8×10^4	−9.1	2.6
Q8·F′GG[h]	H-Gly-Gly-**Phe**-OH	2.2×10^4	−7.5	1.5
Q8·F′GG[h]	H-**Tyr**-Gly-Gly-OH	3×10^3	−9.6	3.6
Q8·F′GG[h]	H-Gly-**Tyr**-Gly-OH	4×10^3	−4.7	−0.2
Q8·F′GG[h]	H-Gly-Gly-Tyr-OH	nd	nd	nd
Q8·F′GG[h]	H-Lys-Gly-Gly-OH	nd	nd	nd
Q8·F′GG[h]	H-Glu-Gly-Gly-OH	nd	nd	nd
Q8·F′GG[h]	H-Leu-Gly-Gly-OH	nd	nd	nd

[a] 10 mM sodium phosphate, pH 7.0, 300 K.[30] [b] 10 mM sodium phosphate, pH 7.0, 300 K.[40] [c] 10 mM sodium phosphate, pH 7.0, 303 K.[41] [d] 10 mM sodium phosphate, pH 7.4, 298 K.[42] [e] 10 mM sodium phosphate, 0.5 mM dithiothreitol, pH 7.4, 298 K, Cys* = intramolecular disulfide.[42] [f] 10 mM sodium phosphate, pH 7.0, 300 K.[43] [g] 10 mM HEPES, pH 7.0, temperature not reported.[44] [h] 10 mM sodium phosphate, pH 7.0, 298 K, F′ = 2,3,4,5,6-pentafluorophenylalanyl.[45] [i] Not detected. [j] Not reported. Putative binding sites are in bold.

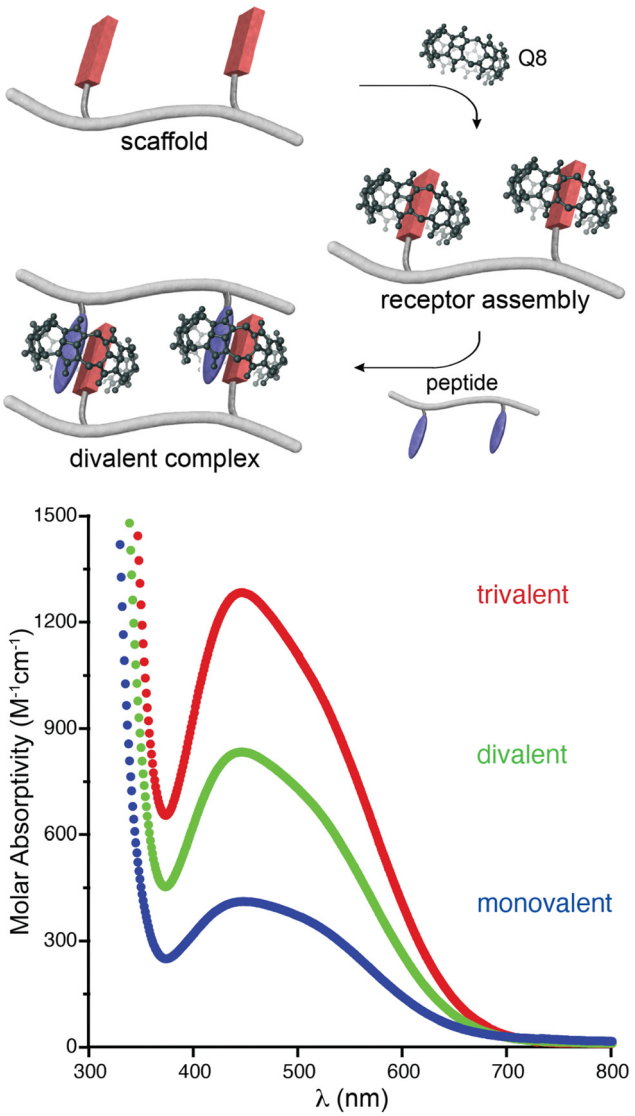

Fig. 7 (top) Schematic of the self-assembly of Q8 onto a divalent scaffold and the divalent binding of the resulting receptor to a divalent peptide. (bottom) UV-visible spectra showing the additive molar absorptivities of monovalent, divalent, and trivalent complexes.[47] Reproduced with permission from ref. 47. Copyright 2009 American Chemical Society.

is remarkable that the linker length showed no significant influence on the binding thermodynamics, as we would have expected greater loss in entropy for the longer chain.

2.3. Dimerization of peptides by cucurbit[8]uril

Early on we were interested to know whether Q8 could bind peptides in the absence of MV and hypothesized that the additional space in the Q8 cavity could accommodate an additional portion of one peptide or part of a second peptide. Twelve peptides of sequence H-X-Gly-Gly-OH, H-Gly-X-Gly-OH, and H-Gly-Gly-X-OH (X = Trp, Phe, Tyr, His), were tested for binding to Q8 by ITC.[18] Binding was only measurable for H-Trp-Gly-Gly-OH and H-Phe-Gly-Gly-OH, and binding to these peptides was found to occur in a 2 : 1 peptide : Q8 stoichiometry (*i.e.*, homodimerization of peptides). NMR data showed that binding occurs site-selectively at the N-terminal aromatic residue. Mass spectrometry confirmed the presence of 2 : 1 peptide : Q8 complexes. The thermodynamic constants for homoternary complex formation are reported in Table 3. The ternary equilibrium constant (K_{ter}: Q8 + 2 peptide → Q8·(peptide)$_2$) values for Q8·(H-Trp-Gly-Gly-OH)$_2$ and Q8·(H-Phe-Gly-Gly-OH)$_2$ were modest (10^9 – 10^{11} M^{-2}) and showed that Q8 prefers Phe to Trp in this context.[18] When looking at these values here and elsewhere, it is important to note the molecularity of complexation and not to confuse the magnitude of a K_{ter} value with that of a binary K_a value. For example, a K_{ter} value of 1.5×10^{11} M^{-2} is roughly equivalent to each molecule of peptide binding with a K_a value of 4×10^5 M^{-1}. Nonetheless, the *sequence-selectivity* of binding in this system is extraordinary. Due to the lower limit of detection for the ITC instrument of $\sim 10^2$ M^{-1}, the selectivity of Q8 for H-Phe-Gly-Gly-OH *versus* H-Gly-Phe-Gly-OH is at least 1000-fold in terms of the affinity per peptide. All twelve peptides had an aromatic side chain, but only Trp and Phe bound measurably, indicating that the identity of the residue is important. All six Trp- and Phe-containing peptides had an N-terminal amine, but only the two peptides containing an N-terminal Trp or Phe bound measurably, indicating that the ammonium group alone is insufficient to drive binding. Instead, the combination of hydrophobic inclusion of a Phe or Trp side chain and electrostatic interaction with the proximal ammonium group is necessary for tight binding. In contrast to our first study,[30] these results convinced us that the N-terminal residue could be a highly selective epitope that allows recognition in more complex environments and applications. Additionally, this early study established the foundation for an important technique that would later be used by numerous research groups, discussed in detail in Section 3.3.1: using Q8 to induce the homodimerization of proteins.[18]

We attempted to delineate the affinities of each peptide in the stepwise formation of the ternary complexes.[18] In the case of H-Trp-Gly-Gly-OH, the observed affinity for the first guest is approximately 4-fold higher than that of the second guest, which is consistent with non-cooperative binding (*i.e.*, the binding of the first guest does significantly influence the stability of binding of the second guest). In the case of H-Phe-Gly-Gly-OH, the data did not yield confident values for the stepwise binding constants. Based on the curvature of the ITC data and on NMR experiments showing the formation of the Q8·(H-Phe-Gly-Gly-OH)$_2$ complex in mixtures containing less than a 2 : 1 mol ratio of peptide : Q8, we concluded that binding is positively cooperative but were unable to unambiguously determine stepwise binding constants. Subsequently, Huskens, Jonkheijm, and coworkers reported a detailed investigation of cooperativity in the Q8·(H-Phe-Gly-Gly-OH)$_2$ system and concluded that binding is most likely to be non-cooperative.[49]

In collaboration with the late P. John Hart at UT Health San Antonio, we obtained crystal structures of the ternary Q8·(H-Phe-Gly-Gly-OH)$_2$ complex (Fig. 8) and the binary Q8·H-Trp-Gly-Gly-OH complex.[18] In both crystal structures, the aromatic side

Table 2 Thermodynamic data for Q8-mediated multivalent peptide binding

Self-assembled receptor	Peptide	K_a (M^{-1})	ΔH (kcal mol^{-1})	$-T\Delta S$ (kcal mol^{-1})
Ac-Gly_2-Viol·Q8-Gly_2-NH_2[a]	Ac-Gly_2-**Trp**-Gly_2-NH_2	2.2×10^4	−10.8	4.9
Ac-Gly_2-Viol·Q8-Gly_2-NH_2[a]	Ac-Gly_3-**Trp**-Gly_3-NH_2	2.2×10^4	−11.0	5.0
Ac-Gly_3-Viol·Q8-Gly_3-NH_2[a]	Ac-Gly_2-**Trp**-Gly_2-NH_2	1.9×10^4	−10.8	4.9
Ac-Gly_3-Viol·Q8-Gly_3-NH_2[a]	Ac-Gly_3-**Trp**-Gly_3-NH_2	2.2×10^4	−11.0	4.9
Ac-(Gly_2-Viol·Q8-Gly_2)$_2$-NH_2[a]	Ac-Gly_2-**Trp**-Gly_2-NH_2	1.7×10^4	−12.8	7.0
Ac-(Gly_2-Viol·Q8-Gly_2)$_2$-NH_2[a]	Ac-Gly_3-**Trp**-Gly_3-NH_2	1.5×10^4	−13.0	7.2
Ac-(Gly_3-Viol·Q8-Gly_3)$_2$-NH_2[a]	Ac-Gly_2-**Trp**-Gly_2-NH_2	1.8×10^4	−11.8	5.9
Ac-(Gly_3-Viol·Q8-Gly_3)$_2$-NH_2[a]	Ac-Gly_3-**Trp**-Gly_3-NH_2	1.4×10^4	−12.3	6.6
Ac-(Gly_2-Viol·Q8-Gly_2)$_2$-NH_2[a]	Ac-(Gly_2-**Trp**-Gly_2)$_2$$NH_2$	5.0×10^5	−24.2	16.3
Ac-(Gly_2-Viol·Q8-Gly_2)$_2$-NH_2[a]	Ac-(Gly_3-**Trp**-Gly_3)$_2$$NH_2$	4.6×10^5	−24.8	17.1
Ac-(Gly_3-Viol·Q8-Gly_3)$_2$-NH_2[a]	Ac-(Gly_2-**Trp**-Gly_2)$_2$$NH_2$	5.5×10^5	−23.4	15.6
Ac-(Gly_3-Viol·Q8-Gly_3)$_2$-NH_2[a]	Ac-(Gly_3-**Trp**-Gly_3)$_2$$NH_2$	5.0×10^5	−24.3	16.5
Ac-(Gly_2-Viol·Q8-Gly_2)$_3$-NH_2[a]	Ac-Gly_2-**Trp**-Gly_2-NH_2	1.7×10^4	−12.2	6.4
Ac-(Gly_2-Viol·Q8-Gly_2)$_3$-NH_2[a]	Ac-Asp_2-(Gly_2-**Trp**-Gly_2)$_3$-Asp_2-NH_2	4.7×10^6	−39.4	30.2

[a] 10 mM sodium phosphate, pH 7.0, 300 K; Viol-Q8 indicates a viologen-modified residue bound to Q8; Ac-indicates an acetylated N-terminal amine.[47] Putative binding sites are in bold.

chains are bound deeply within the Q8 cavity, the N-terminal ammonium groups are bound in close proximity to multiple C═O groups on the Q8 portal, the first peptide NH group hydrogen bonds to a C═O group on Q8, and the second peptide NH group forms at least one stabilizing dipole–dipole interaction with a C═O group on Q8. In addition, the indole NH group forms a bifurcated hydrogen bond with two C═O groups on the opposite portal of Q8. These structures provided a molecular basis with atomic detail for the recognition of peptides by Q8. They revealed the shape and electrostatic complementarity of Q8 with N-terminal Phe and Trp, showing that the Q8 cavity is the right size for certain side chains, and that the C═O groups of Q8 are preorganized to make multiple stabilizing electrostatic interactions with peptides.

Recently, Scherman and coworkers demonstrated the ability to direct the heterodimerization of peptides using the noncanonical amino acid, 2,3,4,5,6-pentafluorophenylalanine (Phe_{F5}, or F′).[45] They showed that Q8 binds to a tripeptide containing N-terminal Phe_{F5} (H-Phe_{F5}-Gly-Gly-OH, or F′GG) with a K_a value of 6.6×10^5 M^{-1}, and the resulting Q8·H-Phe_{F5}-Gly-Gly-OH complex selectively forms heteroternary complexes with eight different tripeptides, with highest affinity for H-Trp-Gly-Gly-OH and H-Phe-Gly-Gly-OH. The electron-poor Phe_{F5} allows for complementary polar-pi interactions with the relatively electron-rich side chains of Trp, Phe, and Tyr. Shifting the aromatic amino acid away from the N-terminus led to a notable decrease in K_a of the second guest. Heterodimerization was not observed for nonaromatic peptides (H-X-Gly-Gly-OH, X = Lys, Glu, Leu). To demonstrate the utility and selectivity of heteropeptide dimers, they applied the heterodimerization technique to on-resin recognition. Resin functionalized with N-terminal Phe_{F5} showed selectivity for aromatic peptides in a mixture and ~98% recycling efficiency through multiple cycles of peptide recognition and competitive displacement.

2.4. Recognition of nonterminal Phe by cucurbit[8]uril

Scherman and coworkers investigated the binding of Q8 to peptides containing Phe at non-terminal sites.[50] They reported data on three pentapeptides derived from the $A\beta_{1-42}$ amyloid peptide of sequence H-X_1-X_2-Phe-X_3-X_4-NH_2 (–NH_2═C-terminal primary amide). Q8 bound two equivalents of peptide with K_{ter} values comparable to or greater than those observed for H-Trp-Gly-Gly-OH and H-Phe-Gly-Gly-OH.[18] The peptide H-Val-Ile-Phe-Ala-Glu-NH_2 showed a remarkably high K_{ter} value of 1.6×10^{13} M^{-2} (Table 3). These results made clear that binding at the N-terminal position may not be as important as originally believed, and that non-terminal Phe is a viable target for micromolar binding of peptides.[50]

Scherman and coworkers followed this work with a large combinatorial screen of non-terminal sites *via* a phage-display library of cyclic peptides against a surface-immobilized Q8·viologen complex (Fig. 9).[42] From the selection experiments, they reported the most repeated three heptapeptide sequences with the corresponding 3-mer motifs: cAsn-Thr-Gly-Ser-Pro-Tyr-Glu (motif -Ser-Pro-Tyr-), cGln-Asn-Pro-Asn-Gln-Lys-Phe (motif -Gln-Lys-Phe-), and cLeu-Lys-Leu-Gly-Glu-Lys-Trp (motif -Glu-Lys-Trp-). When in cyclic form, all three sequences were shown to bind Q8·MV in a 1:1 stoichiometry and with modest affinities (K_a = 4–22 $\times 10^4$ M^{-1}, Table 1), but only cGln-Asn-Pro-Asn-Gln-Lys-Phe bound Q8 when in linear form, suggesting a possible role for structural rigidity in peptide binding. The tripeptide epitope from this sequence (-Gln-Lys-Phe-) was incorporated into three different solvent-exposed loops (BC, DE, and FG) in the Tn3 domain derived from the third fibronectin type-III domain of tenascin C. The binding affinities of Q8·MV to these domains was determined by ITC (K_a = 6.4–61 $\times 10^4$ M^{-1}, Table 1), with one domain giving approximately 7-fold higher affinity than the others. Phe was confirmed as the target site by its mutation to Ala. This study showed that non-terminal Phe is a viable target in the context of a protein, and that disordered loops are viable targets for cucurbit[*n*]urils. This study also supported the finding that non-terminal Phe is preferred to Trp in a broader sequence context and when not located at the N-terminus.[42] These two studies highlight the importance of neighboring sequence context on binding affinity.

Table 3 Thermodynamic data for homoternary complexes

Host	Amino acid, peptide, or protein	K_{ter} (M^{-2})	ΔH (kcal mol^{-1})	$-T\Delta S$ (kcal mol^{-1})
Q8[a]	Tryptophan	6.9×10^7	−17.1	6.3
Q8[a]	Phenylalanine	1.1×10^8	−15.2	4.2
Q8[a]	All 18 other amino acids	nd[m]	nr[n]	nr
Q8[b]	H-**Trp**-Gly-Gly-OH	3.6×10^9	−22.8	9.7
Q8[b]	H-Gly-Trp-Gly-OH	nd	nr	nr
Q8[b]	H-Gly-Gly-Trp-OH	nd	nr	nr
Q8[b]	H-**Phe**-Gly-Gly-OH	1.5×10^{11}	−29.6	14.2
Q8[b]	H-Gly-Phe-Gly-OH	nd	nr	nr
Q8[b]	H-Gly-Gly-Phe-OH	nd	nr	nr
Q8[b]	H-Tyr-Gly-Gly-OH	nd	nr	nr
Q8[b]	H-Gly-Tyr-Gly-OH	nd	nr	nr
Q8[b]	H-Gly-Gly-Tyr-OH	nd	nr	nr
Q8[b]	H-His-Gly-Gly-OH	nd	nr	nr
Q8[b]	H-Gly-His-Gly-OH	nd	nr	nr
Q8[b]	H-Gly-Gly-His-OH	nd	nr	nr
Q8[c]	H-**Phe**-Gly-Gly-OH	2.3×10^{10}	−25.3	11.2
Q8[c]	H-**Phe**-Gly_6-OH	4.4×10^9	−23.0	9.8
Q8[d]	H-Ala-Glu-**Phe**-Arg-His-NH_2	3.0×10^{10}	−15.3	0.9
Q8[d]	H-Leu-Val-**Phe**-Ile-Ala-NH_2	7.7×10^9	−9.0	4.5
Q8[d]	H-Val-Ile-**Phe**-Ala-Glu-NH_2	1.6×10^{13}	−20.8	2.8
Q8[e]	H-**Phe**-Leu-NH_2	1.9×10^{11}	−26.7	11.3
Q8[e]	H-**Tyr**-Ala-Leu-NH_2	8.7×10^7	−18.1	7.3
Q8[f]	H-**Phe**-Gly-Gly-Gly-Cys-OH	2.3×10^{13}	−21.8	6.2
Q8[g]	H-**Phe**-Gly-Gly-OH	1.7×10^{12}	nr	nr
Q8[h]	H-**Tyr**-His-OH	2.4×10^8	nr	nr
Q8[i]	mCFP-**F**GG	2.5×10^{13}	−29.3	10.6
Q8[j]	Caspase-9-**F**GG	2.7×10^{12}	−23.7	5.3
Q8[k]	GST-**F**GG	2.9×10^{12}	−13.2	−3.8
Q8[l]	Aβ **4**–16	5.5×10^{10}	nr	nr
Q8[l]	Aβ 1–16	nd	nr	nr

[a] 10 mM sodium phosphate, pH 7.0, 300 K.[32] [b] 10 mM sodium phosphate, pH 7.0, 300 K.[18] [c] PBS: 10 mM sodium phosphate, 1.8 mM potassium phosphate, 137 mM NaCl, 2.7 mM KCl, pH 7.4, 298 K.[49] [d] 10 mM sodium phosphate, pH 7.4, 298 K.[50] [e] 10 mM sodium phosphate, pH 7.0, 298 K.[51] [f] Pure water, 298 K.[52] [g] Pure water, 298K.[53] [h] 50 mM sodium acetate, pH 4.74.[54] [i] Monomeric cyan fluorescent protein modified with N-terminal FGG, 10 mM sodium phosphate, pH 7.0, 303 K.[55] [j] Caspase-9 modified with N-terminal FGG, 10 mM sodium phosphate, pH 7.0, 303 K.[56] [k] Glutathione-*S*-transferase modified with N-terminal FGG, 20 mM sodium phosphate, 1 mM EDTA, pH 7.4, 298 K.[57] [l] 10 mM sodium phosphate, pH 7.4, 298 K.[58] [m] Not detected. [n] Not reported. Putative binding sites are in bold.

2.5. Dipeptide recognition *via* pair-inclusion within cucurbit[8]uril

We continued to be interested in exploring the effects of peptide sequence context on the binding of peptides by Q8, but our earlier work required the peptide to be intrinsically fluorescent *via* a Trp residue.[40] In collaboration with the Scherman and Bielawski groups, we replaced MV with an auxiliary guest of similar size and charge, tetramethylbenzobis(imidazolium) (MBBI, Fig. 10),[59] which is intrinsically fluorescent. The binding affinities of MBBI and MV for Q8 were shown to be essentially identical, as were the binding affinities of Q8·MBBI and Q8·MV for H-Trp-Gly-Gly-OH, H-Gly-Trp-Gly-OH, and H-Gly-Gly-Trp-OH (Table 1). Therefore, MBBI is an excellent surrogate for MV with respect to targeting Trp. The bright fluorescence of MBBI is quenched slightly in the presence of Q8, and the fluorescence of the Q8·MBBI complex is further quenched upon binding Trp-containing peptides.

As an intrinsically fluorescent component of the sensor, MBBI has the potential to respond to the binding of nonfluorescent peptides. To this end, we synthesized a series of 105 tripeptides of sequence H-Phe-Var_1-Ala-NH_2, H-Phe-Ala-Var_2-NH_2, H-Tyr-Var_1-Ala-NH_2, H-Tyr-Ala-Var_2-NH_2, H-Trp-Var_1-Ala, and H-Trp-Ala-Var_2-NH_2 (Var_1 and Var_2 = all 20 amino acids except Trp and Cys).[60] The peptides were synthesized using parallel solid-phase synthesis, and the relative extent of binding to Q8·MBBI was analyzed indirectly by comparing the relative change in MBBI fluorescence in the presence of peptide. Fluorescence intensity decreased for almost all of the Trp-containing peptides and increased for almost all of the Phe-containing peptides. We hypothesized that these results were due to the simultaneous inclusion of MBBI and Trp inside the Q8 cavity, which quenches Trp fluorescence, whereas Phe-containing peptides have the ability to dimerize with Q8 with higher overall affinity than a heteroternary complex, and therefore Phe-containing peptides are likely to displace MBBI and increase fluorescence. These hypotheses were not explored further.

The interesting results of this study were in the Tyr series (Fig. 11). We observed that fluorescence increased for certain peptides and decreased for their sequence isomers. For example, the peptide H-Tyr-Leu-Ala-NH_2 showed an increase in fluorescence, whereas the peptide H-Tyr-Ala-Leu-NH_2 showed a decrease in fluorescence. NMR studies showed that H-Tyr-Leu-Ala-NH_2 binds Q8 with slow exchange kinetics on the NMR timescale. This allowed us to conveniently determine a 1 : 1 Q8 : peptide binding stoichiometry and to observe that MBBI is fully displaced upon addition of one equivalent of peptide. This

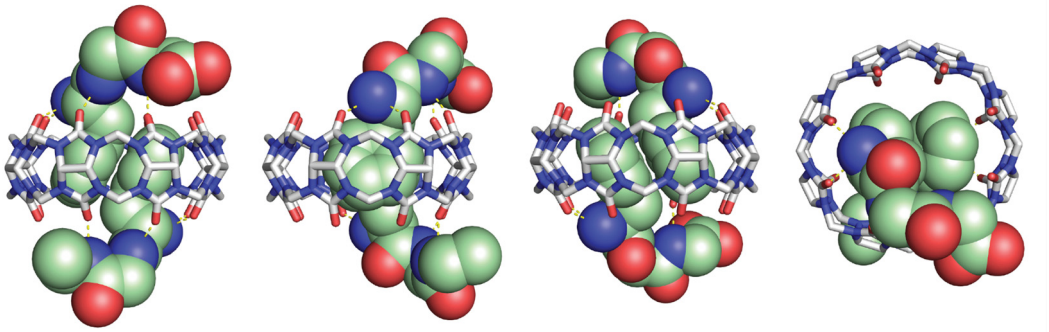

Fig. 8 Rendering of the crystal structure of the Q8·(H-Phe-Gly-Gly-OH)$_2$ complex shown from different viewing angles. The peptide is shown as space-filling, and Q8 as sticks. Peptide carbons are green. Q8 carbons are grey. Oxygens are red. Nitrogens are blue. Hydrogens are not shown. Yellow dashes show key intermolecular electrostatic interactions.[18]

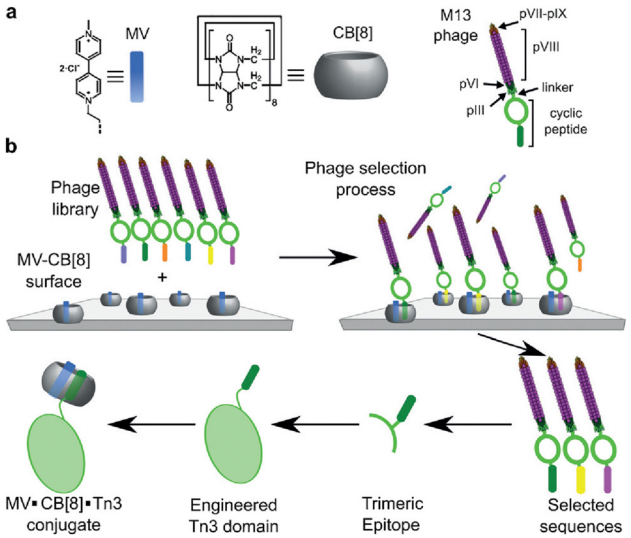

Fig. 9 Selection of non-terminal peptide binding sites by a Q8·viologen complex using phage display, followed by engineering abundant epitopes into disordered loops on the surface of a protein. CB[8] is Q8.[42] Reproduced with permission from ref. 42. © 2016 Wiley-VCH GmbH & Co. KGaA, Weinheim.

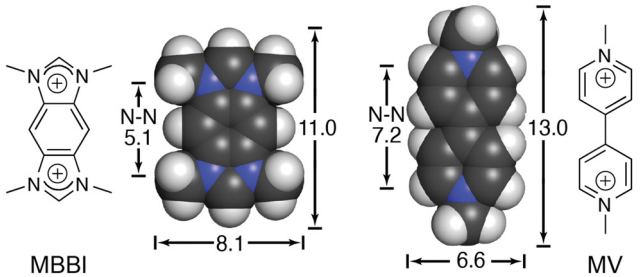

Fig. 10 Chemical formulas and space-filling models of MBBI and MV, showing size comparisons in Angstroms.[59] Reproduced with permission from ref. 59. © 2010 Wiley-VCH Verlag GmbH & Co. KGaA, Weinheim.

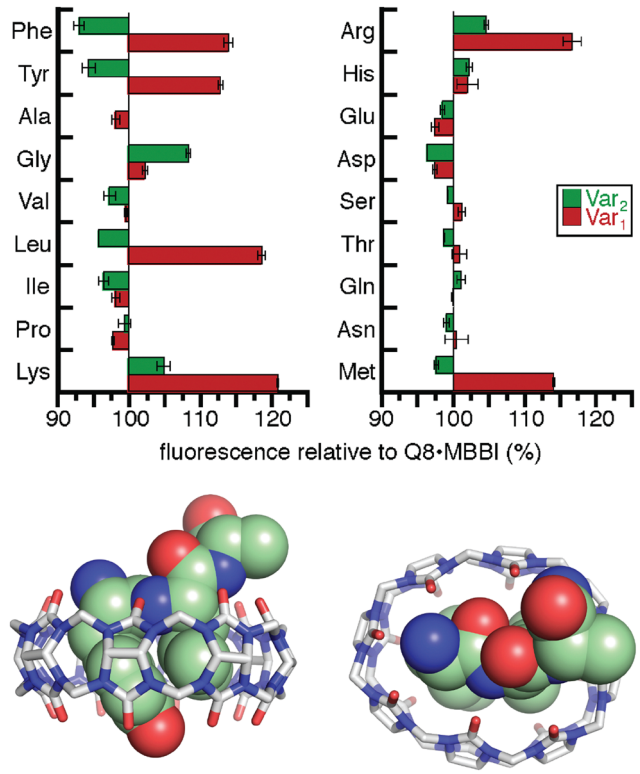

Fig. 11 (top) Relative change in fluorescence of 1 : 1 : 1 peptide : Q8 : MBBI relative to Q8·MBBI under the same condition.[60] The peptide sequences are H-Tyr-Var$_1$-Ala-NH$_2$ and H-Tyr-Ala-Var$_2$-NH$_2$. Reproduced with permission from ref. 60. Copyright 2015 American Chemical Society. (bottom) Rendering of the semiempirical NMR structure of the Q8·H-Tyr-Leu-Ala-NH$_2$ complex in two views. The peptide is shown as space-filling, and Q8 as sticks. Peptide carbons are green. Q8 carbons are grey. Oxygens are red. Nitrogens are blue. Hydrogens are not shown.

result was surprising given that prior work would predict that Q8 should homodimerize the peptides in a 2 : 1 peptide : Q8 ratio. The NMR data also revealed large upfield chemical shift perturbations of the signals corresponding to the side chains of both Tyr and Leu residues, which indicates their simultaneous inclusion within the Q8 cavity. ITC data showed a range of binding constants in the low micromolar to high nanomolar range (Table 4). A semiempirical model of the Q8·H-Tyr-Leu-

Table 4 Thermodynamic data for binary Q8·peptide complexes

Host	Peptide	K_a (M^{-1})	ΔH (kcal mol^{-1})	$-T\Delta S$ (kcal mol^{-1})
Q8[a]	H-**Tyr-Leu**-Ala-NH_2	1.4×10^8	−15.5	4.3
Q8[a]	H-**Tyr**-Ala-Leu-NH_2	2.9×10^4	−9.5	3.4
Q8[a]	H-Ala-**Tyr-Leu**-NH_2	3.2×10^5	−14.1	6.5
Q8[a]	H-**Tyr-Lys**-Ala-NH_2	5.0×10^6	−15.5	6.3
Q8[a]	H-**Tyr-Tyr**-Ala-NH_2	1.4×10^6	−16.1	7.7
Q8[a]	H-**Tyr-Phe**-Ala-NH_2	3.5×10^6	−16.1	7.2
Q8[b]	H-**Met-Phe**-Ala-NH_2	7.1×10^6	−20.1	10.6
Q8[b]	H-**Met-Tyr**-Ala-NH_2	4.0×10^6	−18.2	9.3
Q8[b]	H-**Tyr-Met**-Ala-NH_2	7.7×10^5	−16.6	8.5
Q8[b]	H-Ala-**Met-Tyr**-NH_2	1.6×10^5	−13.8	6.6
Q8[b]	H-Met-Ala-Tyr-NH_2	nd[h]	nr[i]	nr
Q8[b]	H-**Met-Leu**-Ala-NH_2	1.4×10^6	−15.8	7.4
Q8[b]	H-**Leu-Met**-Ala-NH_2	1.7×10^6	−12.1	3.5
Q8[b]	H-Ala-Met-Leu-NH_2	nd	nr	nr
Q8[b]	H-Met-Ala-Leu-NH_2	nd	nr	nr
Q8[b]	H-**Met-Lys**-Ala-NH_2	3.9×10^5	−13.7	6.0
Q8[b]	H-**Lys-Met**-Ala-NH_2	1.2×10^6	−10.9	2.6
Q8[b]	H-Ala-Met-Lys-NH_2	nd	nr	nr
Q8[b]	H-Met-Ala-Lys-NH_2	nd	nr	nr
Q8[b]	H-Met-Ala-Ala-NH_2	nd	nr	nr
Q8[b]	H-**Met-Tyr**-Gly-Gly-Tyr-NH_2	6.3×10^6	−19.4	10.1
Q8[b]	H-**Met-Leu**-Gly-Gly-Tyr-NH_2	3.3×10^6	−16.9	7.9
Q8[b]	H-**Leu-Met**-Gly-Gly-Tyr-NH_2	6.3×10^6	−22.9	13.5
Q8[b]	H-**Met-Lys**-Gly-Gly-Tyr-NH_2	2.4×10^6	−16.9	8.2
Q8[b]	H-**Met-Lys**-Ala-Gly-Tyr-NH_2	1.1×10^6	−16.9	8.3
Q8[b]	H-**Met-Lys**-Val-Gly-Tyr-NH_2	1.6×10^5	−15.9	8.8
Q8[b]	H-Met-Ile-Gly-Gly-Tyr-NH_2	nd	nr	nr
Q8[b]	H-Met-Val-Gly-Gly-Tyr-NH_2	nd	nr	nr
Q8[b]	H-**Met-Arg**-Gly-Gly-Tyr-NH_2	4.8×10^5	−12.4	4.6
Q8[b]	H-Met-Ser-Gly-Gly-Tyr-NH_2	nd	nr	nr
Q8[b]	H-Met-Gly-Gly-Gly-Tyr-NH_2	nd	nr	nr
Q8[c]	H-**Tyr-Leu**-NH_2	8.2×10^6	−13.6	4.2
Q8[c]	H-**Tyr-Leu**-Ala-NH_2	8.1×10^6	−12.0	2.6
Q8[c]	H-**Tyr**-Ala-Leu-NH_2	2.7×10^4	−6.2	0.2
Q8[c]	H-**Tyr-Leu**-Ala-Ala-NH_2	7.1×10^6	−11.0	1.7
Q8[c]	H-Ala-Ala-**Tyr-Leu**-Ala-Ala-NH_2	1.8×10^5	−11.6	4.4
Q8[c]	H-**Leu-Tyr**-NH_2	1.3×10^7	−13.7	4.0
Q8[c]	H-**Leu-Tyr**-Ala-NH_2	1.3×10^7	−12.0	2.3
Q8[c]	H-Ala-**Leu-Tyr**-NH_2	1.3×10^6	−11.7	3.4
Q8[c]	H-**Phe-Leu**-Ala-NH_2	1.0×10^7	−12.0	2.4
Q8[c]	H-Ala-**Phe-Leu**-Ala-NH_2	2.1×10^6	−11.4	2.8
Q8[c]	H-**Leu-Phe**-NH_2	6.6×10^6	−12.3	3.0
Q8[c]	H-**Phe-Leu**-NH_2	1.3×10^7	−11.4	1.7
Q8[d]	H-**Tyr-Met**-Ala-NH_2	1.0×10^6	−11.0	2.8
Q8[d]	H-**Tyr-Lys**-Ala-NH_2	3.1×10^6	−11.4	2.6
Q8[d]	H-**Tyr-Arg**-Ala-NH_2	1.6×10^6	−11.1	2.7
Q8[d]	H-**Tyr-Met**-NH_2	6.1×10^5	−12.3	4.4
Q8[d]	H-**Tyr-Lys**-NH_2	2.5×10^6	−12.7	4.0
Q8[d]	H-**Tyr-Tyr**-NH_2	8.9×10^5	−11.6	3.5
Q8[d]	H-**Met-Tyr**-NH_2	3.9×10^6	−19.2	10.2
Q8[d]	H-**Lys-Tyr**-NH_2	2.4×10^6	−11.8	3.0
Q8[e]	H-His-Phe-OH	3.3×10^3	nr	nr
Q8[e]	H-His-Leu-OH	3.3×10^3	nr	nr
Q8[e]	H-His-Tyr-OH	1.5×10^3	nr	nr
Q8[e]	H-Gly-His-OH	$< 10^2$	nr	nr
Q8[e]	H-Leu-His-OH	9.3×10^4	nr	nr
Q8[e]	H-Gly-Gly-His-OH	$< 10^2$	nr	nr
Q8[e]	H-His-Gly-Gly-OH	$< 10^2$	nr	nr
Q8[f]	H-**Lys-Phe**-Gly-Gly-Tyr-OH	3.0×10^9	−16.6	3.6
Q8[f]	H-**Phe-Lys**-Gly-Gly-Tyr-OH	3.0×10^6	−13.9	5.0
Q8[f]	H-**Leu-Tyr**-Gly-Gly-Gly-OH	8.3×10^8	−17.0	4.7
Q8[f]	H-**Tyr-Leu**-Gly-Gly-Gly-OH	6.7×10^6	−14.9	5.5
Q8[g]	H-Gly-Gly-**Phe-Lys**-Gly-Gly-Tyr-OH	1.2×10^7	−13.4	3.7
Q8[g]	H-Gly-Gly-**Lys-Phe**-Gly-Gly-Tyr-OH	1.7×10^7	−14.2	4.3
Q8[g]	H-Gly-Gly-**Phe-Phe**-Gly-Gly-Tyr-OH	9.1×10^4	−5.8	−1.1
Q8[g]	H-Gly-Gly-**Lys-Lys**-Gly-Gly-Tyr-OH	1.1×10^5	−8.7	1.8
Q8[g]	H-Gly-Gly-**Phe-Arg**-Gly-Gly-Tyr-OH	5.9×10^6	−14.3	5.0
Q8[g]	H-Gly-Gly-**Arg-Phe**-Gly-Gly-Tyr-OH	2.9×10^5	−11.9	4.4
Q8[g]	H-Gly-Gly-Arg-Arg-Gly-Gly-Tyr-OH	$< 10^3$	nd	nd
Q8[g]	H-Gly-Gly-**Trp-Lys**-Gly-Gly-Tyr-OH	6.7×10^5	−12.0	4.0

Table 4 (*continued*)

Host	Peptide	K_a (M^{-1})	ΔH (kcal mol^{-1})	$-T\Delta S$ (kcal mol^{-1})
Q8[g]	H-Gly-Gly-**Lys-Trp**-Gly-Gly-Tyr-OH	2.2×10^6	−13.0	4.3
Q8[g]	H-Gly-Gly-Trp-Trp-Gly-Gly-Tyr-OH	$< 10^3$	nd	nd
Q8[g]	H-Gly-Gly-**Tyr-Leu**-Gly-Gly-Tyr-NH_2	1.8×10^6	−14.9	6.3
Q8[g]	H-Gly-Gly-**Leu-Tyr**-Gly-Gly-Tyr-NH_2	4.4×10^6	−14.9	5.8
Q8[g]	H-Gly-Gly-Tyr-Tyr-Gly-Gly-Tyr-NH_2	$< 10^3$	nd	nd
Q8[g]	H-Gly-Gly-Leu-Leu-Gly-Gly-Tyr-NH_2	5.6×10^4	−13.6	7.1
Q8[g]	H-Gly-Ala-**Lys-Phe**-Ala-Gly-Tyr-NH_2	1.1×10^6	−12.0	3.7
Q8[g]	H-Gly-Ala-**Phe-Lys**-Ala-Gly-Tyr-NH_2	3.6×10^6	−11.3	5.1
Q8[g]	H-Gly-Ala-**Phe-Lys**-Gly-Gly-Tyr-NH_2	1.0×10^5	−10.8	4.0
Q8[g]	H-Gly-Gly-**Phe-Lys**-Ala-Gly-Tyr-NH_2	2.3×10^5	−9.0	1.6

[a] 10 mM sodium phosphate, pH 7.0, 300 K.[60] [b] 10 mM sodium phosphate, pH 7.0, 300 K.[61] [c] 10 mM sodium phosphate, pH 7.0, 298 K.[51] [d] 10 mM sodium phosphate, pH 7.0, 298 K.[62] [e] 50 mM sodium acetate, pH 4.74, 298 K.[54] [f] 10 mM sodium phosphate, pH 7.0, 300 K.[63] [g] 10 mM sodium phosphate, pH 7.0.[64] [h] Not detected. [i] Not reported. Putative binding sites are in bold.

Ala-NH_2 complex from NMR-derived distance restraints (Fig. 11) is consistent with a binding mode in which the peptide backbone folds to allow the side chains of Tyr and Leu to bind within the Q8 cavity. Therefore, we termed this binding mechanism the "pair-inclusion motif." These results showed that Q8 can bind certain dipeptide sites with high affinity, and that the sequence and location of the binding site can have a strong influence on binding affinity. This study also demonstrated the value of MBBI as a critical component of a turn-on peptide sensor.[60]

Excited by the discovery that Q8 can bind peptides *via* inclusion of the side chains of neighboring residues, we considered that the additional complexity of a dipeptide binding site should allow us to identify other possible sequences that bind Q8 with high affinity. The additional binding interface enabled by pair-inclusion should allow inclusion of non-aromatic residues. To this end, we synthesized and screened a series of 144 peptides of sequence H-Var_1-Var_2-Ala-NH_2 (Var_1 = Tyr, Phe, Ile, Leu, Met, Pro, Arg, Lys, and Var_2 = all 20 amino acids except Trp and Cys).[61] The peptides were synthesized using parallel solid-phase synthesis, and the relative extent of binding to Q8·MBBI was analyzed indirectly by comparing the relative change in the fluorescence of Q8·MBBI in the presence *vs.* absence of peptide. The patterns of fluorescence suggested that certain peptides with N-terminal Met bind tightly to Q8. A detailed structure–activity investigation by ITC and NMR yielded several determinants for sub-micromolar binding *via* the pair-inclusion motif (Fig. 12) (Table 4). Specifically, when the first residue is Met, then the second residue should be Leu, Tyr, Phe, Lys, or Arg; the first two resides can be reversed in sequence; and the third residue should be Gly or Ala. Therefore, the pair-inclusion motif allowed for targeting N-terminal Met, which is found in all newly translated eukaryotic proteins, as well as entirely nonaromatic binding sites.[61]

Scherman and coworkers were also motivated by the 2015 discovery of pair-inclusion binding[60] and considered that the proposed mechanism may be inaccurate and that our results could potentially be explained by the formation of 2:2 (Q8:peptide) complexes.[51] Using a combination of binding enthalpy and entropy data determined by ITC, ^{1}H NMR chemical shift

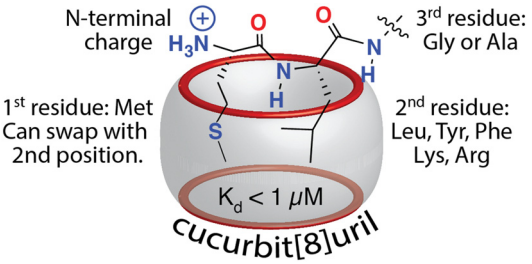

Fig. 12 Sequence determinants for high-affinity binding of N-terminal dipeptide sites by Q8.[61] Reproduced with permission from ref. 61. Copyright 2018 American Chemical Society.

perturbation (Fig. 13), and diffusion constants determined by diffusion ordered NMR spectroscopy (DOSY), they identified patterns that correlate to 1:1, 2:1, and 2:2 guest:Q8 complexes[65] and applied this approach to the study of Q8·peptide complexes in the pair-inclusion motif.[51] The data unambiguously corroborated our conclusions on the

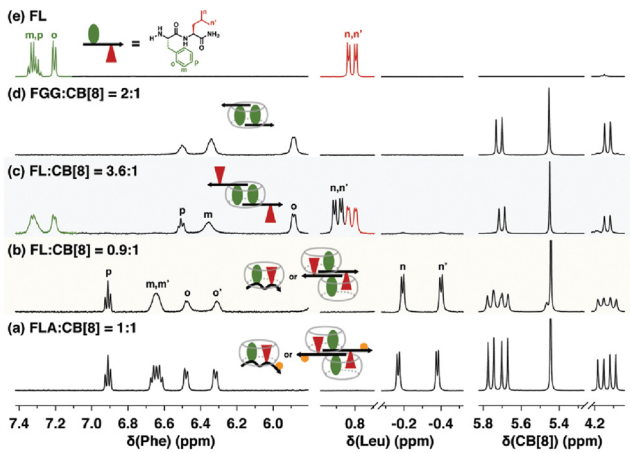

Fig. 13 ^{1}H NMR spectra of H-Phe-Leu-Ala-NH_2 (FLA) and H-Phe-Leu-NH_2 (FL) at various ratios with Q8, showing patterns of signal perturbation that indicate the binding modes shown schematically. CB[8] is Q8.[51] Reproduced from ref. 51 with permission from the Royal Society of Chemistry.

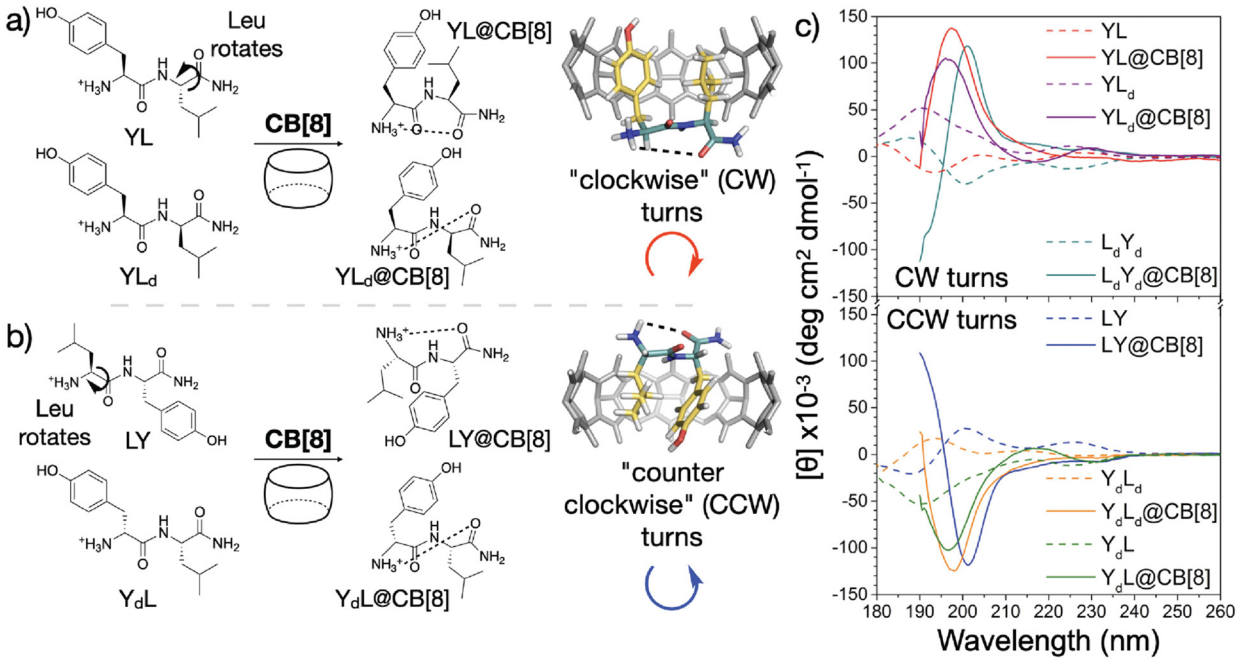

Fig. 14 Model for sequence-dependent folding of peptides by Q8 as monitored by circular dichroism spectroscopy (right). CB[8] is Q8.[62] Reproduced with permission from ref. 62. Copyright 2021 American Chemical Society.

mechanism of pair-inclusion complexation, including that the binding stoichiometry is 1 : 1 peptide : Q8, not 2 : 2, and that the side chains of two neighboring residues in a single peptide molecule include simultaneously within the cavity of a single Q8 molecule.

Recently, Scherman and coworkers investigated the nature of peptide folding induced by Q8 in the pair-inclusion motif.[62] A series of dipeptides known to bind Q8 *via* pair-inclusion was investigated by circular dichroism (CD) spectroscopy, and the CD spectra effectively invert depending on the stereochemistry of the peptide. They proposed a model of "clockwise" or "counterclockwise" folding in order to insert both neighboring side chains into the Q8 cavity (Fig. 14). This concept was used to design a peptide with a central dipeptide binding site that bends upon treatment with Q8, as observed by fluorescence resonance energy transfer.

Recently we reported an investigation of Q8 binding at nonterminal sites *via* the pair-inclusion motif.[64] A library of 64 peptides of sequence H-Gly-X_1-X_2-Gly-NH_2 (X = Phe, Leu, Lys, Met, Arg, Tyr, Trp, Pro) was synthesized in parallel and screened by fluorescence for binding to the Q8·MBBI complex (Fig. 15). Relatively high increases in fluorescence were observed for X_1-X_2 sequences Tyr-Leu, Leu-Tyr, Phe-Leu, Leu-Phe, Tyr-Lys, Lys-Tyr, Phe-Arg, Arg–Phe, Leu-Lys, Lys-Leu, Phe-Lys, Lys-Phe, and Phe-Met. The strongest increase was observed for Phe-Lys. Detailed studies of binding to purified heptapeptides of sequence H-Gly-Gly-X_1-X_2-Gly-Gly-Tyr-OH using ITC and NMR revealed the highest affinities for X_1-X_2 = Lys-Phe (1.7×10^7 M^{-1}) and Phe-Lys (1.2×10^7 M^{-1}). Several other submicromolar complexes were identified (Table 4). A study of the effects of the neighboring sequence revealed that while Gly to

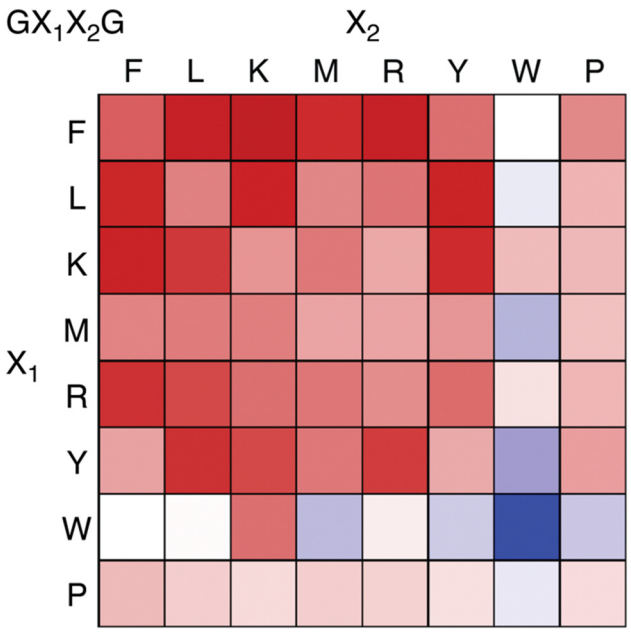

Fig. 15 Fluorescence assay heat map, showing the change in fluorescence of the Q8·MBBI complex upon addition of peptide.[64] Color saturation correlates to the extent of change in fluorescence, with red indicating an increase in fluorescence, and blue indicating a decrease. Reproduced with permission from ref. 64. Copyright 2024 American Chemical Society.

Ala mutations flanking the Lys-Phe site had only a modest decrease in affinity, the same mutations flanking the Phe-Lys site led to a loss of almost three orders of magnitude in affinity. In all cases where affinity was observable, the binding stoichiometry was 1 : 1 peptide : Q8, and NMR studies show

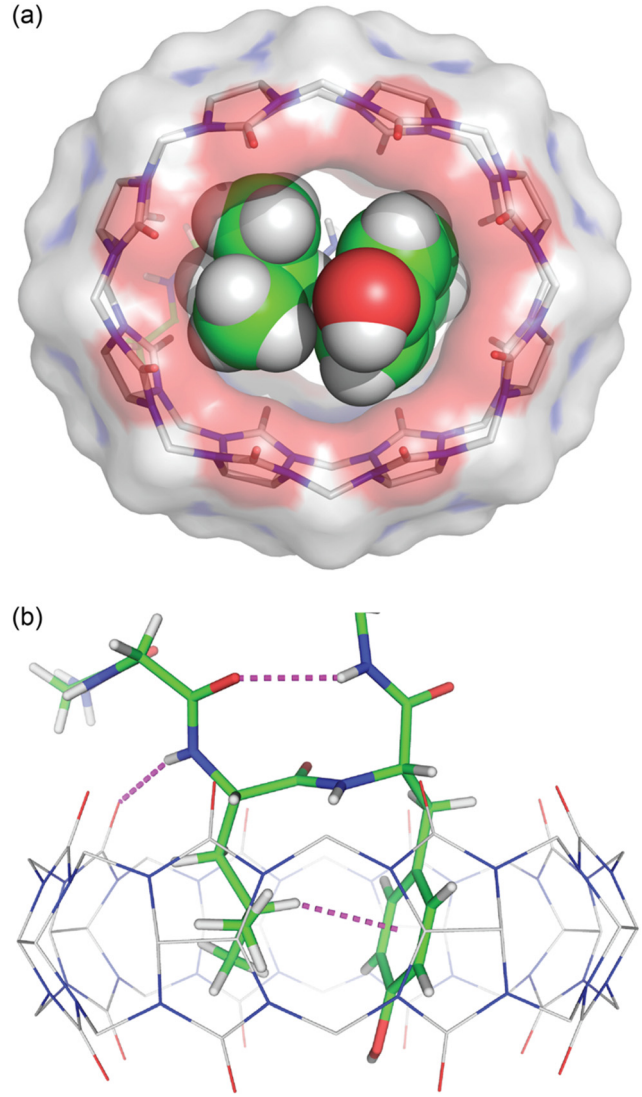

Fig. 16 Crystal structure of the Q8·H-Gly-Gly-Leu-Tyr-Gly-Gly-Gly-OH complex.[64] (top) Rendering that illustrates the inclusion of the Leu and Tyr side chains (space-filling models) within the cavity of Q8 (sticks with a solvent-accessible surface), and the deformation of Q8 from D_{8h} symmetry upon binding. (bottom) Rendering that illustrates the Q8-induced β-hairpin turn, with the Gly_5 NH···Leu_3 O═C hydrogen bond, Leu_3 NH···Q8 hydrogen bond, and Leu_3-Tyr_4 CH···π interaction shown as dashed lines. CCDC ID 2312293. Reproduced with permission from ref. 64. Copyright 2024 American Chemical Society.

simultaneous inclusion of both side chains at the target dipeptide site.[64]

We obtained a crystal structure of the Q8·H-Gly-Gly-Leu-Tyr-Gly-Gly-Gly-OH complex at 0.79 Å resolution.[64] The structure confirmed unambiguously our proposed model for the pair-inclusion motif,[60] with the side chains of Leu and Tyr bound within the cavity of Q8 and complementary electrostatic interactions between peptide and Q8. The unanticipated result of this study is the observation that four contiguous residues, Gly-Leu-Tyr-Gly, form a type II β-turn in which the amide NH of Gly_5 forms an intramolecular hydrogen bond with the carbonyl oxygen of Gly_2 (Fig. 16).

In a subsequent study, we investigated the binding of Q8 to peptides containing the lead Lys-Phe and Phe-Lys dipeptide sites located at the N-terminus.[63] It was found that Q8 binds with extraordinarily high affinity to H-Lys-Phe-Gly-Gly-Tyr-OH (3.0×10^9 M^{-1}) and H-Leu-Tyr-Gly-Gly-Gly-OH (8.3×10^8 M^{-1}) and with 1000-fold and 120-fold selectivity over their sequence isomers H-Phe-Lys-Gly-Gly-Tyr-OH (3.0×10^6 M^{-1}) and H-Tyr-Leu-Gly-Gly-Gly-OH (6.7×10^6 M^{-1}), respectively. We obtained sub-Å resolution crystal structures of the complexes of Q8 with sequence isomers, Q8·H-Leu-Tyr-Gly-Gly-Gly-OH and Q8·H-Tyr-Leu-Gly-Gly-Gly-OH (Fig. 17). These structures correlated well with the structure of Q8 bound at a non-terminal Leu-Tyr site (*vide supra*) and revealed a few differences that may explain the observed sequence-selectivity. In particular, the side chain of the N-terminal Tyr in Q8·H-Tyr-Leu-Gly-Gly-Gly-OH buries more deeply than that of the non-terminal Tyr in Q8·H-Leu-Tyr-Gly-Gly-Gly-OH, allowing contact between the N-terminal ammonium group and proximal Q8 C═O groups. In the Q8·H-Tyr-Leu-Gly-Gly-Gly-OH complex, this effect pushes the Tyr side chain so deeply that its hydroxyl group resides outside of the Q8 portal and needs a water molecule to mediate its electrostatic

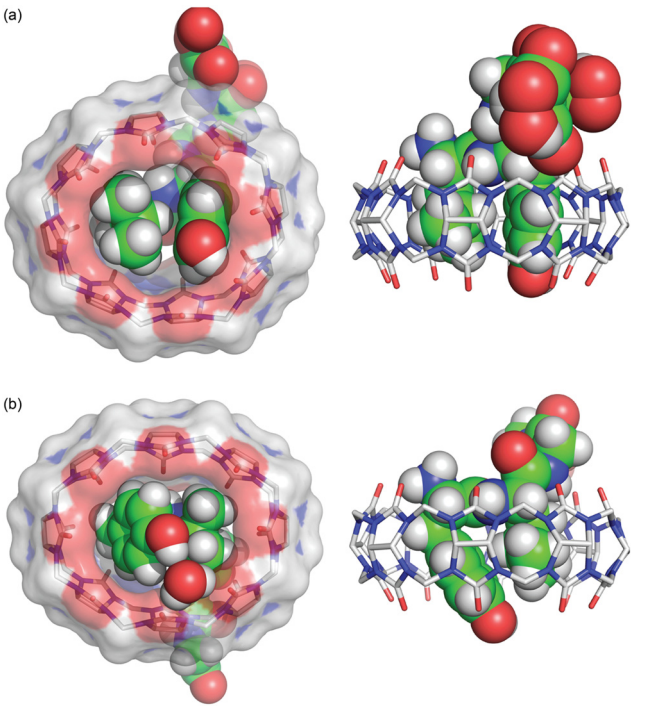

Fig. 17 Crystal structure of the isomeric complexes (top) Q8·H-Leu-Tyr-Gly-Gly-Gly-OH and (bottom) Q8· H-Tyr-Leu-Gly-Gly-Gly-OH.[63] (left) Rendering that illustrates the inclusion of the Leu and Tyr side chains (space-filling models) within the cavity of Q8 (sticks with a solvent-accessible surface), the relative deformation of Q8 from D_{8h} symmetry upon binding, and the interaction of the Tyr hydroxyl group with a Q8 O═C group either directly (Q8·H-Leu-Tyr-Gly-Gly-Gly-OH) or *via* an ordered water molecule (Q8·H-Tyr-Leu-Gly-Gly-Gly). (right) Rendering that illustrates the relative depth of the peptide within the Q8 cavity and the corresponding alignment of electrostatically complementary groups. CCDC ID 2313004 and 2314758. Reproduced from ref. 63 with permission from the Royal Society of Chemistry.

contact with the Q8 portal. In the Q8·H-Leu-Tyr-Gly-Gly-Gly-OH complex, however, the Tyr hydroxyl group is positioned to form a direct hydrogen bond with Q8.[63]

2.6. Aromatic peptide recognition by cucurbit[7]uril

Q7 has a smaller cavity than Q8 and can only accommodate the side chain of one aromatic residue. Kim, Inoue and coworkers first reported the high-affinity and selective binding of peptides by Q7 in 2006.[66] They reported a K_a value of 1.4×10^7 M^{-1} for H-Phe-Leu-NH_2 in 0.1 M NaCl with 2.6-fold selectivity over H-Phe-Phe-NH_2 18-fold selectivity over H-Phe-Ala-NH_2, and 480-fold selectivity over H-Phe-Pro-NH_2 (Table 5). The decrease in affinity for a Pro residue at the second position is likely due to limited conformational freedom and steric interactions, but it remains unclear to us why Leu at the second position significantly increases affinity. Diastereomeric sequences (*e.g.*, H-Phe-D-Ala-OH) were compared, and Q7 bound with modest 2–10-fold diastereoselectivity, sometimes favoring the native sequence and sometimes favoring the diastereomer. This study demonstrated that N-terminal Phe is also a high-affinity site for Q7, and that the identity of the second residue can significantly influence binding affinity.[66]

Kim, Inoue, and coworkers followed this work with a study of Q7 binding to dipeptides containing Phe, Tyr, or Trp residues.[67] In pure water, Q7 was reported to bind H-Phe-Gly-OH with a K_a value of 3.0×10^7 M^{-1}, with 8-fold selectivity over H-Tyr-Gly-OH and with 54-fold selectivity over H-Trp-Gly-OH (Table 5). This finding was analogous to the selectivity of Q8 for N-terminal Phe *versus* N-terminal Trp,[18] and it showed that Q7 binds well to N-terminal Tyr, whereas Q8 does not bind measurably to H-Tyr-Gly-Gly-OH. NMR spectra showed the selective upfield perturbation of aromatic signals upon binding of H-Phe-Gly-OH or H-Tyr-Lys-OH to Q7, which corroborated Q7 binding at the N-terminal Phe or Tyr, respectively. Q7 was shown to bind H-Phe-Gly-OH with 23 000-fold selectivity over its sequence isomer, H-Gly-Phe-OH. Similarly, N-terminal Tyr and N-terminal Trp were preferred over their sequence isomers by 18 000-fold and 2000-fold, respectively.[67] This degree of sequence-selectivity is truly remarkable. The thermodynamic data presented in the supporting information for that paper showed that substituting Gly with Ala does not significantly influence binding affinity.[62] This is important because although Gly is the simplest amino acid residue, Ala has a β carbon and is therefore more representative of the other amino acids. These data also showed that the observed binding affinity is reduced by ~20-fold for H-Phe-Gly-OH and H-Phe-Ala-OH in the presence of 0.1 M NaCl. This result is consistent with the competition of Na^+ for binding at the Q7 portals. Q7 binds Na^+ with a K_a value of 2600 M^{-1},[74] and a simple competition model (Q7·Na^+ + peptide → Q7·peptide + Na^+) would predict a reduction of 258-fold in binding affinity at this concentration. Therefore, these data suggest that Na^+ does not fully compete with organic guests for binding to cucurbit[*n*]urils. This assertion would be consistent with the availability of multiple sites and binding geometries for metal cations at the C═O portals, and this discrepancy signifies a fundamental complication in the analysis of all Q*n* binding data determined under different experimental conditions.

In the time since this study, there have been many binding constants reported for Q7 in complex with aromatic peptides,[44,68,71,73,75] and there is general agreement in the trends observed (Table 5). One point of interest is the comparison of Q7 binding to H-Phe-Gly-Gly-NH_2 *versus* H-Gly-Phe-Gly-NH_2,[69] in which the binding site has moved to the center of a peptide *versus* a terminal position. In this case, the selectivity for the N-terminal *versus* non-terminal position is only 14-fold. This result is in contrast to the 84-fold selectivity of Q7 for H-Phe-Gly-NH_2 *versus* Gly-Phe-NH_2 and the 23 000-fold selectivity of H-Phe-Gly-OH *versus* H-Gly-Phe-OH.[67] The differences between these data sets suggest that the continuing peptide chain is involved in complexation and works to mitigate sequence-selectivity. This is a minor caution against the use of dipeptides to model the behavior of longer peptides or proteins.

In a pair of molecular dynamics computational studies, Li and coworkers predicted that Q7 should bind best to an aromatic residue at the N-terminus, and that placing a basic residue at the third position of the H-X-Gly-Z-OH tripeptide (X = Phe, Tyr, Trp; Z = His, Lys, Arg) should significantly increase binding affinity due to interaction of the basic side chain with the portal C═O groups of Q7.[76,77] Although there are not yet experimental studies to verify these predictions, they are interesting to consider.

2.7. Molecular recognition of insulin by cucurbit[7]uril

It was clear that cucurbit[*n*]urils could bind strongly and selectively to N-terminal aromatic sites on peptides, but it was not clear early on whether this binding would translate to folded proteins. In contrast to peptides, the folded structures of proteins have limited solvent accessibility and constrained conformational mobility, which are of particular concern when a ligand needs to fully encapsulate a portion of the protein. This translation from peptide to protein would validate the use of Q*n*-mediated peptide recognition as affinity tags for proteins. Brunsveld and coworkers genetically engineered proteins to contain the Phe-Gly-Gly (*i.e.*, FGG) sequence at the N-terminus and showed that this modification did not significantly influence the binding affinity to Q8, as discussed in detail below (Table 3).[78] This study was the first to demonstrate the use of Q*n*–peptide interactions as protein affinity tags.

In parallel with these studies, we were also learning that Q7 can bind to a native protein containing an N-terminal Phe residue.[68] Human insulin comprises a 21-mer A-chain and 30-mer B-chain linked covalently *via* two disulfide bonds. We reported a structure and activity study showing that Q7 binds site-selectively to the Phe residue at the N-terminus of the B-chain (*i.e.*, Phe^{B1}).[68] ITC data showed that Q7 binds regular human insulin in 10 mM sodium phosphate, pH 7.0, with a K_a value of 1.5×10^6 M^{-1} and with more than 10 000-fold selectivity *versus* a Glu^{B1}, Glu^{B27} mutant ($K_a < 100$ M^{-1}) (Table 6). The similarity in Q7 binding affinity for insulin *versus*

Table 5 Thermodynamic data for binary Q7·peptide complexes

Host	Peptide	K_a (M^{-1})	ΔH (kcal mol^{-1})	-TΔS (kcal mol^{-1})
Q7[a]	H-**Phe**-Ala-OH	7.9×10^5	−7.3	−0.7
Q7[a]	H-**dPhe**-Ala-OH	1.3×10^6	−7.8	−0.6
Q7[a]	H-**Phe**-Pro-OH	2.9×10^4	−5.9	−0.2
Q7[a]	H-**Phe**-dPro-OH	5.0×10^4	−6.5	0.1
Q7[a]	H-**Phe**-Phe- NH_2	5.3×10^6	−8.8	−0.4
Q7[a]	H-**dPhe**-Phe- NH_2	1.3×10^6	−6.9	−1.4
Q7[a]	H-**Phe**-Leu-NH_2	1.4×10^7	−8.7	−1.1
Q7[a]	H-**Phe**-dLeu-NH_2	1.7×10^6	−5.8	−2.7
Q7[b]	H-**Phe**-Gly-OH	3.0×10^7	−11.3	1.1
Q7[b]	H-Gly-**Phe**-OH	1.3×10^3	−7.2	2.9
Q7[b]	H-**Tyr**-Gly-OH	3.6×10^6	−10.6	1.6
Q7[b]	H-Gly-**Tyr**-OH	2.0×10^2	−5.5	2.4
Q7[b]	H-**Trp**-Gly-OH	5.6×10^5	−10.7	2.8
Q7[b]	H-Gly-**Trp**-OH	2.8×10^2	−4.3	1.0
Q7[b]	H-**Phe**-Ala-OH	1.9×10^7	−11.8	1.9
Q7[b]	H-Ala-**Phe**-OH	1.3×10^3	−8.3	4.0
Q7[c]	H-**Phe**-Gly-OH	1.7×10^6	−7.7	−0.9
Q7[c]	H-**Phe**-Ala-OH	7.9×10^5	−7.3	−0.7
Q7[c]	H-**Phe**-Gly-NH_2	3.7×10^6	−7.4	−1.6
Q7[c]	H-Gly-**Phe**-NH_2	4.4×10^4	−7.3	1.0
Q7[c]	H-**Phe**-Ala-NH_2	8.1×10^6	−9.9	0.5
Q7[c]	H-Ala-**Phe**-NH_2	4.5×10^4	−7.7	1.4
Q7[c]	H-**Tyr**-Gly-NH_2	1.1×10^7	−10.2	0.6
Q7[c]	H-Gly-**Tyr**-NH_2	7.5×10^4	−9.4	2.7
Q7[d]	H-**Phe**-Gly-Gly-OH	2.8×10^6	−17.5	8.7
Q7[d]	H-Gly-**Phe**-Gly-OH	2.2×10^4	−9.3	3.3
Q7[d]	H-Gly-**Tyr**-Gly-OH	2.7×10^3	−2.2	−2.5
Q7[e]	H-**Phe**-Gly-Gly-NH_2	3.2×10^6	−13.4	4.4
Q7[e]	H-Gly-**Phe**-Gly-NH_2	2.3×10^5	−9.8	2.4
Q7[e]	H-***t*BuPhe**-Gly-Gly-NH_2	4.8×10^6	−16.2	7.1
Q7[e]	H-**AmPhe**-Gly-Gly-NH_2	1.1×10^9	−14.2	1.8
Q7[e]	H-Gly-**AmPhe**-Gly-NH_2	2.0×10^6	−8.2	−0.5
Q7[f]	H-**AmPhe**-Gly-Asn-Gln-NH_2	2.0×10^7	−16.9	6.8
Q7[f]	H-**Phe**-Gly-Asn-Gln-NH_2	7.1×10^6	−15.6	6.1
Q7[f]	H-**AmPhe**-Val-Asn-Gln-NH_2	1.3×10^7	−15.7	6.0
Q7[f]	H-**Phe**-Val-Asn-Gln-NH_2	4.0×10^6	−14.5	5.3
Q7[g]	H-**Phe**-Gly-Gly-Gly-Cys	1.2×10^7	−13.8	4.15
Q7[h]	H-Thr-Gly-Ala-**Phe**-Met-NH_2	1.3×10^4	nr[n]	nr
Q7[h]	H-Thr-Gly-dAla-**Phe**-Met-NH_2	2.6×10^4	nr	nr
Q7[h]	H-Thr-Gly-Ala-**Phe**-Leu-NH_2	3.5×10^3	nr	nr
Q7[h]	H-Thr-Gly-Ser-**Phe**-Met-NH_2	1.9×10^4	nr	nr
Q7[h]	H-Thr-Gly-Gly-**Phe**-Met-NH_2	1.4×10^4	nr	nr
Q7[h]	H-Thr-Gly-Ala-**Phe**-Leu-OH	1.8×10^3	nr	nr
Q7[h]	H-**Phe**-Met-NH_2	1.5×10^7	nr	nr
Q7[h]	H-**Phe**-Leu-NH_2	2.7×10^7	nr	nr
Q7[h]	H-**Phe**-Leu-OH	2.1×10^6	nr	nr
Q7[i]	H-Thr-Gly-Ala-**Phe**-Met-NH_2	3.2×10^3	nr	nr
Q7[i]	H-Thr-Gly-Ala-**Phe**-Leu-NH_2	1.4×10^4	nr	nr
Q7[i]	H-Thr-Gly-Ala-**Phe**-Leu-OH	2.4×10^3	nr	nr
Q7[i]	H-**Phe**-Met-NH_2	2.6×10^7	nr	nr
Q7[i]	H-**Phe**-Leu-NH_2	1.4×10^7	nr	nr
Q7[i]	H-**Phe**-Leu-OH	2.1×10^6	nr	nr
Q7[j]	H-**Phe**-Met-NH_2	1.4×10^7	−22.7	12.9
Q7[j]	H-**Tyr**-Met-NH_2	6.4×10^5	−20.0	12.1
Q7[j]	H-**Trp**-Met-Gly-NH_2	2.3×10^5	−20.1	12.7
Q7[j]	H-**AmPhe**-Met-NH_2	5.3×10^8	−10.5	−1.8
Q7[k]	H-His-Phe-OH	5.0×10^2	nr	nr
Q7[k]	H-His-Leu-OH	5.0×10^2	nr	nr
Q7[k]	H-His-Tyr-OH	1.1×10^2	nr	nr
Q7[k]	H-Gly-His-OH	3.3×10^2	nr	nr
Q7[k]	H-Leu-His-OH	2.2×10^4	nr	nr
Q7[k]	H-**Tyr**-His-OH	1.2×10^5	nr	nr
Q7[k]	H-Gly-Gly-His-OH	$<10^2$	nr	nr
Q7[l]	H-Pro-Leu-Ile-Tyr-Leu-Arg-Leu-Leu-Arg-Gly-Gln-Phe-OH	nd[m]	nr	nr
Q7[l]	H-Arg_7-OH	nd	nr	nr
Q7[l]	H-Leu-Arg-Arg-Trp-Ser-Leu-Gly-OH	nd	nr	nr
Q7[l]	H-Leu-Arg-Arg-Trp-pSer-Leu-Gly-OH	nd	nr	nr
Q7[l]	H-**Trp**-Lys-Arg-Thr-Leu-Arg-Arg-Leu-OH	4.1×10^4	nr	nr

Table 5 (*continued*)

Host	Peptide	K_a (M^{-1})	ΔH (kcal mol^{-1})	-TΔS (kcal mol^{-1})
Q7[l]	H-**Trp**-Lys-Arg-pThr-Leu-Arg-Arg-Leu-OH	4.1×10^4	nr	nr
Q7[l]	H-**Phe**-Arg_7-OH	2.9×10^7	nr	nr

[a] 0.1 M NaCl, 298 K, dPhe is the D-isomer.[66] [b] Pure water, 298 K.[67] [c] 0.1 M NaCl, 298 K.[67] [d] 10 mM sodium phosphate, pH 7.0, 300 K.[68] [e] 10 mM sodium phosphate, pH 7.0, 300 K, *t*BuPhe is 4-*tert*-butylphenylalanine, AmPhe is 4-aminomethylphenylalanine.[69] [f] 10 mM sodium phosphate, pH 7.0, 300 K.[70] [g] Pure water, 298 K.[52] [h] 10 mM ammonium phosphate, pH 7.2, 310 K.[71] [i] 10 mM sodium phosphate, pH 7.0, 298 K.[72] [j] 10 mM ammonium phosphate, pH 7.2, 300 K.[73] [k] 50 mM sodium phosphate, pH 4.74, 298 K.[54] [l] 10 mM ammonium phosphate, pH 7.0, temperature not reported, pSer is phosphoserine, pThr is phosphothreonine.[44] [m] Not detected. [n] Not reported. Putative binding sites are in bold.

Table 6 Thermodynamic data for binary Q7·protein complexes

Host	protein	K_a (M^{-1})	Δ*H* (kcal mol^{-1})	$-T\Delta S$ (kcal mol^{-1})
Q7[a]	Human insulin	1.5×10^6	−10.8	2.3
Q7[a]	Human insulin Phe^{B1}Glu Thr^{B27}Glu	nd[l]	nr[m]	nr
Q7[b]	Human growth hormone	5.9×10^5	nr	nr
Q7[c]	Glutathione-*S*-transferase	nd	nr	nr
Q7[c]	Glutathione-*S*-transferase Gln207*t*BuPhe	2.3×10^5	nr	nr
Q7[c]	Glutathione-*S*-transferase Arg108*t*BuPhe	4.1×10^4	nr	nr
Q7[d]	Human insulin	4.4×10^6	nr	nr
Q7[e]	Human insulin	3.8×10^7	nr	nr
Q7[e]	Human insulin B1–13	1.1×10^6	nr	nr
Q7[e]	Human insulin B1–13 Phe^{B1}Ala	1.7×10^4	nr	nr
Q7[e]	Human insulin B14–30	5.4×10^3	nr	nr
Q7[e]	Human insulin B14–30 Phe^{B24}Ala	5.5×10^3	nr	nr
Q7[e]	Human insulin B14–30 Phe^{B25}Ala	7.9×10^4	nr	nr
Q7[e]	Human insulin B14–30 Phe^{B24}Ala Phe^{B25}Ala	6.6×10^3	nr	nr
Q7[f]	Human insulin Phe^{B1}AmPhe	1.0×10^7	−10.8	2.3
Q7[g]	Human insulin	2.3×10^6	nr	nr
Q7[g]	Human insulin Phe^{B1}Ala N-terminal benzoic acid	1.1×10^4	nr	nr
Q7[g]	human insulin Phe^{B1}Ala N-terminal phenylacetic acid	8.2×10^4	nr	nr
Q7[g]	Human insulin	2.8×10^6	nr	nr
Q7[g]	Human insulin Phe^{B1}Ala N-terminal benzoic acid	$<10^3$	nr	nr
Q7[g]	Human insulin Phe^{B1}Ala N-terminal phenylacetic acid	$<10^3$	nr	nr
Q7[h]	Human insulin Pro28Asp	1.9×10^6	nr	nr
Q7[h]	Pramlintide	2.6×10^4	nr	nr
Q7[i]	Aβ 1–40	7.1×10^4	nr	nr
Q7[i]	Aβ 1–40 Phe4Ala	5.2×10^4	nr	nr
Q7[i]	Aβ 1–40 Phe19Ala	5.1×10^4	nr	nr
Q7[i]	Aβ 1–40 Phe20Ala	5.1×10^4	nr	nr
Q7[i]	Aβ 1–40 Phe4Ala Phe19Ala Phe20Ala	6.8×10^3	nr	nr
Q7[i]	Aβ 1–42	2.9×10^4	nr	nr
Q7[j]	Aβ 4–16	1.1×10^6	nr	nr
Q7[j]	Aβ 1–16	1.0×10^4	nr	nr
Q7[k]	Human calcitonin	6.7×10^4	nr	nr
Q7[k]	Human calcitonin Tyr12Ala	2.6×10^4	nr	nr
Q7[k]	Human calcitonin Phe16Ala	2.0×10^4	nr	nr
Q7[k]	Human calcitonin Phe19Ala	2.7×10^4	nr	nr
Q7[k]	Human calcitonin Phe22Ala	3.2×10^4	nr	nr
Q7[k]	Human calcitonin Tyr12Ala Phe16Ala Phe19Ala Phe22Ala	nd	nr	nr

[a] 10 mM sodium phosphate, pH 7.0, 300 K.[68] [b] 10 mM sodium phosphate, pH 7.0, 298 K.[79] [c] PBS: 10 mM sodium phosphate, 1.8 mM potassium phosphate, 137 mM NaCl, 2.7 mM KCl, pH 7.4, 298 K.[75] [d] 20 mM PBS, 298 K.[80] [e] 0.1% formic acid, pH 2.7, 298 K.[81] [f] 10 mM sodium phosphate, pH 7.0, 300 K.[70] [g] 10 mM sodium phosphate, pH 3.5, 300 K.[80] [h] Pure water.[81] [i] 20 mM PBS, 298 K.[82] [j] 20 mM sodium phosphate, 150 mM NaCl pH 7.0, 298 K.[58] [k] 20 mM PBS, 298 K.[83] [l] Not detected. [m] Not reported.

H-Phe-Gly-Gly-OH (2.8×10^6 M^{-1}) also supported the translation of peptide recognition to protein recognition. In essence, human insulin has a built-in affinity tag for Q7. The submicromolar affinity of this complex, however, would be insufficient to bind effectively at the picomolar to nanomolar physiological concentrations of insulin.

An interesting observation of this study involves one disparity between peptide and protein binding. Q7 binds weakly to non-terminal Phe and Tyr residues in the context of small peptides, H-Gly-Phe-Gly-OH and H-Gly-Tyr-Gly-OH, with K_a values of 2.2×10^4 M^{-1} and 2.7×10^3 M^{-1}, respectively. However, Q7 binding was not measurable to the Glu^{B1}, Glu^{B27} mutant, which has two surface-exposed, non-terminal Phe residues and four surface-exposed, non-terminal Tyr residues.[68] This disparity is perhaps due to the neighboring sequence context or, more likely, to the difference in the

accessibility of the side chain of a target site to encapsulation by Q7 when located on a peptide *versus* on the surface of a folded protein. A high-resolution crystal structure of the Q7·insulin complex shed some light on this issue.[68] The asymmetric unit comprised two molecules of insulin, one of which is bound to one molecule of Q7 at the Phe^{B1} position (Fig. 18). The aromatic side chain of Phe^{B1} is buried within the Q7 cavity, and the N-terminal ammonium group is proximal to Q7 C=O groups, with a binding interface of ~200 Å^2. Therefore, the molecular basis for the recognition of N-terminal Phe by Q7 is congruent with that of Q8.[18]

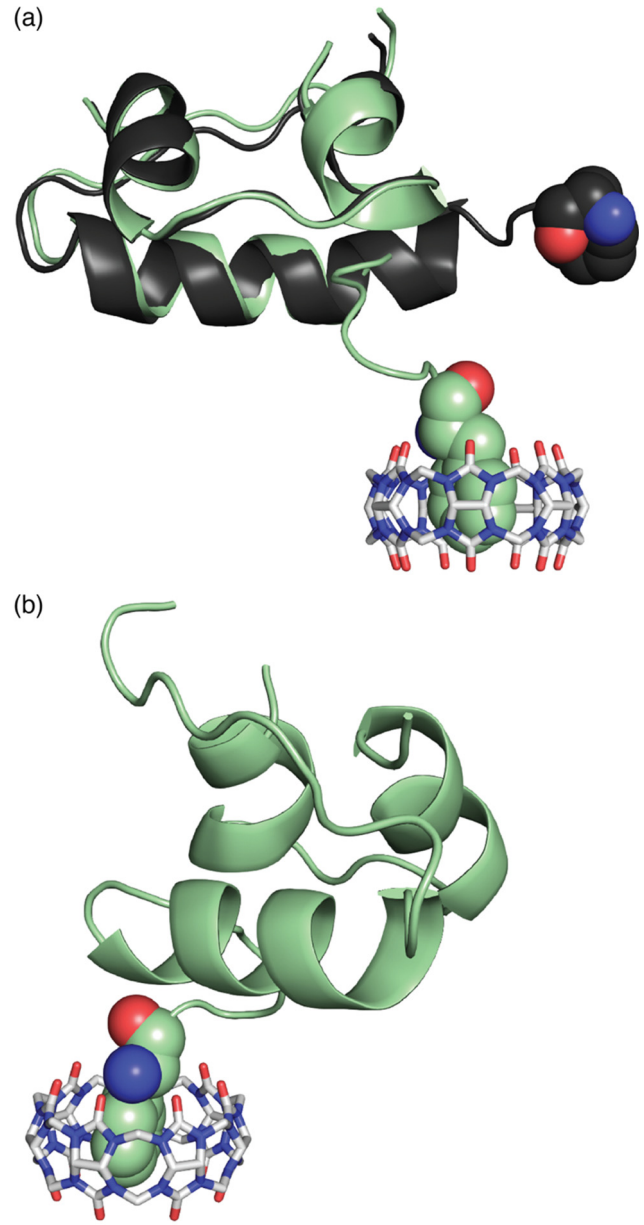

Fig. 18 Crystal structure of the Q7·insulin complex.[68] Q7 is shown as a stick model. The Q7-bound insulin molecule is shown in green. The insulin molecule not bound to Q7 is shown in black. The Phe^{B1} position is rendered as space-filling. (a) Superposition with minimized RMSD over all alpha carbons. This rendering shows the N-terminal region of the B-chain unfolding from an alpha helix upon binding to Q7 and unfolding to separate from the rest of the protein. (b) This rendering shows the proximity of the N-terminal ammonium group with Q7 C=O groups. PDB ID 3Q6E.

Superposition of the two insulin molecules in the asymmetric unit was useful for studying the relationship between insulin structure and Q7 binding (Fig. 17).[68] Structural homology between the two insulins is extensive, with a 0.37 Å root-mean-square deviation (RMSD) over 35 alpha carbons. The largest deviation is at residues B1–B4, which unfold in order to present a fully solvent-accessible site for Q7 to encapsulate. Akin to short peptides, it is common for protein termini to be more disordered and solvent-exposed than other regions of the protein.[84] This observation suggested a more general principle, which is that extensive solvent accessibility is an essential feature of protein recognition by cucurbit[*n*]urils. This feature of cucurbit[*n*]urils is perhaps an advantage for targeting intrinsically disordered regions of proteins, which are known to be essential for the function of many proteins and to be implied in the etiology of many diseases.[85] The observation by Scherman and coworkers that Q8 can bind to sites on disordered loops (*vide supra*)[42] supports this hypothesis.

Like cucurbit[*n*]urils, natural sequence-selective receptors for proteins also require those sites to be fully solvent-accessible. For example, N-recognin proteins are part of the N-degron pathway of protein homeostasis that defines the biological lifetime of a protein by the identity of its N-terminal residue (*i.e.*, the N-end rule).[10,86] N-recognins in both prokaryotes and eukaryotes include the unfolded N-terminal residue of their protein targets within their active sites (Fig. 19). This is also true for many proteases, kinases, and other biomolecular receptors that target proteins sequence-selectively.[10] In this context, cucurbit[*n*]urils behave as synthetic N-recognins.

We were concerned that although Q7 binds site-selectively to Phe^{B1}, it may not bind with selectivity for insulin *versus* other proteins. In an initial test of protein selectivity, we used a fluorescent indicator displacement assay to measure the relative extent of binding of Q7 to native human insulin, the Glu^{B1}, Glu^{B27} mutant of human insulin, human serum albumin,

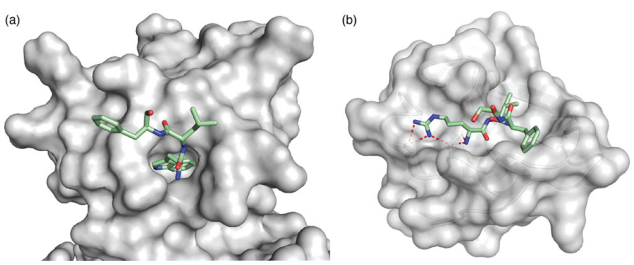

Fig. 19 Crystal structures of N-recognins bound to their cognate peptide termini. (a) ClpS bound to Trp-Leu-Phe, showing burial of the N-terminal indole side chain deep within a cavity (PDB ID: 3GQ1).[87] (b) UBR box of UBR2 bound to Arg-Ile-Phe, showing several electrostatic contacts (<3 Å, red dashed lines) with Asp side chains in the binding site (PDB ID: 3NY3).[88] N-recognins are shown as grey solvent exposed surfaces. Peptides are shown as sticks with green carbons, red oxygens, and blue nitrogens.

human immunoglobulin G, and bovine carbonic anhydrase.[68] Q7 was highly selective for native human insulin *versus* the other four proteins, but this result did not imply selectivity in a biological context. Therefore, we carried out a selectivity study using a multiplex method. In collaboration with the Isaacs group at University of Maryland, we covalently conjugated Q7 to sepharose beads and used the resulting "Q7-resin" to selectively isolate human insulin and human growth hormone (hGH, K_a = 5.9 × 10^5 M^{-1}) from a simple mixture of proteins.[79] The insulin and hGH were released by treating the resulting resin with a high-affinity competitor, *N*,*N*′-diethyl-1,6-diaminohexane, but not a low-affinity competitor, diethylamine, thus demonstrating selective recognition in a mixture. We repeated this experiment in human serum with both insulin and hGH added at 10–100 μM and showed selective enrichment of these proteins. This remarkable result shows that the N-terminal residue is a highly selective epitope capable of conferring protein recognition in the presence of high concentrations (500–700 μM) of other proteins.

2.8. Recognition of lysine and methylated lysine

Receiving less attention until recently is the Lys residues in peptides and proteins. Kim, Inoue, and coworkers first showed that Q6 can bind N-terminal Lys.[67] Buried in the supporting information of their 2008 paper is the fascinating result that Q6 binds N-terminal Lys in the peptide H-Lys-Ala-NH_2 with a K_a value of 1.6 × 10^4 M^{-1} (Table 7). Nau and coworkers reported weak affinity of Q7 for the amino acid lysine (K_a = 800 M^{-1}).[89] Gamal-Eldin and Macartney then showed that methylating the ε-amino group of Lys, which is used to regulate DNA transcription, increases the affinity for Q7 by 3.4-fold, 110-fold, and 3600-fold for mono-, di-, and trimethylation, respectively.[90] Crowley and coworkers engineered a dimethyl Lys residue ($LysMe_2$) into a disordered loop of the *Ralstonia solanacearum* lectin protein (RSL*) and estimated a K_a value of ∼10^3 M^{-1} in 20 mM potassium phosphate, 50 mM NaCl, pH 6.0, *via* chemical shift perturbation of the side chain resonances of the $LysMe_2$ residue.[91] The crystal structure showed Q7 binding in different modes, but the dimethylammonium group is buried in the cavity of Q7 and exists in two states in the crystal, showing that it is free to move within the Q7 cavity (Fig. 20). This group engineered an additional solvent-accessible $LysMe_2$ binding site into RSL* and showed Q7 binding at both sites in solution and in the solid state.[92] Additional work with this system was used for engineering crystalline protein architectures.[93–95] Zhong, Hooley, and coworkers showed that Q7 shifts the electrophoretic mobility of methylated histone peptides, allowing for more efficient separation by capillary electrophoresis.[96]

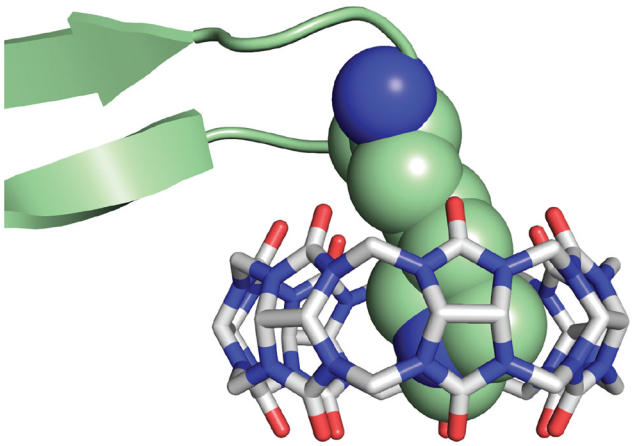

Fig. 20 Close-up rendering of the crystal structure of the Q7·RSL* complex, showing Q7 bound to the $LysMe_2$ residue.[91] Only one of the two conformations of the $LysMe_2$ side chain is shown, and it is rendered as space-filling with green carbons. Q7 is rendered as sticks with grey carbons. Oxygens are red. Nitrogens are blue. PDB ID 6F7W.

In contrast to the work on Q7 and methylated lysines, Crowley recently investigated Q6 binding to unmodified Lys residues in several proteins and found that Q6 can recognize Lys, but not $LysMe_2$, and that recognition depends heavily on the sequence context.[97] High-affinity binding of Q6 at N-terminal Met-Lys, but not at non-terminal Met-Lys, was inferred by observation of slow exchange kinetics on the NMR timescale. Binding of Q8 to N-terminal Met-Lys in the context of a protein demonstrates that the pair-inclusion motif within short peptides translates to folded proteins.

2.9. Recognition of noncanonical residues

Excited by the development of techniques for incorporating noncanonical amino acids into proteins, we were interested to explore the capacity of Q7 to bind chemically modified Phe residues. To this end, we screened a small library of modified phenylalanines for binding to Q7 and found that 4-*tert*-butyl-phenylalanine (*t*BuPhe) and 4-aminomethyl-phenylalanine (AmPhe) bind Q7 with 20–30-fold increased binding affinity (Table 5).[69] N-terminal *t*BuPhe is not a significant improvement over N-terminal Phe, but N-terminal AmPhe binds Q7 with a K_a value of 1.1 × 10^9 M^{-1} in 10 mM sodium phosphate, pH 7.0. The extraordinary 340-fold enhancement in affinity is perhaps due to the deep burial of the side chain within the Q7 cavity, enabling both the side chain ammonium group and the N-terminal ammonium group to bind to opposite portals of Q7, as supported by NMR data.[69] In a subsequent study, we confirmed the relatively high affinity of Q7 for the AmPhe residue in the peptide H-AmPhe-Met-NH_2 (5.3 × 10^8 M^{-1}).[73]

Encouraged by these results, we pursued the incorporation of the AmPhe residue into a protein. Human insulin was chosen as the target due to the presence of an N-terminal Phe residue at the B1 position. By mutating this residue to AmPhe,

Table 7 Thermodynamic data for binary Q6·peptide complexes

Host	protein	K_a (M^{-1})	ΔH (kcal mol^{-1})	$-T\Delta S$ (kcal mol^{-1})
Q6[a]	H-Leu-Ala-NH_2	6.5 × 10^2	−2.9	1.0
Q6[a]	H-Leu-Phe-NH_2	4.0 × 10^2	−2.7	−0.9
Q6[a]	H-Phe-Leu-NH_2	5.0 × 10^1	−1.4	−0.7
Q6[a]	H-Lys-Ala-NH_2	1.6 × 10^4	−2.8	−2.9

[a] 0.1 M NaCl, 298 K.[67]

we hoped to increase the affinity of Q7 by orders of magnitude while only adding an aminomethyl group to the protein. Aminomethyl insulin (*i.e.*, human insulin F^{B1}AmPhe) was produced in a four-step semisynthesis starting from commercially available, recombinant regular human insulin[70] and found to bind Q7 with a K_a value of 1.0×10^7 M^{-1}, a modest 7-fold increase over regular human insulin. Surprised by this result, we evaluated the binding of Q7 to four tetrapeptide analogues of the N-terminal region of the B-chain of human insulin, including the native B1–4 sequence if H-Phe-Val-Asn-Gln-NH_2 (4.0×10^6 M^{-1}) as parent, the less sterically hindered Val^{B2}Gly mutant, H-Phe-Gly-Asn-Gln-NH_2 (7.1×10^6 M^{-1}), and the Phe^{B1}AmPhe mutants of both, *i.e.*, H-AmPhe-Val-Asn-Gln-NH_2 (1.3×10^7) and H-AmPhe-Gly-Asn-Gln-NH_2 (2.0×10^7 M^{-1}). While we were disappointed that the affinity of Q7 for AmPhe in these contexts is weaker than in H-AmPhe-Gly-Gly-NH_2 and H-AmPhe-Met-NH_2, it was interesting to observe that the binding of Q7 to aminomethyl insulin is remarkably similar to its B1–4 tetrapeptide analogue, H-AmPhe-Val-Asn-Gln-NH_2.

Recently, Liu and coworkers reported a general method for inhibiting protein activity site-selectively by incorporating a single *t*BuPhe residue and blocking activity with Q7.[75] A single *t*BuPhe was incorporated at carefully chosen sites near the active sites of glutathione-*S*-transferase, protein tyrosine kinase, and tumor necrosis factor alpha. Q7 inhibited the activities of these proteins, while adding H-Phe-Gly-Gly-OH as a competitor restored protein activity.

2.10. Lessons learned from molecular recognition studies

These molecular recognition studies have yielded several principles for targeting small sites on peptides and proteins with cucurbit[*n*]urils in a site-selective and sequence-predictive manner and with affinities that are compatible with a range of possible applications, as detailed in Section 3. Targeting the N-terminal residue, as a unique epitope, offers the most straightforward approach to high affinity and selectivity. N-terminal Phe can be targeted by Q7 in a 1 : 1 (Q7 : polypeptide) stoichiometry and by Q8 in a 1 : 2 (Q8 : polypeptide) stoichiometry, both with sub-micromolar affinities. Most residues can be tolerated at the second position, but Pro significantly destabilizes binding. N-terminal Tyr can be bound by Q7 in a 1 : 1 (Q7 : polypeptide) stoichiometry and with low-micromolar affinity, whereas N-terminal Lys-Phe, and Leu-Tyr can be bound in a 1 : 1 (Q8 : polypeptide) stoichiometry and with low- to sub-nanomolar affinities. Q8 can also target N-terminal Met with submicromolar affinity, in which the identities of the second (Leu, Met, Lys, Arg, Phe, and Tyr preferred) and third residues (Gly and Ala preferred) are important. Entirely nonaromatic sequences are possible in the pair-inclusion motif. In some cases, the first and second residues of an N-terminal dipeptide site can be swapped, while in other cases (*e.g.*, Lys-Phe *vs.* Phe-Lys and Leu-Tyr *vs.* Tyr-Leu), there is sequence selectivity of several orders of magnitude. The molecular basis for recognition in these motifs is supported by extensive NMR and crystallographic data. N-terminal sites are likely to be tolerated by proteins due to their propensity to unfold and become fully accessible to encapsulation by the host. Similarly, sites located in disordered loops are also likely to be accessible. Non-terminal sites containing Phe or AmPhe are accessible to Q7 at low micromolar affinity, whereas numerous dipeptide sequences are accessible to Q8 binding, with affinities reaching mid-nanomolar for the sequences Lys-Phe and Phe-Lys. N-terminal and non-terminal Trp can be targeted by preformed complexes including Q8 and a cofactor, and binding is essentially independent of the neighboring sequence context.

The studies described in this section also demonstrate several properties of Q*n*·peptide complexes that make them particularly well suited to applications involving affinity tags for proteins and peptides: (1) binding occurs in purely aqueous solution (*i.e.*, no organic solvent) and is compatible with a wide range of buffer conditions, including salts of different types, salt concentrations up to physiologic level (*e.g.*, PBS, serum), and pH from neutral to acidic. (2) The binding affinities are mostly in the range of 10^5–10^9 M^{-1}, which enable working concentrations to be in the useful high micromolar to low nanomolar range. (3) Binding is observable and quantifiable by numerous methods. (4) Site-selectivity is relatively high for certain sequences (*e.g.*, Q7 binding to N-terminal Phe, or Q8 binding to N-terminal Lys-Phe) and relatively low for others (*e.g.*, Q8·MV binding to non-terminal Trp), which allows for adaptation to a diverse range of applications. (5) The rules for sequence recognition and the various modes of binding are sufficiently well understood to accurately predict binding. (6) Target binding sites can be engineered into proteins with minimal to no loss in affinity while maintaining site-selectivity. (7) N-terminal and non-terminal sites can be targeted with high affinity and selectivity. (8) Q8 can noncovalently couple peptides and proteins to an auxiliary guest that can add functionality *via* heteroternary complex formation. (9) Q8 can reversibly homodimerize peptides and proteins. (10) Q7 and Q8 can bind peptides and proteins with high affinity in a 1 : 1 ratio. 11) Q7 retains its recognition properties when attached to a solid support. These favorable characteristics have enabled the demonstration of a broad range of applications, as described in detail in Section 3.

3. Applications of peptide and protein recognition by cucurbit[*n*]urils

The molecular recognition properties detailed in Section 2 have facilitated the development of numerous applications involving the site-specific binding of cucurbit[*n*]urils, particularly Q7 and Q8, to peptides and proteins, as reviewed comprehensively in this section. One can view these applications as ways to create or improve affinity tags for polypeptides, or to extend the classical idea of an affinity tag to new applications such as protein dimerization, oligomerization, and polymerization, or dynamic surfaces and reversible materials. We hope these examples will inspire the next generation of scientists to build programmable and functional devices and materials.

3.1. Sensor development

Chemical sensors interact with a target chemical and, upon interaction, transduce an observable signal that can be amplified and read out by the user.[98] Sensors that are selective for peptides and proteins are highly useful for the detection and quantification of desired polypeptide targets *in vitro*, *in vivo* (*e.g.*, probes), and *ex vivo* (*e.g.*, medical diagnostics). The selective recognition of polypeptides by Q7 and Q8 satisfies the first requirement of a chemical sensor. This section reviews the work of numerous groups to couple this binding to a signal transduction mechanism in order to create functional sensors.

3.1.1. Optical polypeptide sensing. In the original studies investigating polypeptide recognition by cucurbit[*n*]urils, we reported that peptide binding to Q8·MV is accompanied by the growth of a visible charge-transfer absorbance and the quenching of Trp fluorescence.[30] This experiment was built directly on the report by Kim and coworkers that the binding of 2,6-dihydroxynaphthalene to Q8·MV is accompanied by the appearance and growth of a visible charge-transfer absorbance and the quenching of naphthalene fluorescence.[28] As described in Section 2.1, we used this approach to rapidly screen the binding of Q8·MV to a library of Trp-containing peptides,[40] and to quantify the extent of valency in multivalent complexes containing Q8·viologen·Trp binding units.[47]

Methyl viologen is limited as an optical sensor due to its lack of intrinsic fluorescence. Several alternative auxiliary guests for Q8 have been developed with intrinsic fluorescence (Fig. 21). Kaifer and coworkers replaced MV as a first guest for Q8 with 2,7-dimethyldiazaphenanthrenium (DPT^{2+}) and 2,7-dimethyldiazapyrenium (DAP^{2+}), which have limited rotational freedom, compared to MV, and are intrinsically fluorescent.[99] The resulting Q8·guest complexes bound to indole, tryptophan, and serotonin, which quenched the fluorescence of the first guest. We followed this work with a report on the use of tetramethylbenzobis(imidazolium) (MBBI) as an intrinsically fluorescent sensing component for peptides, as described in more detail in Section 2.5.[43]

Biedermann, Nau, and coworkers reported the use of complexes of Q8 with various aromatic chromophores, including DAP, MDPP, and MVE (Fig. 21), to sense by CD spectroscopy the binding and reaction of chiral guests including aromatic amino acids and peptides as well as the proteins somatostatin and insulin.[100] Biedermann and coworkers recently demonstrated enhanced sensitivity using fluorescence-detected CD to detect amino acids, peptides, and proteins.[101]

Aryal, Huang, Hunter, and coworkers reported a sensor for aromatic amino acids and peptides based on a water-soluble perylene-monimide, PMI (Fig. 20).[102] The Q8·PMI complex has a K_a value of 1.3×10^4 M^{-1} and causes PMI to deaggregate and increase in fluorescence by up to 19-fold. Upon competitive displacement of PMI with phenylalanine-containing peptides, the fluorescence decreases in a concentration-dependent manner. Schmuck, Nau, and coworkers demonstrated a ratiometric fluorescence sensor based on Q8 and a bis(pyrene), AP-1 (Fig. 17).[103] Q8 interrupts the intramolecular pyrene excimer, which is restored upon the competitive binding of phenylalanine-containing peptides and insulin to Q8. The ratio of pyrene monomer fluorescence emission to excimer emission was used as the sensing metric.

Hennig, Nau, and coworkers applied Q*n*-based optical sensing to measure the transport of cell-penetrating peptides across phospholipid membranes.[44] Q8·DAP and Q7·berberine complexes were trapped within liposomes and used to detect the permeation of unlabeled Phe- and Trp-containing peptides into the liposome at effective concentrations equal to or higher than the K_d value for the peptides. Biedermann, Nau, and coworkers extended this method to the time-resolved, quantitative determination of membrane permeability for a wide array of analytes using Q8 in complex with DAP, MVE, and MBBI.[104]

Li and coworkers developed a sensor based on the Q8-induced flocculation of Au nanoparticles.[105] The nanoparticles were modified with peptides containing a C-terminal Cys for covalent attachment to the Au surface and an N-terminal Trp to induce nanoparticle aggregation *via* the Q8-mediated dimerization of Trp residues. Because the aggregation of Au

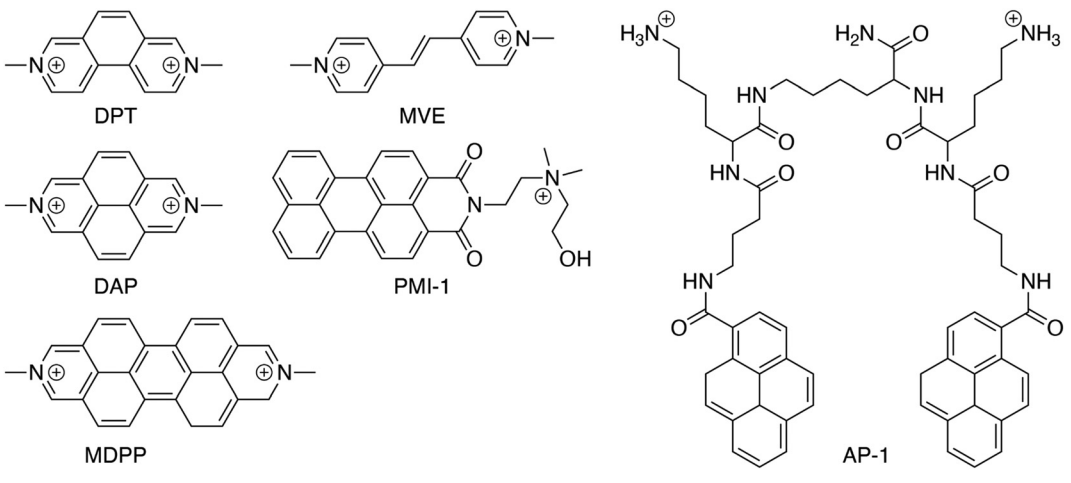

Fig. 21 Chemical formulas of guests used for sensor development with cucurbit[*n*]urils.

nanoparticles modulates their plasmon absorbance, introducing a protein that targets the surface-bound peptide, competitively displaces Q8, and drives disaggregation of the nanoparticles allows for optical detection of the protein with a lower limit of detection of 0.2 nM. Hou and coworkers used the H-Phe-Gly-Gly-OH peptide as an example analyte to demonstrate a novel detection platform in which Q8 is bound to surfactant molecules at an interface, and sensing is activated by addition of the peptide and competitive displacement of the surfactant.[106]

Cao and coworkers reported the formation and adaptive chirality of an achiral Q8-based supramolecular organic framework (SOF) and its use as a chiroptical sensor for polypeptides.[107] SOFs are formed upon the complexation of tetra(6-coumarinylmethyl-pyridinium)tetraphenylethylene (TPE) units with Q8. Through the addition of Phe or Trp containing dipeptides with L- or D- stereochemistry, the TPE units can be induced to have a rotational conformation of *M*- or *P*-, producing mirror-image circular dichroism and circularly polarized luminescence signals upon binding. Taking advantage of adaptive chirality, SOFs were able to distinguish dipeptides H-Phe-Ala-OH, H-Ala-Phe-OH, and H-Phe-Phe-OH, as well as proteins somatostatin and regular human insulin, with CD spectra characteristic of either *M*- or *P*-SOFs. They then exchanged the TPE unit with a hexaphenylbenzene (HPB) derivative, tetra(6-coumarinylmethyl-pyridinium)hexaphenylbenzene, and distinguished L-Trp-X from L-Phe-X dipeptides based on the adaptive chirality of the SOF.[108] Importantly, chiral induction of the SOF was only observed when Trp and Phe were placed at the N-terminus, allowing distinction between L-Trp/Phe-X and L-X-Trp/Phe. The adaptive chirality and chiroptical sensing properties of the supramolecular organic framework may be applied to determine enantiopurity of amino acids and distinguish biological chiral molecules.

3.1.2. Electrochemical polypeptide sensing. In addition to optical detection, the redox properties of viologens have enabled their use in the electrochemical detection of polypeptides. Li and coworkers reported a technique for quantifying a solution-phase protein *via* its binding to a surface-bound peptide presenting a non-terminal Trp residue (Fig. 22).[109] Protein-binding peptides containing one or more aromatic residues and modified with an alkanethiol group were self-assembled on a gold electrode and then treated with their cognate protein binding partner. The residual, unbound sites were then bound by Q8·MV, which served as an electrochemical reporter. Negative potential applied at the electrode reduces the proximal MV groups, which was read out by square-wave voltammetry. The technique was highly selective and sensitive for tumor necrosis factor-α and *amyloid* β 1–42 oligomer, with a lower limit of detection in the mid-picomolar range.

Yuan, Chia, and coworkers described the incorporation of Q8·MV into a sensor for microRNA by binding to Trp-labeled DNA strands used in a target cycling and strand displacement amplification method.[110] Trp-labeled oligonucleotide strands produced in the reaction cycling bind to a sensor electrode coated with Q8·MV groups and are released by single-electron

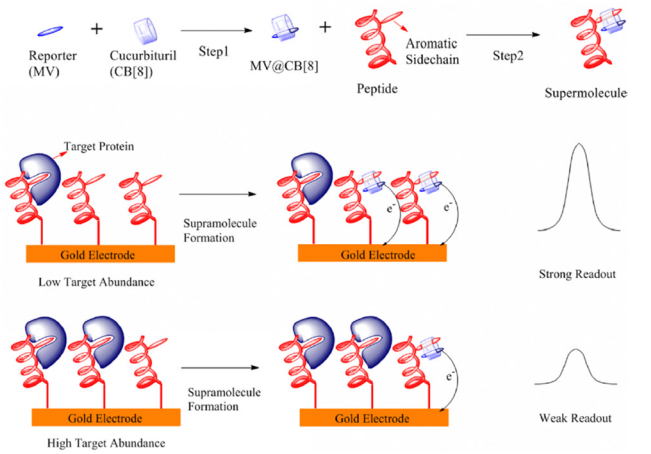

Fig. 22 Protein sensing technique through electrochemical readout at a gold surface. CB[8] is Q8.[109] Reproduced with permission from ref. 109. Copyright 2012 American Chemical Society.

reduction of the viologen, followed by oxidative regeneration of the sensor.

3.1.3. Enhancing polypeptide detection with cucurbit[*n*]urils. We collaborated with the Kim group at Korea University to demonstrate that the addition of Q7 to protein samples following peptic digestion increases mass spectrometric signal abundance and sequence coverage for peptides containing N-terminal Phe.[111] The observed signal enhancement was attributed to the C=O portals of Q7 stabilizing positive charges and thus increasing proton affinities of the bound guests, which improves ionization efficiency. The addition of Q7 also resulted in increased fractionalization of peptides, which was also attributed to charge stabilization and interactions with the carbonyl portals.

The selectivity of Q7 for N-terminal Phe has also been applied to signal enhancement by surface enhanced Raman scattering (SERS).[112] Camden, Webber, and coworkers demonstrated how the addition of Q7 to samples can improve the sensitivity and detection limits of peptides and proteins with N-terminal Phe *via* SERS by increasing the concentration of analyte in proximity to the nanoparticle surface.

3.1.4. Measuring photocleavage. Pischel, Basílio, and coworkers demonstrated the light-induced dimerization of peptides by Q8.[53] H-Phe-Gly-Gly-OH was modified N-terminally with a photo-cleavable 6-nitroveratryloxycarbonyl group (NVoc). 1 : 1 binding of NVoc-FGG with Q8 was confirmed by ITC, NMR spectroscopy, and mass spectrometry. Photodeprotection of the NVoc-FGG·Q8 complex triggered the dimerization of H-Phe-Gly-Gly-OH in Q8, as confirmed by NMR spectroscopy. This approach points toward the use of stimuli-responsive supramolecular chemistry in biological contexts.

3.2. Measuring and inhibiting protease activity

Proteases are enzymes that catalytically hydrolyze peptide bonds and are involved in digestion, protein maturation, protein homeostasis, viral processing, and many other processes. As such, proteases are important targets for

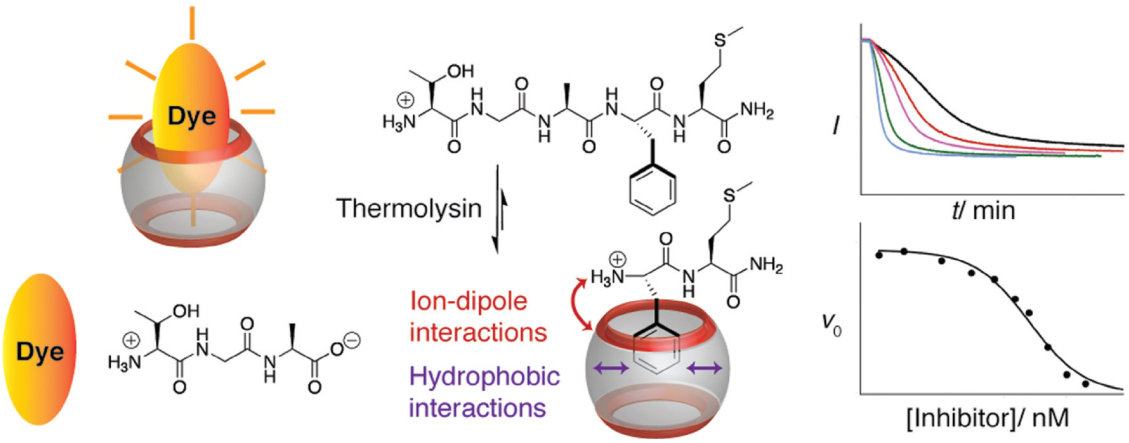

Fig. 23 Supramolecular tandem enzyme assay for real-time measurement of the proteolysis of enkephalin-type peptides with thermolysin, using Q7 and acridine orange as the reporter pair. (top right) Fluorescence intensity as a function of time at different concentrations of substrate, used to measure k_{cat}/K_M. (bottom right) Reaction rate as a function of inhibitor concentration, used to measure the inhibitory constant.[71] Reproduced with permission from ref. 71. Copyright 2011 American Chemical Society.

measurement and control using synthetic ligands. The selective recognition of peptides and proteins by cucurbit[*n*]urils therefore provides fertile ground for the development of applications involving proteases.

3.2.1. Measuring protease activity. Nau and coworkers have pioneered the use of supramolecular chemistry to measure enzyme activity using label-free "supramolecular tandem enzyme assays".[113] These assays comprise an indicator-displacement assay coupled with an enzyme-catalyzed reaction. Briefly, a host such as Q7 binds with different affinities to the starting material *versus* the product of an enzymatic reaction. By incorporating a fluorescent indicator guest that is displaced competitively by either the starting material or the product, the progress of the enzyme-catalyzed reaction can be monitored continuously *via* the change in the fluorescence of the indicator. The enzyme-catalyzed reaction is slower than the supramolecular competition chemistry, and therefore the assay reports enzyme activity in real time. Although this method has been used to monitor a wide range of reactions, we focus here on reactions involving the binding of amino acids and peptides. Hennig, Bakirci, and Nau measured the kinetics of the decarboxylation of amino acids using Q7 and the fluorescent dye dapoxyl as the reporter pair.[114] Initially, the Q7·dapoxyl complex (K_a = 2 × 10^4 M^{-1}) produced a strong fluorescence due to its stability in the presence of the weakly binding enzyme substrates lysine, arginine, histidine, and ornithine. The decarboxylation of these substrates produces cadaverine, agmatine, histamine, and putrescine, respectively, which bind strongly to Q7 and competitively displace the dye, producing a corresponding decrease in fluorescence intensity. Li and coworkers reported an application of the supramolecular tandem enzyme assay to continuously monitor the oxidation of peptides H-Tyr-Leu-Ala-NH2 and H-Dopa-Leu-Ala-NH2 (Dopa = 3-hydroxytyrosyl) by tyrosinase using a Q8·thioflavin-T reporter pair.[115] This method was also used to monitor inhibition of tyrosinase by kojic acid.

In collaboration with the Nau group at Jacobs University Bremen, we reported a method for monitoring proteolysis by the endopeptidase thermolysin, which cleaves on the N-terminal side of hydrophobic residues such as Phe and Leu, using Q7 and acridine orange as the reporter pair (Fig. 23).[71] The substrate peptides contained a non-terminal Phe residue, which binds relatively weakly to Q7, whereas the product peptides contained an N-terminal Phe, which competitively displaces acridine orange and results in a decrease in fluorescence intensity. This method was used to rapidly determine the Michaelis Menten k_{cat}/K_M values for the proteolysis of a series of unlabeled enkephalin-based peptides, thereby profiling the substrate selectivity of this enzyme. We also used the assay to measure the inhibitory constant of a known protease inhibitor.

Hennig, Nau, and coworkers combined this method for monitoring enzyme kinetics with their aforementioned technique for detecting peptide membrane permeation to demonstrate the dual-color chemosensing of a compartmentalized reaction network.[116] The compartmentalized liposomal system was designed to detect the enzymatic cleavage of enkephalin-related peptides in the extravesicular space by a Q7·methylene blue reporter pair, and to detect the membrane permeation of the cleaved product in the intravesicular space by either Q8·2-anilinonaphthalene-6 sulfonic acid or Q7·berberine reporter pairs. The dyes enabled selective optical excitation and emission, providing a way to kinetically discriminate between two sequential reactions, cleavage and permeation.

3.2.2. Inhibiting protease activity. Nau and coworkers first reported the inhibition of enzyme-mediated proteolysis through sequence-selective binding of the substrate peptides with Q7.[117] In a subsequent study, we demonstrated that Q7 can be used in conjunction with porcine methionine aminopeptidase (APN) to selectively inhibit its exopeptidase activity (Fig. 24).[73] In the presence of Q7, the digestion of the enkephalin-type peptide H-Thr-Gly-Ala-Phe-Met-NH_2 was halted after removal of the first three residues because the

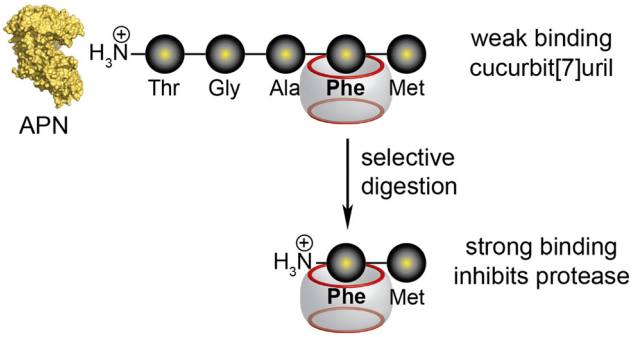

Fig. 24 Schematic for the sequence-specific inhibition of a nonspecific protease.[73] Reproduced with permission from ref. 73. Copyright 2013 American Chemical Society.

H-Phe-Met-NH_2 product binds tightly to Q7. This reaction was quantitative in the presence of one molar equivalent of Q7, thereby demonstrating an effective method for peptide processing. Q7 completely protected H-Phe-Met-NH_2 and H-AmPhe-Met-NH_2 from APN proteolysis for 24 hours, but protection was not complete for the weaker binding H-Tyr-Met-NH_2 and H-Trp-Met-NH_2, which indicates the importance of sequence-selectivity and working concentrations in this method.[73]

Gong, Cao, and coworkers used this approach to measure the activity of APN.[118] Au nanoparticles coated with H-Phe-Gly-Gly-Phe-Glu-Leu-Leu-Cys-OH peptides were flocculated upon addition of Q8, akin to the method reported by Li and coworkers, *vide supra*.[105] APN was introduced to remove the N-terminal Phe, which prevents flocculation and allows for the measurement of enzymatic activity. This approach was reported to have improved detection limit and response time compared to other methods for measuring APN activity.

3.3. Protein assembly

The formation of protein dimers, oligomers, polymers, discrete assemblies, and indistinct aggregates is ubiquitous in nature. Therefore, the ability to measure or control these processes has significant potential value in bioscience and biotechnology. This section illuminates the practicality of applying cucurbit[*n*]urils toward these ends. In the context of affinity tags, this is an area of new development made possible by the dimerizing capability of Q8.

3.3.1. Discrete peptide assembly. Masson and coworkers reported the formation of well-defined supramolecular architectures from cucurbit[*n*]uril, coordinated Pt^{II}, and peptide building units.[119] Q8·(Pt-Cys-$(Gly)_3$-Phe)$_2$ assemblies were constructed *in situ* by dimerizing platinum terpyridyl complexes within Q8 and grafting Phe-$(Gly)_3$-Cys peptides to the Pt^{II} centers. The assemblies were used to selectively target Q7 and Q8 *via* the N-terminal Phe residues, leading to a series of supramolecular pseudorotaxanes and pseudocatenanes. Notable structures formed from the Q8·(Pt-Cys-$(Gly)_3$-Phe)$_2$ assemblies included a "pendant necklace" with 2:2 FGGGC-Pt/Q8 stoichiometry in head-to-head and head-to-tail arrangements at the terpyridyl units and Phe residues, respectively, a structure with the same stoichiometry but in dual head-to-head arrangements, and a head-to-tail dimer with a 4:4 FGGGC-Pt/Q8 stoichiometry.

3.3.2. Discrete protein assembly. Protein dimerization is essential for controlling biological processes such as signaling, aggregation, and apoptosis. Brunsveld and coworkers have demonstrated the power of engineering proteins with minimal affinity tags, such as FGG at the N-terminus, and using Q8 to induce protein dimerization by binding to these sites. They first showed that the Q8-mediated dimerization of FGG-protein tags can be used to selectively and reversibly dimerize fluorescent proteins.[78] Monomeric yellow fluorescent protein (mYFP) and cyan fluorescent protein (mCFP) were genetically engineered with the code for FGG upstream of the protein gene and a self-splicing intein domain further upstream of the FGG-tag. This clever design allows for the FGG-mXFP proteins to be generated conveniently by autocleavage of the intein and subsequent elution from a chitin resin. They observed fluorescence resonance energy transfer (FRET) upon the Q8-mediated homodimerization of FGG-mYFP (*via* homo-FRET) as well as the Q8-mediated heterodimerization of FGG-mYFP and FGG-mCFP (*via* hetero-FRET). Q8-mediated dimerization of FGG-mYFP was reversible upon the addition of methyl viologen as a competitive guest for Q8. Brunsveld and coworkers reported the extension of this approach to the supramolecular control of protein tetramerization (Fig. 25).[120] They engineered double mutants (S208F and V224L) of yellow and cyan fluorescent proteins to form dimerizing mutants dYFP and dCFP with Phe-Gly-Gly at each N-terminus. The resulting FGG-dYFP and FGG-dCFP formed heterodimers along a protein–protein interface. These dimers were induced to dimerize upon addition of Q8 to form stable protein tetramers.

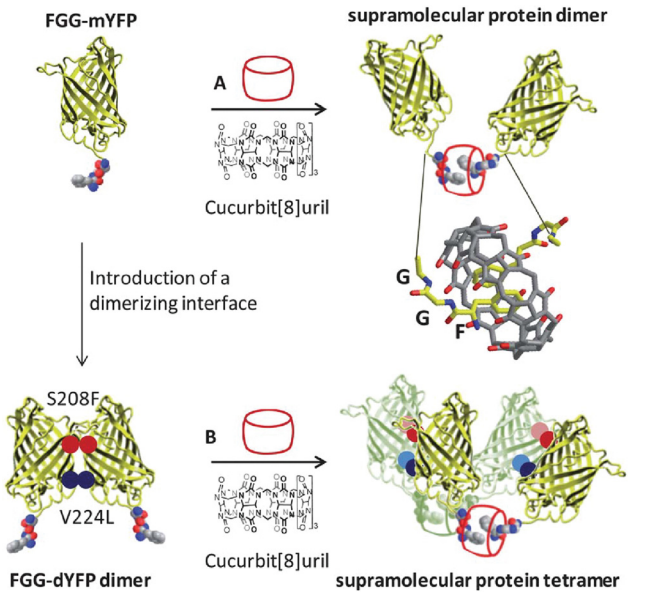

Fig. 25 Design of a protein tetramer by Q8-mediated dimerization of an FGG-modified protein dimer.[120] Reproduced from ref. 120 with permission from the Royal Society of Chemistry.

Brunsveld and coworkers reported the structure of a Q8-mediated protein dimer using dynamic light scattering and solution-based small angle X-ray scattering to show that the Q8-mediated dimer of FGG-mYFP forms a Z-shaped structure that retains the size and shape of the individual YFP subunits and with a relatively compact contact area between the proteins.[121] The parallel, coplanar alignment of the beta barrels helps to explain the efficient FRET between the proteins.

Q8-mediated protein dimerization was then applied to controlling the activity of the enzyme caspase-9, which normally exists in monomeric form and is activated by dimerization. Brunsveld and coworkers engineered a mutant of caspase-9 to contain an N-terminal FGG-tag (*i.e.*, FGG-casp-9) and showed that enzyme activity was increased 50-fold upon dimerization with Q8.[122] This enhancement was dependent on the concentration of Q8 and could be reversed in a concentration-dependent fashion by addition of the tripeptide H-Phe-Gly-Gly-OH as a competitive inhibitor. The activity of a control caspase-9 mutant with N-terminal H-Met-Gly-Gly- was not affected by Q8. They recently extended supramolecular control of caspase-9 activity by engineering a light-sensitive peptide cage for Q8.[123] The cage contained two N-terminal FGG-tags and two photo-cleavable amino-3-(2-nitrophenyl)propanoic acid residues. Upon photocleavage, the affinity of the cage for Q8 substantially decreases, thus liberating Q8 to drive the dimerization of FGG-casp-9 monomers. The activity of caspase-9 activated by photocleavage of the cage was comparable to that of caspase-9 activated by uncaged Q8. Notably, this approach to enzyme activation avoids modification of the enzyme active site, thereby providing an additional measure of control.

Brunsveld and coworkers reported the use of Q8 to drive split-enzyme complementation and restore enzymatic activity for the heterocomplexation of split-luciferase fragment pairs.[124] An N-terminal FGG-tag was incorporated into the two protein fragments, and Q8-mediated combination of the NFluc437 and CFluc398 fragments resulted in enzymatic activity in a concentration-dependent manner. Memantine, a high-affinity guest for Q8, was shown to be an effective competitor to reverse this process. Ottmann, Brunsveld, and coworkers then reported the use of Q8 to mediate supramolecular protein assembly with a 14–3–3 protein dimer.[125] Estrogen receptor α (ERα) has a 14–3–3 protein-binding domain at its C-terminus. An N-terminal FGG-tag was added to ERα, and addition of Q8 induced protein dimerization. The affinity of ERα for 14–3–3 protein was enhanced significantly in the presence of Q8. When the FGG-ERα peptide was acetylated at the N-terminal amine (Ac-FGG), no binding to Q8 was observed. Importantly, they were able to determine the crystal structure of the Q8-bound protein tetramer (Fig. 26), showing stacking of Phe side chains within the Q8 cavity and chelation of the N-terminal ammonium groups by Q8 C=O groups, in a manner identical to the Q8·(H-Phe-Gly-Gly-OH)$_2$ structure.[18] Akin to the Q7·insulin crystal structure,[63] the binding site on FGG-ERα is fully solvent-accessible. Brunsveld and coworkers then used Q8-mediated activation of FGG-modified caspase-8 to overcome limitations in studying the mechanism of dimerization and activation by circumventing the need to mutate the dimerization interface.[126] Utilizing Q8-mediated activation of caspase-9, Ottman, Brunsveld, Merkx, and coworkers designed a synthetic self-activating protease signaling network in which dimerization and activation of FGG-caspase-9 by Q8 was shown to activate a 14–3–3 scaffold inhibited by ExoS peptides, thus triggering 14–3–3-templated split-luciferase complementation.[127] This method demonstrates the control of common mechanisms for intracellular signaling by a modular supramolecular platform.

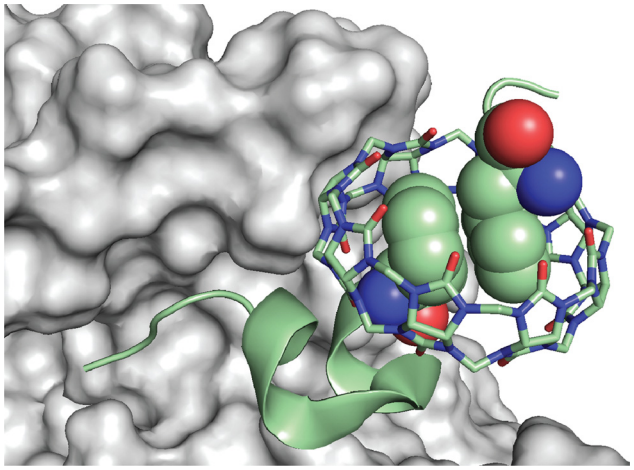

Fig. 26 Rendering of the crystal structure of the Q8·(14–3–3·FGG-ERα)$_2$ complex.[125] The solvent-accessible surface of 14–3–3 is shown in grey. The backbone of FGG-ERα is shown as a green ribbon. The N-terminal Phe residues are shown as space-filling. Q8 is shown as sticks. Carbons are green, oxygens are red, and nitrogens are blue. PDB ID 5N10.

Dankers, Brunsveld, and coworkers reported the reversal of Q8-mediated dimerization of FGG-mYFP using a bivalent guest presenting two N-terminal Phe-Gly-Gly-Gly peptides linked with a penta(ethylene glycol).[128] They measured a K_a value of 9.0×10^6 M^{-1} for Q8 binding to the bivalent guest, and they proposed the formation of an interesting pseudocatenane structure. Using fluorescence polarization anisotropy, FGG-modified yellow fluorescent protein was dimerized when bound to Q8. When the FGG-modified penta(ethylene glycol) was introduced as a competitor, it reversed protein dimerization.

3.3.3. Protein oligomers and polymers. Controlling the assembly of protein-based materials is a goal with wide-ranging biomedical applications, including therapeutics, diagnostics, tissue engineering, and imaging. Liu and coworkers first reported the Q8-induced linear assembly of proteins into nanowires.[57] Building on the ability of His-tagged glutathione S-transferase (GST) to dimerize *via* metal chelation of the His tags, they engineered a GST variant with an N-terminal FGG-tag and showed that the resulting FGG-GST homodimers could be induced to form supramolecular protein polymers upon addition of Q8. Further studies were carried out to demonstrate the use of GST as a selenoenzyme glutathione peroxidase (GPX) mimic by incorporating the catalytic selenocysteine into the substrate-binding pocket of FGG-GST. In the presence of

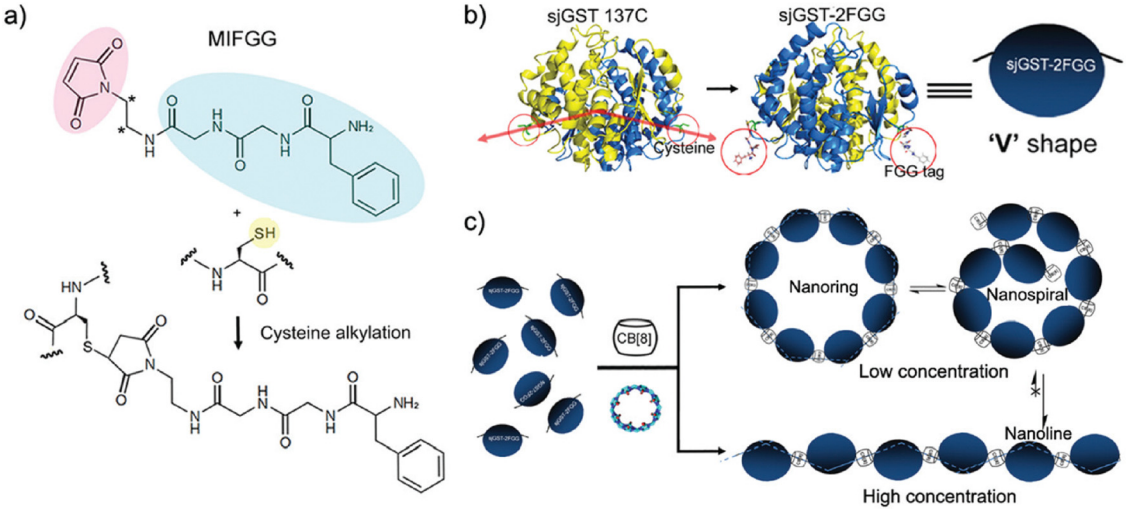

Fig. 27 Conjugating FGG-maleimide to Cys side chains allows for Q8 to mediate protein assembly. CB[8] is Q8.[130] Reproduced from ref. 130 with permission from the Royal Society of Chemistry.

Q8, Se-FGG-GST produced nanowires that reduced mitochondrial oxidative stress.

Liu, Li and coworkers then fused GST to a redox-sensitive mutually exclusive protein (MEP) and fused an N-terminal FGG-tag.[129] The tagged protein spontaneously formed homodimers that could be induced to form larger assemblies by addition of Q8. The morphologies of the assemblies could be controlled reversibly *via* the redox properties of the protein in order to assemble into nanowires or nanorings. To circumvent the need for genetic engineering, Liu and coworkers then conjugated a maleimide group to the C-terminus of H-Phe-Gly-Gly- in order to make a compound that can be conjugated to the side chain of any solvent-exposed Cys residue.[130] They demonstrated the utility of this approach by attaching the conjugate to the Cys side chains of a variant GST. The Cys groups on the GST homodimer projected in a V shape, and Q8 induced the assembly of the homodimers into linear supramolecular polymers, rings, and spirals in a concentration-dependent fashion (Fig. 27). Liu, Hou, and coworkers conjugated a pyridinium derivative to a protein engineered with a single Cys residue and formed two-dimensional protein arrays in the presence of Q8.[131] Addition of the tripeptide H-Phe-Gly-Gly-OH competitively reversed assembly formation.

3.3.4. Modulating protein aggregation. The extraordinarily small binding site for Q7 and Q8 has allowed the study of natural proteins and peptides containing those sequences in the context of protein aggregation. Amyloids are aggregates of proteins that assemble into fibrils and have been implicated in the etiology of several diseases. Therefore, techniques for forming and inhibiting amyloids are valuable for understanding amyloidogenesis and for developing therapeutics.

Hugh Kim, Kimoon Kim, and coworkers reported the inhibition of the amyloidogenesis of insulin and β-amyloid ($A\beta_{1-40}$ and $A\beta_{1-42}$) using Q7 (Fig. 28).[132] An insulin : Q7 ratio of 2 : 1 or higher showed inhibition of fibrillation based on a thioflavin T spectroscopic assay, which reports the formation of β-sheets. Although Q7 bound selectively to the Phe^{B1} position, ITC experiments at pH 2.7 showed binding of a second equivalent of Q7 to Phe^{B24} with lower affinity. Phe^{B24} binding was corroborated by molecular dynamics simulations with a partially unfolded insulin structure and suggests that Q7 binding to Phe^{B24} inhibits insulin·insulin dimerization along the interface comprising B11–17 and B24–26. In parallel, Q7 was also shown to suppress the fibrillation of Aβ peptide at high Q7 : peptide ratios. Titration studies revealed a K_a value of 7.1×10^4 M^{-1} in sodium phosphate buffer (Table 6). Binding studies with point mutants of $A\beta_{1-40}$ revealed equal accessibility of Q7 to Phe4, Phe19, and Phe20, and Q7 binding was postulated to inhibit the clustering of these residues and the formation of the partially folded intermediate on the path to amyloid assembly. Q7 binds $A\beta_{1-42}$ and $A\beta_{1-40}$ with similar affinity and suppresses fibrillation. de Oliveira and coworkers used molecular dynamics simulations to suggest that the inhibition of $A\beta_{1-42}$ by Q7 is due to binding of Q7 to Asp1, Lys 16, and Val36, with prevention of protofibril elongation.[133] Bowers and coworkers reported the binding of one and two molar equivalents of Q7 to monomers and dimers, respectively, of the $A\beta_{25-35}$ fragment (Gly-Ser-Asn-Lys-Gly-Ala-Ile-Ile-Gly-Leu-Met), presumably *via* the Lys residue, leading to the suppression of oligomer formation.[134] Li, Hong, and coworkers reported the Q7- and Q8-mediated inhibition of amyloid fibrillation of $A\beta_{1-16}$ and the truncated $A\beta_{4-16}$, which contains an N-terminal Phe.[58] They reported K_a values for Q7 with $A\beta_{4-16}$ of 1.1×10^6 M^{-1} and with $A\beta_{1-16}$ of 1×10^4 M^{-1} (Table 6). Q8 binds two equivalents of $A\beta_{4-40}$ with a ternary binding constant K_{ter} value of 5.5×10^{10} M^{-2} (Table 3), whereas no binding was observed for Q8 with the $A\beta_{1-16}$ peptide. They showed that Q7 and Q8 slow the aggregation of $A\beta_{4-40}$ at a lower concentration than $A\beta_{1-40}$, presumably by binding to the ends of short oligomers, and that Q7 and Q8 reduce the cytotoxicity of $A\beta_{4-40}$. Q7, but not Q8, reduces the cytotoxicity of $A\beta_{1-40}$.

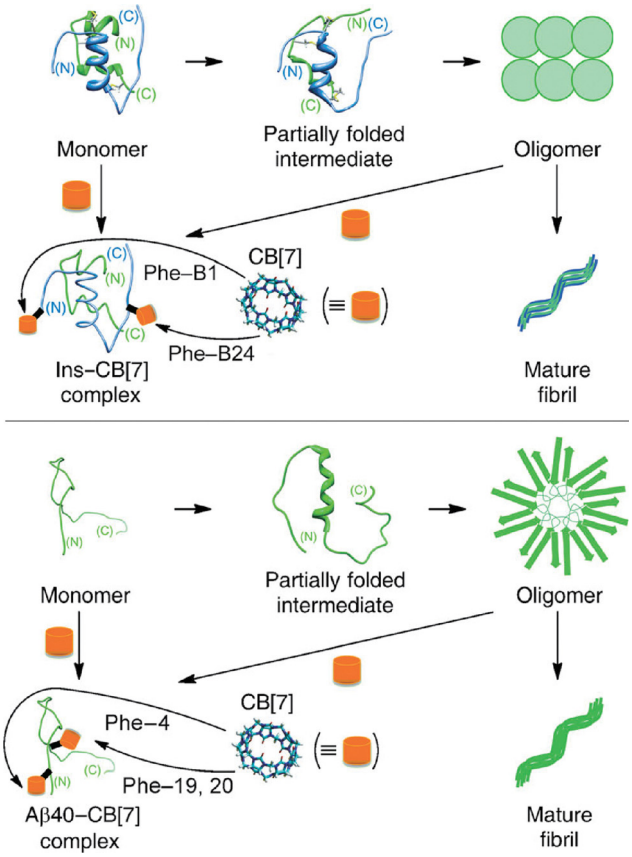

Fig. 28 Schematic for the inhibition of fibrillation using Q7 to stabilize the monomeric forms of (top) insulin and (bottom) $A\beta_{1-40}$. CB[7] is Q7.[132] Reproduced with permission from ref. 132. © 2014 Wiley-VCH Verlag GmbH & Co. KGaA, Weinheim.

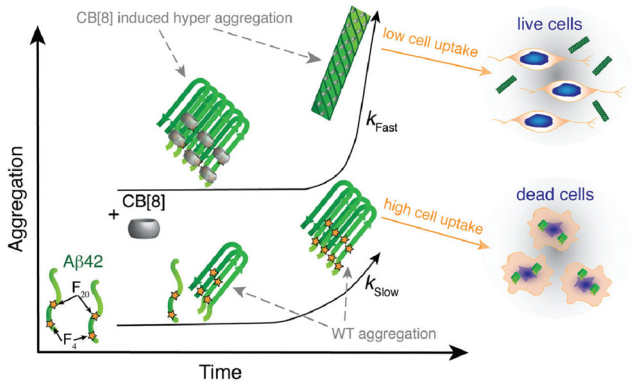

Fig. 29 Time-based aggregation of $A\beta_{1-42}$ in the presence and absence of Q8. Q8 induces the aggregates to grow faster and larger, and cell uptake and toxicity are reduced. CB[8] is Q8.[136] Reproduced from ref. 136 with permission from the Royal Society of Chemistry.

Hugh Kim, Kimoon Kim, and coworkers reported that Q6 can be used to control the length of amyloid fibrils of human insulin.[135] They showed that the length of low polydispersity (1.3) oligomers of insulin can be increased by increasing the Q6 concentration above its solubility limit. They proposed that length control is mediated by the coprecipitation of the Q6·insulin complex, which controls the concentration of available insulin monomer for fibrillation. This approach was extended to the control of the fibrillation for several other proteins, including human islet amyloid polypeptide, hen egg white lysozyme, $A\beta_{1-40}$, and $A\beta_{1-42}$.

Building on their early work showing that Q8 can dimerize fragments of Aβ by binding non-terminal Phe sites, Scherman and coworkers took a different approach to inhibiting the toxicity of amyloid fibrils by *promoting* fibrillation of $A\beta_{1-42}$ with Q8 (Fig. 29).[136] ITC analysis with $A\beta_{1-42}$ *versus* a Phe4Ala Phe19Ala Phe20Ala triple mutant suggested binding of Q8 at the three Phe sites, and CD data suggested pi-stacking between Phe side chains. An excess of Q8 accelerated elongation, and the $A\beta_{1-42}$ aggregates had lower toxicity and cell uptake in the presence *versus* absence of Q8, thus introducing a possible new approach to reducing amyloid toxicity.

Li, Zhu, Chen, and coworkers reported the inhibition of the fibrillation of human calcitonin (hCT) using Q7.[83] Alanine screening of the four aromatic residues showed a reduction in affinity in all mutants. Q7 increased L929 cell viability until it caused cytotoxicity. The addition of Q7 with hCT promoted proliferation, osteogenic differentiation, and osteogenesis of MC3T3 cells. The presence of Q7 was hypothesized to promote the activity of hCT, which would lead to increased cell proliferation. Q7 and hCT administered subcutaneously also resulted in calcitonin release and reduced serum calcium levels, which was thought to be due to the stabilization of calcitonin from fibrillation/aggregation. Q7 also decreased the immunogenicity of hCT. This paper sheds mechanistic light on a prior study by this group that reports a sustained release of hCT from a poly(D,L-lactic acid-*co*-glycolic acid)-*b*-poly(ethylene glycol)-*b*-poly(D,L-lactic acid) block copolymer hydrogel in the presence of excess Q7.[137]

Derrick, van der Walle, and coworkers reported that the colloidal stability of monoclonal antibodies containing an aggregation prone region (APR) is improved in the presence of Q7.[138] Using a combination of dynamic light scattering, intrinsic Trp fluorescence, ITC, and NMR spectroscopy, a comparative analysis of an antibody and its mutant deleting two aromatic residues from the APR makes the case for colloidal stability induced by binding of Q7 to the nonterminal aromatic residues. This group then reported the modulation of fibrillation of the HIV fusion inhibitor enfuvirtide (ENF) using Q7.[139] Alanine screening of the C-terminal Phe suggested single-site binding of Q7 at the C-terminus. Q7 delayed the onset of fibrillation of wild-type ENF. ENF/Q7 and mutant ENF fibrils exhibited comparable morphologies, differing from wild-type ENF fibrils, suggesting the potential for Q7 in determining fibril morphology. Hamilton and coworkers reported the inhibition of islet amyloid polypeptide (IAPP) aggregation through the recognition of N-terminal "hot segments" by Q7.[140] IAPP "hot segments" contain two Phe residues known to drive peptide aggregation. Q7 completely inhibited *de novo* and membrane-catalyzed fibril formation at 10 molar equivalents. Q7 also inhibited elongation and secondary nucleation caused by toxic preformed oligomers and rescued rat insulinoma cells from IAPP assembly-mediated cytotoxicity.

3.4. Supramolecular polymers and hydrogels

The synthesis of materials with dynamic properties is a major aim of modern chemistry. Such materials would have the advantages of being responsive to external stimuli, being self-healing, and having other properties that change in time. This section describes the use of cucurbit[*n*]urils to induce the reversible formation of polymer and hydrogel materials *via* interaction with materials modified with N-terminal aromatic amino acid residues. In a sense, this work could be viewed as utilizing affinity tags for reversible polymerization and gelation.

3.4.1. Linear supramolecular polymers. In parallel with the research of Liu and coworkers on the use of Q8 to reversibly polymerize proteins, as discussed in Section 3.3.2, Zhang and coworkers pursued the use of Q8 to reversibly polymerize water-soluble polymers.[141] They built an octa(ethylene glycol) chain monomer terminated on both ends with FGG-tags. The introduction of Q8 at a Q8 : monomer ratio of 1 : 1 induced supramolecular polymerization in aqueous solution at concentrations higher than the observed K_d (0.27 μM) (Fig. 30). This group then reported a two-step supramolecular polymerization based on a conjugate comprising an FGG-tag linked to diazobenzene.[142] Two equivalents of the conjugate bind to Q8 *via* the N-terminal Phe, and the resulting bivalent supramonomer polymerizes upon addition of a bivalent bis-β-cyclodextrin. Polymerization was reversible both by addition of a competitive guest for Q8 and by photoisomerization of the diazobenzene groups.

Liu, Dong, and coworkers reported the formation of supramolecular polymers from supramonomers comprising a 1 : 2 complex between Q8 and the hexapeptide H-Phe-Gly-Gly-Gly-Gly-Tyr-OH (Fig. 30).[143] Horseradish peroxidase (HRP) was used to induce the covalent cross-coupling of the tyrosine side chains to yield polymers. Liu, Xu, and coworkers added an extra Tyr residue, H-Phe-Gly-Gly-Gly-Tyr-Tyr-OH, which allowed for the crosslinking of polymer chains *via* HRP-mediated cross-coupling to form highly monodisperse, spherical "nanocapsules" (Fig. 31).[144] This hydrogel material was used to deliver doxorubicin antitumor agent and indocyanine green indicator to human breast cancer cells. Several other examples of supramolecular hydrogels are discussed in the next section.

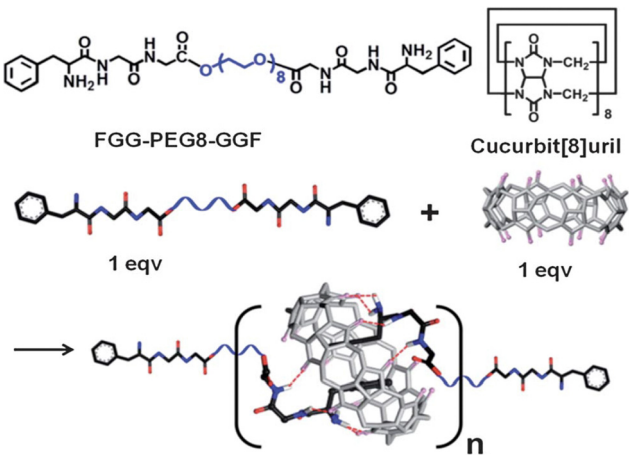

Fig. 30 Supramolecular polymerization of a bifunctional monomer with Q8 in aqueous solution.[141] Reproduced from ref. 141 with permission from the Royal Society of Chemistry.

3.4.2. Supramolecular hydrogels. The formation of supramolecular linear polymers and hydrogels depends on the self-assembly of multivalent compounds using Q8, akin to the work described in Section 2.2.[47] The linear supramolecular polymers use bivalent compounds, whereas hydrogels use compounds of higher valency, which effectively cross-link into network polymers. Scherman and coworkers pioneered the development of stimulus-responsive hydrogels based on the Q8-mediated crosslinking of polyvalent copolymers presenting viologen or naphthyl groups.[145,146] To reduce the toxicity and complexity of the system, this group used Q8 to homodimerize N-terminal Phe or Trp groups grafted onto a poly(styrene)-based backbone.[147] The resulting materials were dynamic, self-healing, cross-linked hydrogels that were stronger with N-terminal Phe groups than with N-terminal Trp groups, presumably due to their relative affinities for Q8. Scherman and coworkers reported supramolecular hydrogels comprising the polysaccharides hyaluronic acid, carboxymethyl cellulose, and hydroxyethyl cellulose grafted with H-Phe-Cys and cross-linked with Q8 (Fig. 32).[148] This approach allowed for hydrogel formation at 1–2 wt%, with stable hydrogels observed for hyaluronic acid and carboxymethyl cellulose with tunable rheological properties. Zhang, Serpe, and coworkers reported a method for synthesizing microgels based on supramolecular monomers ("supramonomers").[149] They synthesized supramonomers by conjugating FGG-tags to an acrylate group and using Q8 to dimerize the tags. These complexes were copolymerized with *N*-isopropylacrylamide to form stimulus-responsive microgels. Additional dynamic control over hydrogel properties was reported by Tan, Chen, and coworkers using a dual-cross-link strategy.[150] They synthesized poly(ε-Lys) and modified some of the α-amine sites with N-terminal Phe. Q8 was used to dimerize the Phe groups, and a dialdehyde-modified poly(ethylene glycol) (PEG) was used to dynamically cross-link the free amines *via* imine formation.

Supramolecular hydrogels have been used to demonstrate several applications in biomedical science. Scherman and coworkers reported the sustained release of bovine serum albumin from a Q8-mediated hydrogel comprising polyvalent copolymers presenting viologen and naphthyl groups.[151] Wang and coworkers reported a strategy for *in situ* activation of an antibiotic using Q8 as the activator (Fig. 33).[152] A polymer comprising a branched poly(ethyleneimine) was modified on the branches with N-terminal-Phe groups and cross-linked in the presence of Q8. The resulting hydrogel showed antibiotic activity with four bacterial cell lines, which was eliminated in the presence of a competitive guest for Q8.

In parallel with the report on supramolecular nanocapsules for drug delivery, as described in the previous section, Wang and coworkers reported the synthesis of supramolecular nanogels for stimulus-responsive drug delivery.[153] N-terminal Phe

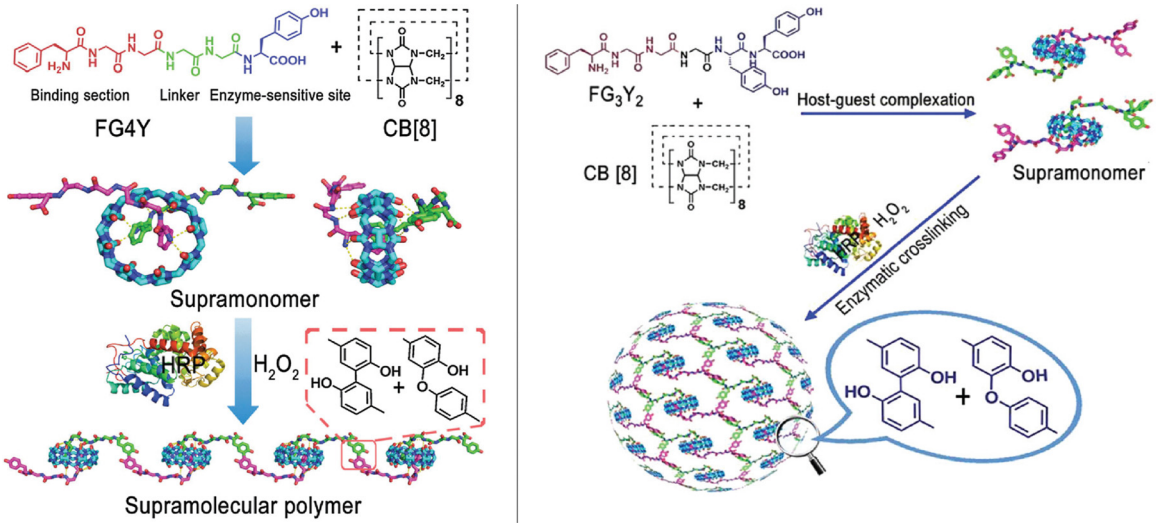

Fig. 31 Supramolecular polymers (left)[144] and hydrogels (right) mediated by Q8. CB[8] is Q8.[144] Reproduced from ref. 143 and 144 with permission from the Royal Society of Chemistry.

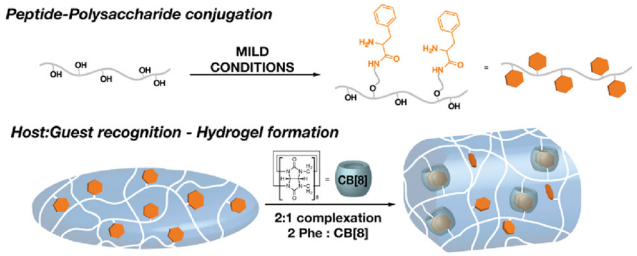

Fig. 32 Supramolecular hydrogels comprising polysaccharides grafted with N-terminal Phe and cross-linked by Q8. CB[8] is Q8.[148] Reproduced with permission from ref. 148. Copyright 2015 American Chemical Society.

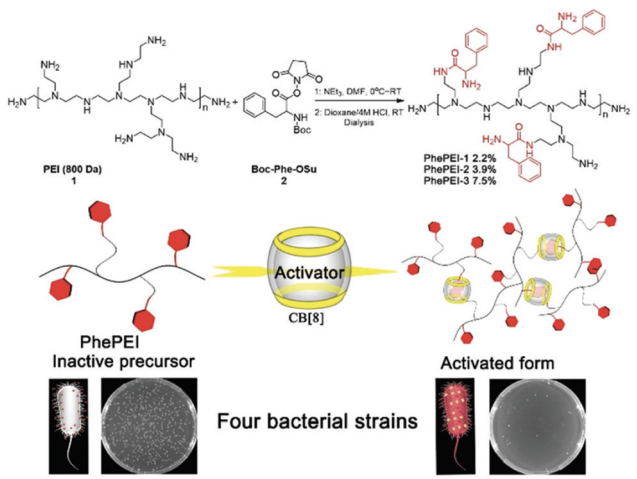

Fig. 33 An eco-friendly, *in situ* antibiotic that is reversibly activated by Q8-induced supramolecular crosslinking. CB[8] is Q8.[152] Reproduced from ref. 152 with permission from the Royal Society of Chemistry.

groups were grafted onto a chitosan scaffold and crosslinked using Q8 to form highly monodisperse and biocompatible hydrogels. The hydrogels released doxorubicin upon treatment with high-affinity competitors and were shown to be cell permeable and to reduce the toxicity of doxorubicin in two cell lines. Hu, Xu, Di, and coworkers reported an alternative approach to stimulus-responsive oral drug delivery for targeting intestinal microbiota (Fig. 34).[154] Mesoporous silica nanoparticles were loaded with the small molecule agent hydrocortisone and then capped with a supramolecular multilayer comprising chitosan grafted with N-terminal Trp groups and hyaluronic acid grafted with azobenzene groups, which were held together by Q8-mediated heteroternary complexes. *In vitro*, the multilayers disassembled in the presence of dithionite, a surrogate for azoreductase that reduces azobenzene to aniline, and released Cy5 fluorescent dye. In mice, the particles accumulated and released hydrocortisone in the colon, where azoreductase is released by intestinal microbiota.

Wang and coworkers reported a stimulus-responsive material that makes use of a specific peptide sequence for multimodal self-assembly and targeted drug delivery (Fig. 35).[155] The peptide H-Phe-Phe-Val-Leu-Lys-OH was designed to have a binding site for Q7 at the N-terminus and a sequence that would self-assemble in the absence of Q7. This peptide was conjugated *via* the Lys side chain to the antitumor agent camptothecin. Q7 complexed with the amphiphilic camptothecin conjugates, forming monodisperse micellar structures and entering cells. The structures decomposed when spermine, which was overexpressed in the cancer cells, competitively released the camptothecin conjugate from Q7. The conjugate then self-assembled into fibrils with improved accumulation, retention, and sustained release of camptothecin.

Das and coworkers reported the synthesis of a supramolecular hydrogel that promotes efficient cell adhesion and proliferation.[156] A peptide of sequence H-Phe-Gly-Gly-Lys-Tyr-Cys-Cys-Tyr-Arg-Gly-Asp-Ser-NH_2 was designed to contain a site for Q8-mediated supramolecular cross-linking *via* the N-terminal Phe, a binding site for integrins at the C-terminus,

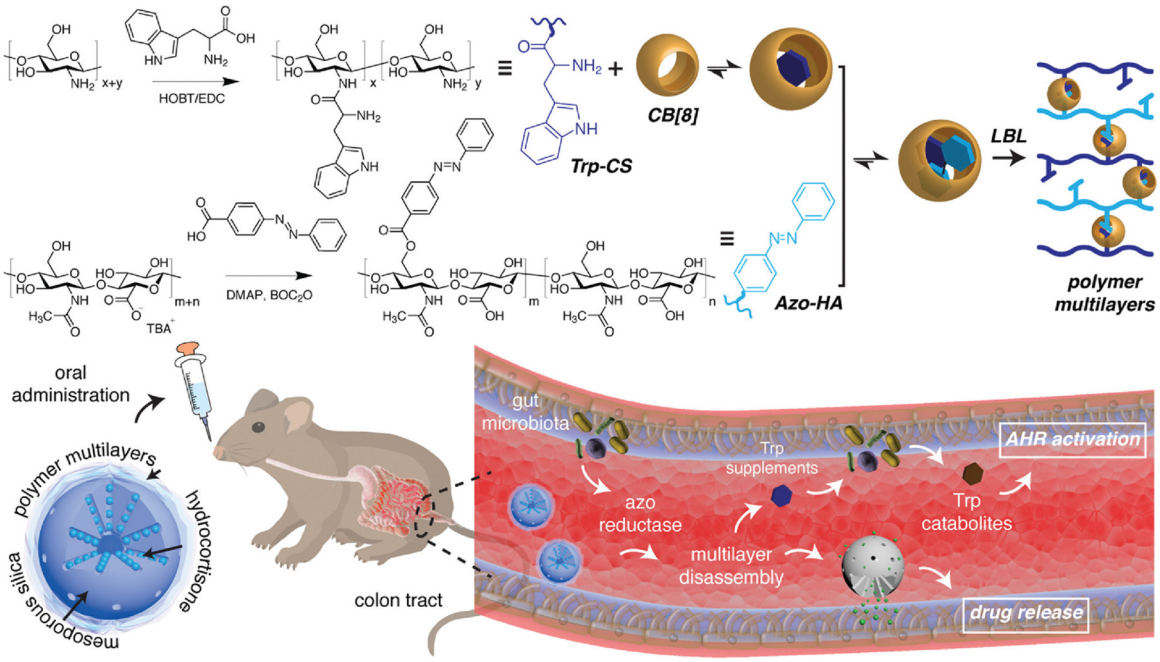

Fig. 34 Mesoporous silica nanoparticles capped with Q8-mediated multilayers that release cargo upon azobenzene reduction. CB[8] is Q8.[154] Reproduced from ref. 154 with permission from the Royal Society of Chemistry.

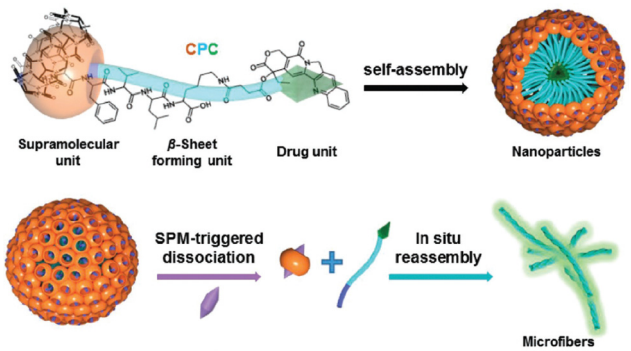

Fig. 35 Drug delivery strategy involving a drug conjugated to a pentapeptide designed to bind Q7, enter cells, release Q7, self-assemble into microfibers, and release the drug.[155] Reproduced with permission from ref. 155. © 2021 Wiley-VCH GmbH.

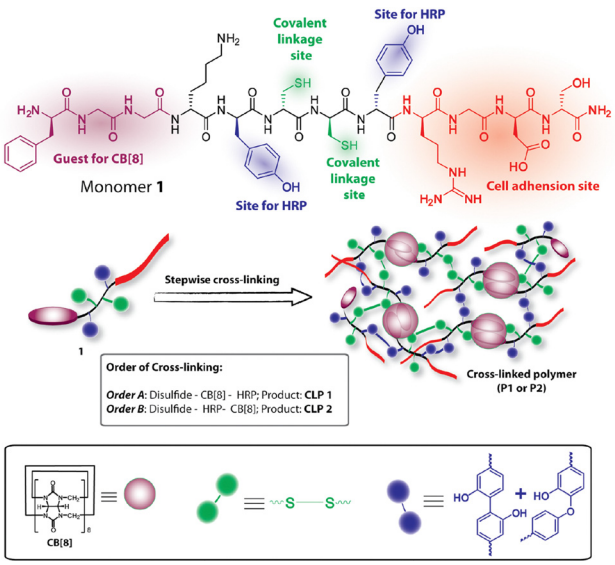

Fig. 36 Highly cross-linked, peptide-based, hydrogel capable of promoting cell adhesion and proliferation. CB[8] is Q8.[156] Reproduced with permission from ref. 156. Copyright 2018 American Chemical Society.

two Cys residues for covalent cross-linking *via* disulfide bond formation, and two Tyr residues for cross-linking *via* horseradish peroxidase (Fig. 36). The three mechanisms for cross-linking allowed for fine-tuning of particle size. Stable hydrogels presented integrin-binding sites on the surface. The particles were noncytotoxic and promoted efficient cell adhesion.

Myung and coworkers reported the synthesis of supramolecular hydrogels that encapsulate cells and are injectable.[157] Norbornene groups were grafted onto gelatin, and the ternary complex Q8·(H-Phe-Gly-Gly-Cys-OH)$_2$ was used to crosslink the polymers into a hydrogel *via* thiol–ene click chemistry with the Cys side chains. The resulting materials were optically transparent and injectable through an 18-gauge needle. Human fibroblasts grown in the hydrogel remained viable long after injection.

Supramolecular hydrogels based on self-assembling peptide amphiphiles (PA) are promising materials for modeling and engineering biological tissue. Mata, Azevedo, and coworkers reported on the Q8-mediated hydrogelation of peptide amphiphile nanofibers as an alternative to ion-based equivalents.[158] PA units comprising an N-terminal palmitoyl tail, a β-sheet-promoting amino acid sequence (V_3A_3), and three ionizable glutamic acid residues were engineered with either a Phe or Trp C-terminal amide. Upon self-assembly, the Phe and Trp

residues are presented at the surface of the nanofibers, allowing recognition and tunable gelation by Q8. Compared with Ca^{2+}-based PA hydrogels, Q8-based hydrogels formed more efficiently and required less Q8 than Ca^{2+} to achieve similar mechanical properties. Cell culture studies demonstrated the cell viability of the hydrogels and point toward the possibility of embedding cells during the gelation process.

3.5. Dynamic surfaces

Dynamic chemistry occurring at solid–liquid interfaces is ubiquitous in living systems and is necessary for many technologies such as heterogeneous catalysis, affinity purification, and sensors. Surfaces presenting ligands or receptors are effectively two-dimensional polyvalent materials. The capability of Q8 to bind two guests presents an opportunity to form polyvalent surfaces that dynamically trap and release ligands. One guest can be tethered to the surface covalently while the other can be the target solution-phase ligand. This section describes several applications involving dynamic surfaces that were made possible by the binding of cucurbit[*n*]urils to polypeptides.

Scherman and coworkers first described the use of dynamic supramolecular surface chemistry involving Q8-peptide interactions (Fig. 37).[159] Viologen groups were patterned on a self-assembled monolayer of alkanethiolates on Au and bound to Q8. Peptides containing an N-terminal Trp were captured selectively by heteroternary complex formation with the surface-bound Q8-viologen complexes and released selectively by single-electron reduction of the viologen. Capture and release were achieved for numerous cycles. This group then reported the synthesis of silica nanoparticles that present catenanes in which viologen axles are threaded through Q8 molecules and then covalently anchored on both ends to the surface.[160] The functional surfaces of these superparamagnetic nanoparticles bound to aromatic compounds, including amino acids and peptides, *via* the Q8 groups, with selectivity for Phe- and Trp-containing peptides *versus* nonaromatic peptides. The captured peptides could then be released from the nanoparticles by single-electron reduction of the viologens. They also used a dynamic surface presenting Q8·viologen groups to select for high-affinity peptides *via* phage display, as mentioned in Section 2.4.[42]

Li and coworkers demonstrated the synthesis of native protein multilayers mediated by Q8.[161] Q8 spontaneously coated a silica surface presenting ammonium groups, and multilayers of hemoglobin and/or catalase were applied, with Q8 adhering the layers. Catalase retained its catalytic activity when assembled. Lysozyme, glucose oxidase, bovine serum albumin, and β-lactoglobulin did not assemble in this fashion, suggesting the necessity of selective binding. Free Q8 was also shown to aggregate solutions of hemoglobin, catalase, glutathione-*S*-transferase, and insulin in a process that was reversible upon the addition of methyl viologen. Q6 and Q7 did not aggregate proteins, suggesting the necessity of the dimerization capacity of Q8.

Jonkheijm and coworkers reported a series of studies demonstrating the power of supramolecular chemistry for making dynamic surfaces that can manipulate living cells. They first reported a bioactive monolayer for cell adhesion with a

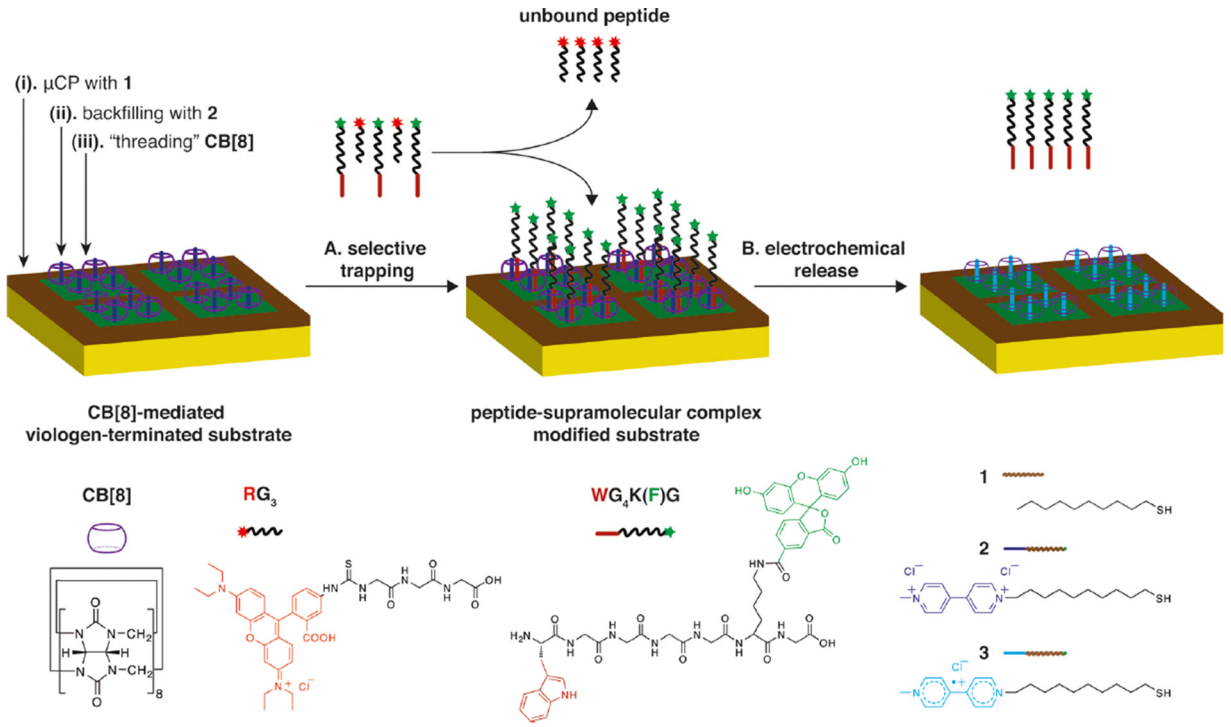

Fig. 37 Reversible, supramolecular capture and release of peptides mediated by the binding and redox properties of the surface-bound viologen. CB[8] is Q8.[159] Reproduced with permission from ref. 159. Copyright 2010 American Chemical Society.

reversible electrochemical switch.[162] Viologen groups were presented on a self-assembled monolayer of alkanethiolates on Au, which recruited Q8. Peptides of sequence H-Trp-Gly-Gly-Arg-Gly-Asp-Ser-OH were designed to contain an N-terminal Trp binding site for the surface-bound Q8·viologen complexes and an RGD site for integrin binding in order to drive cell adhesion. In the presence of Q8, the peptides bound to the surface, and cell adhesion was observed. Cells could then be released electrochemically *via* reduction of the viologen groups. They then engineered bacterial cells to present on their surfaces miniproteins containing a disordered loop with the sequence Gly-Gly-Trp-Gly-Gly.[163] Q8 mediated the assembly of these cells in a concentration-dependent and sequence-selective manner and was inhibited by the competitive binding of H-Phe-Gly_6-OH. These cells also bound to a surface presenting viologen groups and showed enhanced motility, presumably mediated by reversible multivalent interactions at the surface. They then developed a strategy to immobilize knottin miniproteins on a self-assembled monolayer and capture its cognate binding partner, β-trypsin (Fig. 38).[164] Knottins were genetically engineered to contain one or two Gly-Gly-Trp-Gly-Gly sites for binding to surface-immobilized Q8·viologen complexes. Binding was improved for the divalent *versus* monovalent knottins, and surface adhesion of trypsin only occurred for the divalent knottin. All knottins were strong inhibitors of trypsin in solution. In a subsequent study, they produced knottins containing one, two, three, or four Gly-Gly-Trp-Gly-Gly binding sites and found that the binding affinity to surfaces presenting Q8·viologen complexes correlated with the valency of the knottins.[165] The knottins also contained an RGD site for cell adhesion, and the higher valency knottins mediated greater cell elongation and more pronounced focal adhesion.

Brunsveld and coworkers demonstrated the reversible immobilization of a protein on lipid bilayers.[166] A supported bilayer comprising dioleylphosphatidylcholine on silica-coated quartz was prepared and treated with a cholesterol-viologen conjugate, which incorporated into the bilayer to present viologen groups on the surface (Fig. 39). Q8 was used to immobilize yellow fluorescent proteins (YFP) tagged with N-terminal H-Trp-Gly-Gly (WGG-YFP) or H-Met-Gly-Gly (MGG-YFP). Both proteins bound to the surfaces, but MGG-YFP bound more weakly than FGG-YFP. The binding of WGG-YFP *vs.* MGG-YFP was also studied in solution, and although MGG did not bind Q8, MGG-YFP bound Q8 with similar affinity as WGG-YFP, indicating that the Q8·MGG-YFP complex is likely mediated by a nonterminal binding site. Protein binding was reversible upon addition of Q8. Brunsveld, Dankers, and coworkers then used Q8 to reversibly immobilize proteins on the surface of a thermoplastic elastomer.[167] H-Phe-Gly-Gly-Lys was conjugated to a 2-uriedo-4-pyrimidinone (UPy) group *via* the Lys side chain to generate FGGK(UPy). This conjugate was mixed with a thermoelastic polymer and drop-coated or spin-coated onto surfaces. In the presence of Q8, the FGG-containing surfaces pulled down FGG-YFP selectively *versus* MGG-YFP. The complex disassembled when washed.

Wang and coworkers used the Q7·Phe interaction to prepare a dynamic material capable of selectively isolating proteins containing methylated Lys *via* affinity purification.[168] A resin presenting covalently bound Q7 groups was coated with the peptide H-Phe-Gly-Gly-Ala-Ala-Pro-Gly-Phe-pTyr-X-Glu-Ala-Gln (pTyr is phosphotyrosine, X is a noncanonical residue presenting a chloroacetyl group). The C-terminal domain of this peptide binds the protein PLCγ1 and covalently attaches to a Cys residue *via* coupling with the chloroacetyl group. A PLCγ1 domain was inserted into the HP1β CD-PLCγ1-c-SH2 fusion protein, which was then conjugated to the peptide-coated resin. The HP1β CD domain binds selectively to methylated Lys

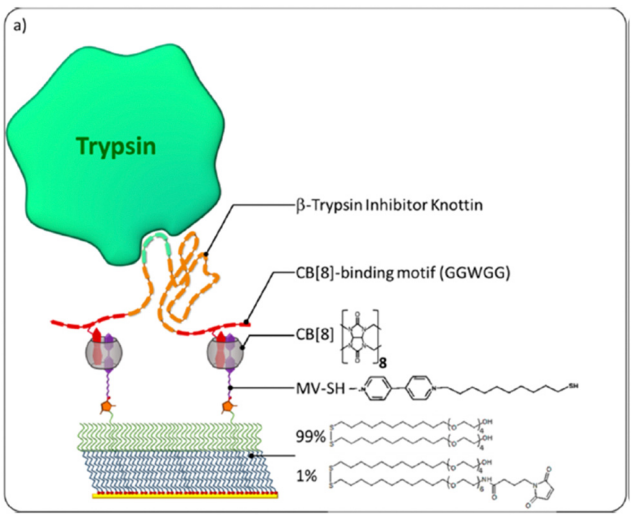

Fig. 38 Surface for reversibly immobilizing functional mini-proteins for enzyme inhibition. CB[8] is Q8.[164] Reproduced with permission from ref. 164. Copyright 2015 American Chemical Society.

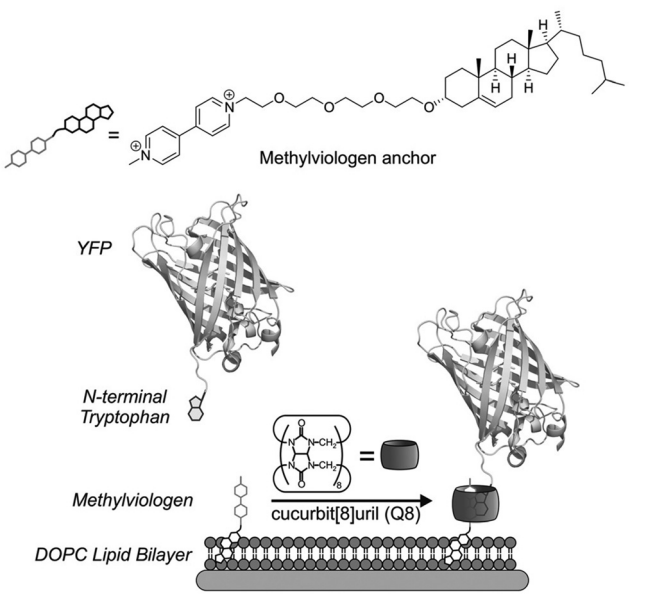

Fig. 39 Reversible immobilization of WGG-labeled proteins on a supported bilayer.[166] Reproduced with permission from ref. 166. © 2015 Wiley-VCH Verlag GmbH & Co. KGaA, Weinheim.

residues, and this material was used to enrich cell extract with methyl Lys-containing proteins, allowing for the identification of 255 proteins *via* mass spectrometric analysis of the trypsinized extract. A gentle elution of the protein of interest was achieved by adding amantadine to competitively release the peptide.

3.6. Protein drug formulation

Conjugating pharmaceutical proteins with poly(ethylene glycol) (PEG) is known to stabilize the proteins, inhibit aggregation, and limit proteolytic degradation. However, the covalent modification complicates isolation and purification of the protein after labeling and may alter protein function. Anderson, Langer, Isaacs, and coworkers demonstrated a novel supramolecular approach to stabilizing biopharmaceuticals by reversibly attaching Q7-PEG conjugates to the native Phe^{B1} affinity tag in human insulin.[169] Q7 was covalently conjugated to PEG chains of varying length (M_n = 5, 10, or 30 kDa) *via* copper-free click chemistry, and the conjugates spontaneously bound to insulin (Fig. 40). PEGylation did not significantly change the secondary structure of insulin or the affinity of Q7 for insulin. With agitation, insulin aggregated in the presence and absence of Q7 and PEG, but not in the presence of Q7-PEG, even after 100 days. The 100-day aged insulin stabilized by Q7-PEG retained its full activity. At pharmaceutical concentrations, Q7-PEG was also able to stabilize proteins without an N-terminal Phe residue. Q7-PEG stabilized an antibody, which was fully active after 24 hours, and Q7-PEG stabilized glucagon, which was fully soluble after 24 h. *In vivo*, insulin and Q7-PEG delivered subcutaneously to diabetic mice prolonged normoglycemia for time durations that correlated with the length of the PEG chain. This observation was believed to be due to delayed absorption *via* lymphatic circulation of the larger molecular weight complexes.

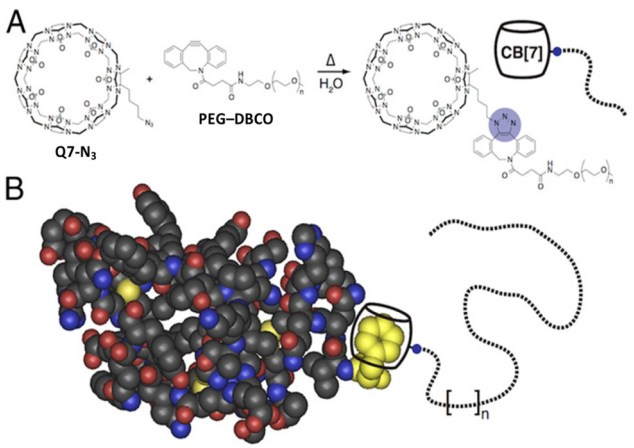

Fig. 40 (A) Copper-free click reaction carried out between azidobutyl-Q7 and PEG polymer with dibenzocyclooctyne-modified PEG chains. (B) Supramolecular PEGylation of insulin *via* the Phe^{B1} residue (yellow). CB[7] is Q7.[169] Reproduced with permission from ref. 169. Copyright 2016 National Academy of Sciences.

Continuing this line of inquiry, Webber, Appel, and coworkers demonstrated that Q7-PEG stabilizes the fast-acting insulin aspart and lispro analogues in their monomeric states and reduces aggregation.[170] They also demonstrated that Q7-PEG can stabilize co-formulations of insulin and pramlintide and improve the pharmacokinetics of this dual hormone therapy.[171] They then conjugated Q7 to proteins and demonstrated that the affinity of guest-conjugated PEG chains to Q7-protein correlates directly to the time of total insulin exposure, which is likely governed by the absorption rate.[172]

One concern in the supramolecular PEGylation of insulin is the prolonged *in vivo* duration of action due to sustained complex formation in the subcutaneous depot. Webber, Chou, and coworkers demonstrated the ability to tune the duration of action while preserving the stabilizing effects of PEGylation by engineering N-terminal acid-modified insulin analogs, which bind with weaker affinity for Q7.[80] Another challenge with supramolecular PEGylation is biodegradability and intracellular accumulation. Seeking a more biocompatible method, Kramer and coworkers demonstrated the stabilization of insulin and calcitonin by Q7 conjugated with zwitterionic polypeptides.[173] Inhibition of protein aggregation was directly correlated with the length of the zwitterionic chain. Treatment of the zwitterionic chain with natural proteases led to steady biodegradation.

3.7. Facilitating polypeptide modification

Site-selective modification of proteins is an area of intense current interest, with broad application in biochemistry and biomedical science. The ability of cucurbit[*n*]urils to bind site-selectively to peptides and proteins has inspired work in this area. Appel and coworkers demonstrated the use of Q7 as a protecting group for protein modification.[174] Q7 was used to bind the Phe^{B1} position of insulin and effectively protect the N-terminal amine from electrophilic attack by keeping it protonated, while a PEG chain was coupled site-selectively and covalently to the unprotected N-terminal amine of the A-chain. Li, Li, and coworkers demonstrated regioselective coupling *via* Michael addition to a Cys residue with a proximal Trp.[175] A peptide presenting a viologen group and a dehydroalanine residue was bound to Q8 and then to a series of peptides, with varying distance between Trp and Cys residues. The efficiency of coupling was shown to depend on the sequence order and the distance between the Trp and Cys residues.

4. Outlook

The applications described in Section 3 exemplify the extraordinary capabilities of cucurbit[*n*]urils in the context of bioscience and biotechnology. From sensing and separations to effectors and inhibitors of protein assembly, the interactions of Q7 and Q8 with peptides and proteins are strong, predictably selective, and compatible with a wide range of useful conditions, including protein mixtures, living cells, and mice. This system is practical in part because Q7 and Q8 are commercially

available and readily accessible synthetically and function in neutral aqueous buffer at working concentrations that are compatible with many measurement techniques. This system is also practical in part because much is known about the chemistry of peptides and proteins, including their chemical synthesis, biosynthesis, and posttranslational modification, and the engineering and use of affinity tags. Q8 provides the powerful capability of reversible, noncovalent dimerization of peptides and proteins with one another and with a functional guest. The principles for molecular recognition in this system described in Section 2 are well understood and enable highly predictive, programmable, and switchable binding. Taken together, these properties are extraordinary and should enable the development of many more applications. We are particularly excited by the recent work on stabilizing protein drug formulations. We envision further development of methods for the selective enrichment and analysis of complex mixtures, the synthesis of functional hydrogels for tissue engineering, the synthesis of probes for biological processes, the creation of selective agents for biological imaging, and the creation of catalysts for site-selective protein modification. It will be exciting to see what the next decade of creativity brings to bear.

Data availability

This review article contains no new data. All presented data are reproduced from other published sources, which are cited within the article.

Conflicts of interest

There are no conflicts to declare.

Acknowledgements

This paper is dedicated to Prof. George M. Whitesides on the occasion of his 85th birthday and in appreciation for his mentorship and his extraordinary contributions to science. We gratefully acknowledge financial support from the National Institutes of Health (GM141708), the Welch Foundation (W-1640 and W-0031), and Trinity University.

References

1 C. L. Young, Z. T. Britton and A. S. Robinson, *Biotechnol. J.*, 2012, **7**, 620–634.
2 J.-C. Janson, *Protein Purification: Principles, High Resolution Methods, and Applications*, Wiley, Hoboken, USA, 3rd edn, 2011.
3 O. Boutureira and G. J. L. Bernardes, *Chem. Rev.*, 2015, **115**, 2174–2195.
4 V. Mishra, Affinity Tags for Protein Purification, *Curr. Protein Pept. Sci.*, 2020, **21**, 821–830.
5 P. N. Hengen, *Trends Biochem. Sci.*, 1995, **20**, 285–286.
6 C. Zhao, L. M. Hellman, X. Zhan, W. S. Bowman, S. W. Whiteheart and M. G. Fried, *Anal. Biochem.*, 2010, **399**, 237–245.
7 J. Arnau, C. Lauritzen, G. E. Petersen and J. Pedersen, *Protein Expression Purif.*, 2006, **48**, 1–13.
8 M. H. Hefti, J. G. Caroline, V. V. der Toorn, R. Dixon and J. A. Vervoort, *Anal. Biochem.*, 2001, **295**, 180–185.
9 E. S. Day, S. M. Cote and A. Whitty, *Biochemistry*, 2012, **51**, 9124–9136.
10 E. Cha, N. Clements, C. Hofman, B. Lavoie, A. Van Zile, L. Warden and A. R. Urbach, in *Supramolecular Protein Chemistry*, ed. P. Crowley, Royal Society of Chemistry, Cambridge, UK, 2020.
11 E. S. Istvan and J. Deisenhofer, *Science*, 2001, **292**, 1160–1164.
12 R. E. McGovern, H. Fernandes, A. R. Khan, N. P. Power and P. B. Crowley, *Nat. Chem.*, 2012, **4**, 527–533.
13 J. Habchi, P. Tompa, S. Longhi and V. N. Uversky, *Chem. Rev.*, 2014, **114**, 6561–6588.
14 M. W. Peczuh and A. D. Hamilton, *Chem. Rev.*, 2000, **100**, 2479–2494.
15 M. Giese, J. Niemeyer and J. Voskuhl, *ChemPlusChem*, 2020, **85**, 985–997.
16 S. Tashiro, M. Kobayashi and M. Fujita, *J. Am. Chem. Soc.*, 2006, **128**, 9280–9281.
17 C. Dolain, Y. Hatakeyama, T. Sawada, S. Tashiro and M. Fujita, *J. Am. Chem. Soc.*, 2010, **132**, 5564–5565.
18 L. M. Heitmann, A. B. Taylor, P. J. Hart and A. R. Urbach, *J. Am. Chem. Soc.*, 2006, **128**, 12574–12581.
19 M. V. Rekharsky, H. Yamamura, Y. H. Ko, N. Selvapalam, K. Kim and Y. Inoue, *Chem. Commun.*, 2008, 2236–2238.
20 J. Lagona, P. Mukhopadhyay, S. Chakrabarti and L. Isaacs, *Angew. Chem., Int. Ed.*, 2005, **44**, 4844–4870.
21 S. J. Barrow, S. Kasera, M. Cao, J. Rowland, J. del Barrio and O. A. Scherman, *Chem. Rev.*, 2015, **115**, 12320–12406.
22 K. Kim, *Cucurbiturils and Related Macrocycles*, Royal Society of Chemistry, Croydon, UK, 1st edn, 2020.
23 F. Biedermann, W. M. Nau and H.-J. Schneider, *Angew. Chem., Int. Ed.*, 2014, **53**, 11158–11171.
24 A. E. Kaifer, *Isr. J. Chem.*, 2018, **58**, 244–249.
25 S. Liu, C. Ruspic, P. Mukhopadhyay, S. Chakrabarti, P. Y. Zavalij and L. Isaacs, *J. Am. Chem. Soc.*, 2005, **127**, 15959–15967.
26 M. V. Rekharsky, T. Mori, C. Yang, Y. H. Ko, N. Selvapalam, H. Kim, D. Sobransingh, A. E. Kaifer, S. Liu, L. Isaacs, W. Chen, S. Moghaddam, M. K. Gilson, K. Kim and Y. Inoue, *Proc. Natl. Acad. Sci. U. S. A.*, 2007, **104**, 20737–20742.
27 J. Kim, I.-S. Jung, S.-Y. Kim, E. Lee, J.-K. Kang, S. Sakamoto, K. Yamaguchi and K. Kim, *J. Am. Chem. Soc.*, 2000, **122**, 540–541.
28 H.-J. Kim, J. Heo, W. S. Jeon, E. Lee, J. Kim, S. Sakamoto, K. Yamaguchi and K. Kim, *Angew. Chem., Int. Ed.*, 2001, **40**, 1526–1529.
29 L. Cao, M. Śekutor, P. Y. Zavalij, K. Mlinarić-Majerski, R. Glaser and L. Isaacs, *Angew. Chem., Int. Ed.*, 2014, **53**, 988–993.

30 M. E. Bush, N. D. Bouley and A. R. Urbach, *J. Am. Chem. Soc.*, 2005, **127**, 14511–14517.
31 K. Kim, J. Kim, I.-S. Jung, S.-Y. Kim, E. Lee and J.-K. Kang, *Cucurbituril derivatives, their preparation methods and uses*, *US Pat.*, US6365734, 2000.
32 P. Rajgariah and A. R. Urbach, *J. Inclusion Phenom. Macrocyclic Chem.*, 2008, **62**, 251–254.
33 C. Chothia, *J. Mol. Biol.*, 1976, **105**, 1–12.
34 A. Radzicka and R. Wolfenden, *Biochemistry*, 1998, **27**, 1664–1670.
35 W. C. Wimley and S. H. White, *Nat. Struct. Biol.*, 1996, **3**, 842–848.
36 D. W. Johnson and F. Hof, *Aromatic Interactions: Frontiers in Knowledge and Application in Supramolecular Chemistry*, Royal Society of Chemistry, Croydon, UK, 2017.
37 L. M. Espinoza-Fonseca, *Mol. BioSyst.*, 2012, **8**, 237–246.
38 T. Clackson and J. A. Wells, *Science*, 1995, **267**, 383–386.
39 A. A. Bogan and K. S. Thorn, *J. Mol. Biol.*, 1998, **280**, 1–9.
40 O. A. Ali, E. M. Olson and A. R. Urbach, *Supramol. Chem.*, 2013, **25**, 863–868.
41 R. P. G. Bosmans, W. E. Hendriksen, M. Verheijden, R. Eelkema, P. Jonkheijm, J. H. van Esch and L. Brunsveld, *Chem. – Eur. J.*, 2015, **21**, 18466–18473.
42 S. Sonzini, A. Marcozzi, R. J. Gubeli, C. F. van der Walle, P. Ravn, A. Herrmann and O. A. Scherman, *Angew. Chem., Int. Ed.*, 2016, **55**, 14000–14004.
43 F. Biedermann, U. Rauwald, M. Cziferszky, K. A. Williams, L. D. Gann, B. Y. Guo, A. R. Urbach, C. W. Bielawski and O. A. Scherman, *Chem. – Eur. J.*, 2010, **16**, 13716–13722.
44 X. Chen, Z. Huang, R. L. Sala, A. M. McLean, G. Wu, K. Sokolowski, K. King, J. A. McCune and O. A. Scherman, *J. Am. Chem. Soc.*, 2022, **144**, 8474–8479.
45 A. Barba-Bon, Y.-C. Pan, F. Biedermann, D.-S. Guo, W. M. Nau and A. Hennig, *J. Am. Chem. Soc.*, 2019, **141**, 20137–20145.
46 F. Biedermann and O. A. Scherman, *J. Phys. Chem. B*, 2012, **116**, 2842–2849.
47 J. J. Reczek, A. A. Kennedy, B. T. Halbert and A. R. Urbach, *J. Am. Chem. Soc.*, 2009, **131**, 2408–2415.
48 M. Mammen, S.-K. Choi and G. M. Whitesides, *Angew. Chem., Int. Ed.*, 1998, **37**, 2754–2794.
49 E. Cavatorta, P. Jonkheijm and J. Huskens, *Chem. – Eur. J.*, 2017, **23**, 4046–4050.
50 S. Sonzini, S. T. J. Ryan and O. A. Scherman, *Chem. Commun.*, 2013, **49**, 8779.
51 G. Wu, D. E. Clarke, C. Wu and O. A. Scherman, *Org. Biomol. Chem.*, 2019, **17**, 3514–3520.
52 H. Barbero and E. Masson, *Chem. Sci.*, 2021, **12**, 9962–9968.
53 R. J. Fernandes, P. Remón, A. J. Moro, A. Seco, A. S. D. Ferreira, U. Pischel and N. Basílio, *J. Org. Chem.*, 2021, **86**, 8472–8478.
54 E. Zaorska and M. Malinska, *Chem. – Eur. J.*, 2024, **30**, e202302250.
55 H. D. Nguyen, D. T. Dang, J. L. J. van Dongen and L. Brunsveld, *Angew. Chem., Int. Ed.*, 2010, **49**, 895–898.
56 D. T. Dang, H. D. Nguyen, M. Merkx and L. Brunsveld, *Angew. Chem., Int. Ed.*, 2013, **52**, 2915–2919.
57 C. Hou, J. Li, L. Zhao, W. Zhang, Q. Luo, Z. Dong, J. Xu and J. Liu, *Angew. Chem., Int. Ed.*, 2013, **52**, 5590–5593.
58 G. Li, W.-Y. Yang, Y.-F. Zhao, Y.-X. Chen, L. Hong and Y.-M. Li, *Chem. – Eur. J.*, 2018, **24**, 13647–13653.
59 F. Biedermann, U. Rauwald, M. Cziferszky, K. A. Williams, L. D. Gann, B. Y. Guo, A. R. Urbach, C. W. Bielawski and O. A. Scherman, *Chem. – Eur. J.*, 2010, 7.
60 L. C. Smith, D. G. Leach, B. E. Blaylock, O. A. Ali and A. R. Urbach, *J. Am. Chem. Soc.*, 2015, **137**, 3663–3669.
61 Z. Hirani, H. F. Taylor, E. F. Babcock, A. T. Bockus, C. D. Varnado, C. W. Bielawski and A. R. Urbach, *J. Am. Chem. Soc.*, 2018, **140**, 12263–12269.
62 D. E. Clarke, G. Wu, C. Wu and O. A. Scherman, *J. Am. Chem. Soc.*, 2021, **143**, 6323–6327.
63 P. Suating, M. B. Ewe, L. B. Kimberly, H. D. Arman, D. J. Wherritt and A. R. Urbach, *Chem. Sci.*, 2024, **15**, 5133–5142.
64 P. Suating, L. B. Kimberly, M. B. Ewe, S. L. Chang, J. M. Fontenot, P. R. Sultane, C. W. Bielawski, D. A. Decato, O. B. Berryman, A. B. Taylor and A. R. Urbach, *J. Am. Chem. Soc.*, 2024, **146**, 7649–7657.
65 G. Wu, M. Olesinska, Y. Wu, D. Matak-Vinkovic and O. A. Scherman, *J. Am. Chem. Soc.*, 2017, **139**, 3202–3208.
66 M. V. Rekharsky, H. Yamamura, C. Inoue, M. Kawai, I. Osaka, R. Arakawa, K. Shiba, A. Sato, Y. H. Ko, N. Selvapalam, K. Kim and Y. Inoue, *J. Am. Chem. Soc.*, 2006, **128**, 14871–14880.
67 M. V. Rekharsky, H. Yamamura, Y. H. Ko, N. Selvapalam, K. Kim and Y. Inoue, *Chem. Commun.*, 2008, 2236.
68 J. M. Chinai, A. B. Taylor, L. M. Ryno, N. D. Hargreaves, C. A. Morris, P. J. Hart and A. R. Urbach, *J. Am. Chem. Soc.*, 2011, **133**, 8810–8813.
69 L. A. Logsdon, C. L. Schardon, V. Ramalingam, S. K. Kwee and A. R. Urbach, *J. Am. Chem. Soc.*, 2011, **133**, 17087–17092.
70 H. R. Anderson, W. L. Reeves, A. T. Bockus, P. Suating, A. G. Grice, M. Gallagher and A. R. Urbach, *Bioconjugate Chem.*, 2023, **34**, 212–217.
71 G. Ghale, V. Ramalingam, A. R. Urbach and W. M. Nau, *J. Am. Chem. Soc.*, 2011, **133**, 7528–7535.
72 R. Jiang, M. Nilam, A. Hennig and W. Nau, *Adv. Mater.*, 2024, **36**, 2306922.
73 L. A. Logsdon and A. R. Urbach, *J. Am. Chem. Soc.*, 2013, **135**, 11414–11416.
74 S. Zhang, L. Grimm, Z. Miskolczy, L. Biczok, F. Biedermann and W. M. Nau, *Chem. Commun.*, 2019, **55**, 14131–14134.
75 W. Cao, W. Qin, Y. Wang, Z. Dai, X. Dai, H. Wang, W. Xuan, Y. Zhang, Y. Liu and T. Liu, *Angew. Chem., Int. Ed.*, 2021, **60**, 11196–11200.
76 F. Ma, X. Zheng and Z. Li, *Phys. Chem. Chem. Phys.*, 2021, **23**, 13724–13733.
77 F. Ma, X. Zheng, L. Xie and Z. Li, *J. Mol. Liq.*, 2021, **328**, 115479.
78 H. D. Nguyen, D. T. Dang, J. L. J. van Dongen and L. Brunsveld, *Angew. Chem., Int. Ed.*, 2010, **49**, 895–898.

79 W. Li, A. T. Bockus, B. Vinciguerra, L. Isaacs and A. R. Urbach, *Chem. Commun.*, 2016, **52**, 8537–8540.
80 R. Meudom, Y. Zhang, M. A. VandenBerg, L. Zou, Y. W. Zhang, M. J. Webber and D. H.-C. Chou, *Acta Pharm. Sin. B*, 2023, **13**, 2281–2290.
81 C. L. Maikawa, A. A. A. Smith, L. Zou, G. A. Roth, E. C. Gale, L. M. Stapleton, S. W. Baker, J. L. Mann, A. C. Yu, S. Correa, A. K. Grosskopf, C. S. Liong, C. M. Meis, D. Chan, M. Troxell, D. M. Maahs, B. A. Buckingham, M. J. Webber and E. A. Appel, *Nat. Biomed. Eng.*, 2020, **4**, 507–517.
82 H. H. Lee, T. S. Choi, S. J. C. Lee, J. W. Lee, J. Park, Y. H. Ko, W. J. Kim, K. Kim and H. I. Kim, *Angew. Chem., Int. Ed.*, 2014, **53**, 7461–7465.
83 H. Shang, A. Zhou, J. Jiang, Y. Liu, J. Xie, S. Li, Y. Chen, X. Zhu, H. Tan and J. Li, *Acta Biomater.*, 2018, **78**, 178–188.
84 E. Jacob and R. Unger, *Bioinformatics*, 2007, **23**, e225–e230.
85 V. N. Uversky, V. Dave, L. M. Iakoucheva, P. Malaney, S. J. Metallo, R. P. Pathak and A. C. Joerger, *Chem. Rev.*, 2014, **114**, 6844–6879.
86 A. Varshavsky, *Proc. Natl. Acad. Sci. U. S. A.*, 2019, **116**, 358–366.
87 G. Roman-Hernandez, R. A. Grant, R. T. Sauer and T. A. Baker, *Proc. Natl. Acad. Sci. U. S. A.*, 2009, **106**, 8888–8893.
88 E. Matta-Camacho, G. Kozlov, F. F. Li and K. Gehring, *Nat. Struct. Mol. Biol.*, 2010, **17**, 1182–1187.
89 D. M. Bailey, A. Hennig, V. D. Uzunova and W. M. Nau, *Chem. – Eur. J.*, 2008, **14**, 6069–6077.
90 M. A. Gamal-Eldin and D. H. Macartney, *Org. Biomol. Chem.*, 2013, **11**, 488–495.
91 F. Guagnini, P. M. Antonik, M. L. Rennie, P. O'Byrne, A. R. Khan, R. Pinalli, E. Dalcanale and P. B. Crowley, *Angew. Chem., Int. Ed.*, 2018, **57**, 7126–7130.
92 F. Guagnini, S. Engilberge, K. O. Ramberg, J. Perez and P. B. Crowley, *Chem. Commun.*, 2020, **56**, 360–363.
93 F. Guagnini, S. Engilberge, R. J. Flood, K. O. Ramberg and P. B. Crowley, *Cryst. Growth Des.*, 2020, **20**, 6983–6989.
94 K. O. Ramberg, F. Guagnini, S. Engilberge, M. A. Wronska, M. L. Rennie, J. Perez and P. B. Crowley, *Chem. – Eur. J.*, 2021, **27**, 1–10.
95 K. O. Ramberg and P. B. Crowley, *J. Struct. Biol.*, 2023, **215**, 107969.
96 J. Lee, L. Perez, Y. Liu, H. Wang, R. J. Hooley and W. Zhong, *Anal. Chem.*, 2018, **90**, 1881–1888.
97 K. O. Ramberg, S. Engilberge, F. Guagnini and P. B. Crowley, *Org. Biomol. Chem.*, 2021, **19**, 837–844.
98 L. You, D. Zha and E. V. Anslyn, *Chem. Rev.*, 2015, **115**, 7840–7892.
99 Y. Ling, W. Wang and A. E. Kaifer, *Chem. Commun.*, 2007, 610–612.
100 F. Biedermann and W. M. Nau, *Angew. Chem., Int. Ed.*, 2014, **53**, 5694–5699.
101 A. Prabodh, Y. Wang, S. Sinn, P. Albertini, C. Spies, E. Spuling, L.-P. Yang, W. Jiang, S. Bräse and F. Biedermann, *Chem. Sci.*, 2021, **12**, 9420–9431.
102 G. H. Aryal, L. Huang and K. W. Hunter, *RSC Adv.*, 2016, **6**, 82566–82570.
103 D. Maity, K. I. Assaf, W. Sicking, C. Hirschhäuser, W. M. Nau and C. Schmuck, *Chem. – Eur. J.*, 2019, **25**, 13088–13093.
104 F. Biedermann, G. Ghale, A. Hennig and W. M. Nau, *Commentat. Biol.*, 2020, **3**, 1–10.
105 L. Wei, X. Wang, C. Li, X. Li, Y. Yin and G. Li, *Biosens. Bioelectron.*, 2015, **71**, 348–352.
106 H. Wang, Y. Fan, B. Chen, J. Lei, S. Yu, X. Chen and X. Hou, *Nat. Commun.*, 2022, **13**, 1906–1914.
107 Y. Li, Q. Li, X. Miao, C. Qin, D. Chu and L. Cao, *Angew. Chem., Int. Ed.*, 2021, **60**, 6744–6751.
108 C. Yan, Q. Li, X. Miao, Y. Zhao, Y. Li, P. Wang, K. Wang, H. Duan, L. Zhang and L. Cao, *Angew. Chem., Int. Ed.*, 2023, **62**, e202308029.
109 H. Li, H. Xie, Y. Cao, X. Ding, Y. Yin and G. Li, *Anal. Chem.*, 2013, **85**, 1047–1052.
110 Y. Chang, Y. Zhuo, Y. Chai and R. Yuan, *Anal. Chem.*, 2017, **89**, 8266–8272.
111 J. W. Lee, M. H. Shin, W. Mobley, A. R. Urbach and H. I. Kim, *J. Am. Chem. Soc.*, 2015, **137**, 15322–15329.
112 J. E. Olson, A. S. Braegelman, L. Zou, M. J. Webber and J. P. Camden, *Appl. Spectrosc.*, 2020, **74**, 1374–1383.
113 G. Ghale and W. M. Nau, *Acc. Chem. Res.*, 2014, **47**, 2150–2159.
114 A. Hennig, H. Bakirci and W. M. Nau, *Nat. Methods*, 2007, **4**, 629–632.
115 Y. Cai and G. Li, *Dyes Pigm.*, 2021, **195**, 109734.
116 R. Jiang, M. Nilam, A. Hennig and W. M. Nau, *Adv. Mater.*, 2024, **36**, 2306922.
117 A. Hennig, G. Ghale and W. M. Nau, *Chem. Commun.*, 2007, 1614–1616.
118 X. Mao, Y. Li, P. Han, X. Wang, S. Yang, F. Zhang, X. Gong and Y. Cao, *Sens. Actuators, B*, 2018, **267**, 336–341.
119 H. Barbero and E. Masson, *Chem. Sci.*, 2021, **12**, 9962–9968.
120 D. T. Dang, J. Schill and L. Brunsveld, *Chem. Sci.*, 2012, **3**, 2679.
121 D. T. Dang, R. P. G. Bosmans, C. Moitzi, I. K. Voets and L. Brunsveld, *Org. Biomol. Chem.*, 2014, **12**, 9341–9344.
122 D. T. Dang, H. D. Nguyen, M. Merkx and L. Brunsveld, *Angew. Chem., Int. Ed.*, 2013, **52**, 2915–2919.
123 P. J. De Vink, T. Van Der Hek and L. Brunsveld, *Chem. Sci.*, 2021, **12**, 6726–6731.
124 R. P. G. Bosmans, J. M. Briels, L.-G. Milroy, T. F. A. de Greef, M. Merkx and L. Brunsveld, *Angew. Chem., Int. Ed.*, 2016, **55**, 8899–8903.
125 P. J. de Vink, J. M. Briels, T. Schrader, L.-G. Milroy, L. Brunsveld and C. Ottmann, *Angew. Chem.*, 2017, **129**, 9126–9130.
126 D. T. Dang, A. H. A. M. van Onzen, Y. L. Dorland and L. Brunsveld, *ChemBioChem*, 2018, **19**, 2490–2494.
127 S. J. A. Aper, A. Den Hamer, S. F. A. Wouters, L. J. M. Lemmens, C. Ottman, L. Brunsveld and M. Merkx, *ACS Synth. Biol.*, 2018, **7**, 2216–2225.
128 M. Ramaekers, S. P. W. Wijnands, J. L. J. van Dongen, L. Brunsveld and P. Y. W. Dankers, *Chem. Commun.*, 2015, **51**, 3147–3150.

129 R. Wang, S. Qiao, L. Zhao, C. Hou, X. Li, Y. Liu, Q. Luo, J. Xu, H. Li and J. Liu, *Chem. Commun.*, 2017, **53**, 10532–10535.
130 X. Li, Y. Bai, Z. Huang, C. Si, Z. Dong, Q. Luo and J. Liu, *Nanoscale*, 2017, **9**, 7991–7997.
131 Y. Li, L. Zhao, H. Chen, R. Tian, F. Li, Q. Luo, J. Xu, C. Hou and J. Liu, *Chem. Commun.*, 2021, **57**, 10620–10623.
132 H. H. Lee, T. S. Choi, S. J. C. Lee, J. W. Lee, J. Park, Y. H. Ko, W. J. Kim, K. Kim and H. I. Kim, *Angew. Chem., Int. Ed.*, 2014, **53**, 7461–7465.
133 O. V. de Oliveira, A. da Silva Gonçalves and N. E. Castilho de Almeida, *J. Biomol. Struct. Dyn.*, 2022, **40**, 9602–9612.
134 N. E. C. de Almeida, T. D. Do, M. Tro, N. E. LaPointe, S. C. Feinstein, J.-E. Shea and M. T. Bowers, *ACS Chem. Neurosci.*, 2016, **7**, 218–226.
135 T. S. Choi, H. H. Lee, Y. H. Ko, K. S. Jeong, K. Kim and H. I. Kim, *Sci. Rep.*, 2017, **7**, 5710.
136 S. Sonzini, H. F. Stanyon and O. A. Scherman, *Phys. Chem. Chem. Phys.*, 2017, **19**, 1458–1465.
137 H. Shang, X. Chen, Y. Liu, L. Yu, J. Li and J. Ding, *Int. J. Pharm.*, 2017, **527**, 52–60.
138 M. Martinez Morales, M. Zalar, S. Sonzini, A. P. Golovanov, C. F. van der Walle and J. P. Derrick, *Mol. Pharmaceutics*, 2019, **16**, 3100–3108.
139 M. Martinez Morales, C. F. van der Walle and J. P. Derrick, *Mol. Pharmaceutics*, 2023, **20**, 3559–3569.
140 D. Maity, Y. Oh, L. Gremer, W. Hoyer, M. Magzoub and A. D. Hamilton, *Chem. – Eur. J.*, 2022, **28**, e202200456.
141 X. Tan, L. Yang, Y. Liu, Z. Huang, H. Yang, Z. Wang and X. Zhang, *Polym. Chem.*, 2013, **4**, 5378.
142 Q. Song, F. Li, X. Tan, L. Yang, Z. Wang and X. Zhang, *Polym. Chem.*, 2014, **5**, 5895–5899.
143 Z. Huang, Y. Fang, Q. Luo, S. Liu, G. An, C. Hou, C. Lang, J. Xu, Z. Dong and J. Liu, *Chem. Commun.*, 2016, **52**, 2083–2086.
144 S. Liu, Z. Huang, F. Li, T. Yan, S. Fu, R. Tian, C. Hou, Q. Luo, J. Xu and J. Liu, *Polym. Chem.*, 2019, **10**, 3566–3570.
145 E. A. Appel, F. Biedermann, U. Rauwald, S. T. Jones, J. M. Zayed and O. A. Scherman, *J. Am. Chem. Soc.*, 2010, **132**, 14251–14260.
146 E. A. Appel, X. J. Loh, S. T. Jones, F. Biedermann, C. A. Dreiss and O. A. Scherman, *J. Am. Chem. Soc.*, 2012, **134**, 11767–11773.
147 M. J. Rowland, E. A. Appel, R. J. Coulston and O. A. Scherman, *J. Mater. Chem. B*, 2013, **1**, 2904.
148 M. J. Rowland, M. Atgie, D. Hoogland and O. A. Scherman, *Biomacromolecules*, 2015, **16**, 2436–2443.
149 Q. Song, Y. Gao, J.-F. Xu, B. Qin, M. J. Serpe and X. Zhang, *ACS Macro Lett.*, 2016, **5**, 1084–1088.
150 J. Zhang, S. Hou, Y. Chen, J. Zhou, H. Chen and Y. Tan, *Soft Matter*, 2019, **15**, 9797–9804.
151 E. A. Appel, X. J. Loh, S. T. Jones, C. A. Dreiss and O. A. Scherman, *Biomaterials*, 2012, **33**, 4646–4652.
152 S. Li, N. Jiang, W. Zhao, Y.-F. Ding, Y. Zheng, L.-H. Wang, J. Zheng and R. Wang, *Chem. Commun.*, 2017, **53**, 5870–5873.
153 Y.-F. Ding, J. Wei, S. Li, Y.-T. Pan, L.-H. Wang and R. Wang, *ACS Appl. Mater. Interfaces*, 2019, **11**, 28665–28670.
154 S. Cheng, H. Shen, S. Zhao, Y. Zhang, H. Xu, L. Wang, B. Di, L. Xu and C. Hu, *Nanoscale*, 2020, **12**, 15348–15363.
155 C. Sun, Z. Wang, K. Yang, L. Yue, Q. Cheng, Y.-L. Ma, S. Lu, G. Chen and R. Wang, *Small*, 2021, **17**, e2101139.
156 P. Dowari, S. Saha, B. Pramanik, S. Ahmed, N. Singha, A. Ukil and D. Das, *Biomacromolecules*, 2018, **19**, 3994–4002.
157 A. C. Madl, C. M. Madl and D. Myung, *ACS Macro Lett.*, 2020, **9**, 619–626.
158 C. Redondo-Gómez, S. Padilla-Lopátegui, A. Mata and H. S. Azevedo, *Bioconjugate Chem.*, 2022, **33**, 111–120.
159 F. Tian, M. Cziferszky, D. Jiao, K. Wahlström, J. Geng and O. A. Scherman, *Langmuir*, 2011, **27**, 1387–1390.
160 X. Ren, Y. Wu, D. E. Clarke, J. Liu, G. Wu and O. A. Scherman, *Chem. – Asian J.*, 2016, **11**, 2382–2386.
161 H. Yang, Q. An, W. Zhu, W. Li, Y. Jiang, J. Cui, X. Zhang and G. Li, *Chem. Commun.*, 2012, **48**, 10633.
162 Q. An, J. Brinkmann, J. Huskens, S. Krabbenborg, J. de Boer and P. Jonkheijm, *Angew. Chem., Int. Ed.*, 2012, **51**, 12233–12237.
163 S. Sankaran, M. C. Kiren and P. Jonkheijm, *ACS Nano*, 2015, **9**, 3579–3586.
164 S. Sankaran, M. de Ruiter, J. J. L. M. Cornelissen and P. Jonkheijm, *Bioconjugate Chem.*, 2015, **26**, 1972–1980.
165 S. Sankaran, E. Cavatorta, J. Huskens and P. Jonkheijm, *Langmuir*, 2017, **33**, 8813–8820.
166 R. P. G. Bosmans, W. E. Hendriksen, M. Verheijden, R. Eelkema, P. Jonkheijm, J. H. van Esch and L. Brunsveld, *Chem. – Eur. J.*, 2015, **21**, 18466–18473.
167 O. J. G. M. Goor, R. P. G. Bosmans, L. Brunsveld and P. Y. W. Dankers, *J. Polym. Sci., Part A: Polym. Chem.*, 2017, **55**, 3607–3616.
168 L. Li, M. Liu, L. Yue, R. Wang, N. Zhang, Y. Liang, L. Zhang, L. Cheng, J. Xia and R. Wang, *Anal. Chem.*, 2020, **92**, 9322–9329.
169 M. J. Webber, E. A. Appel, B. Vinciguerra, A. B. Cortinas, L. S. Thapa, S. Jhunjhunwala, L. Isaacs, R. Langer and D. G. Anderson, *Proc. Natl. Acad. Sci. U. S. A.*, 2016, **113**, 14189–14194.
170 C. L. Maikawa, A. A. A. Smith, L. Zou, C. M. Meis, J. L. Mann, M. J. Webber and E. A. Appel, *Adv. Ther.*, 2020, **3**, 1900094.
171 C. L. Maikawa, A. A. A. Smith, L. Zou, G. A. Roth, E. C. Gale, L. M. Stapleton, S. W. Baker, J. L. Mann, A. C. Yu, S. Correa, A. K. Grosskopf, C. S. Liong, C. M. Meis, D. Chan, M. Troxell, D. M. Maahs, B. A. Buckingham, M. J. Webber and E. A. Appel, *Nat. Biomed. Eng.*, 2020, **4**, 507–517.
172 C. L. Maikawa, A. I. d'Aquino, E. T. Vuong, B. Su, L. Zou, P. C. Chen, L. T. Nguyen, A. A. A. Autzen, J. L. Mann, M. J. Webber and E. A. Appel, *Biomacromolecules*, 2021, **22**, 3565–3573.
173 Z. S. Clauss, R. Meudom, B. Su, M. A. VandenBerg, S. S. Saini, M. J. Webber, D. H. C. Chou and J. R. Kramer, *Biomacromolecules*, 2023, **24**, 481–488.
174 A. A. A. Smith, C. L. Maikawa, G. A. Roth and E. A. Appel, *Org. Biomol. Chem.*, 2020, **18**, 4371–4375.
175 G. Li, J. Hu, H. Chen, Y.-X. Chen and Y.-M. Li, *Chem. Commun.*, 2021, **57**, 6086–6089.

